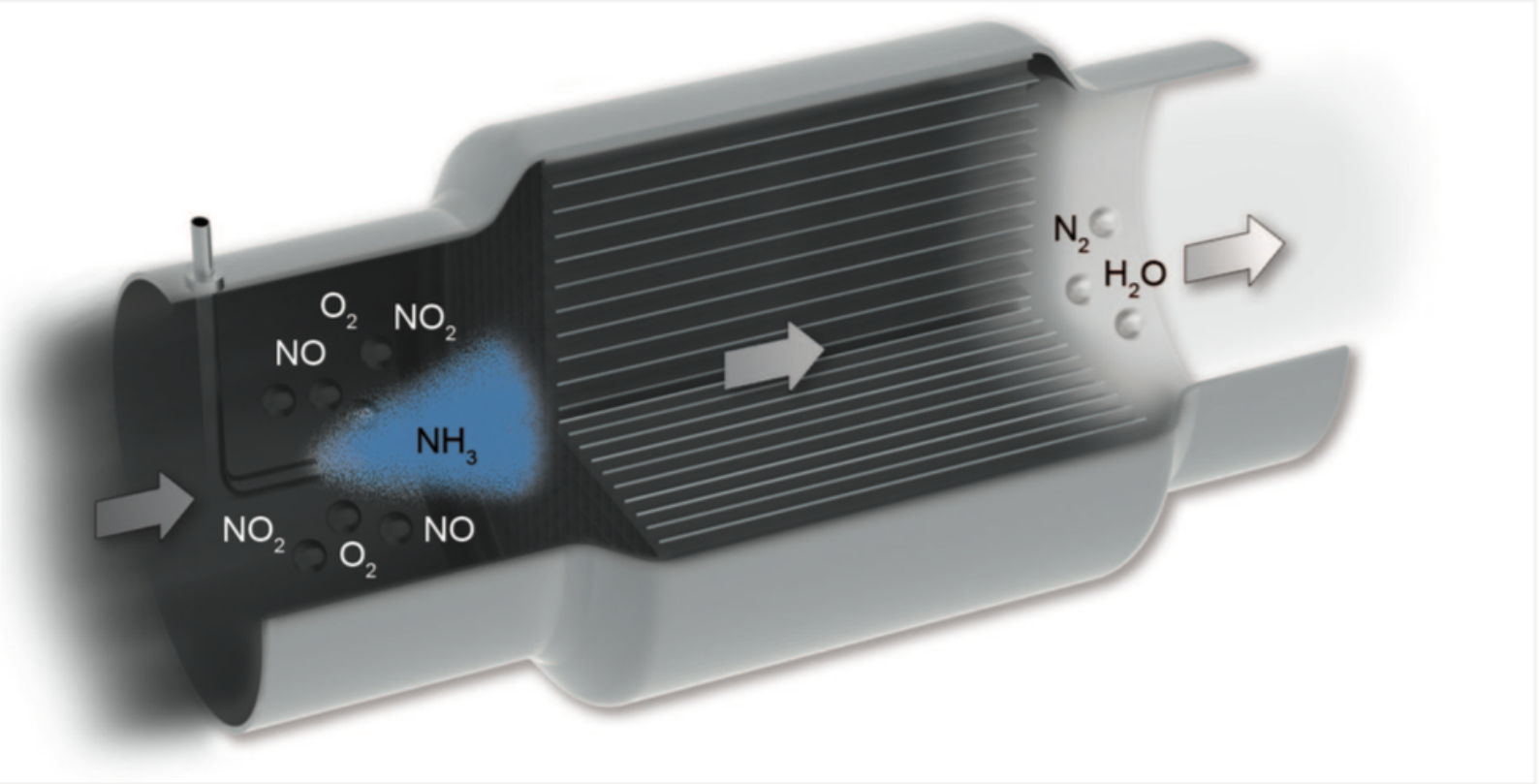

Selective Catalytic Reduction System for Marine Applications

Dynamic Modelling and System Integration

Federico Cattaneo

Technische Universiteit Delft

TU Delft Delft University of Technology

Challenge the future

SELECTIVE CATALYTIC REDUCTION SYSTEM FOR MARINE APPLICATIONS

DYNAMIC MODELLING AND SYSTEM INTEGRATION

by

Federico Cattaneo

in partial fulfillment of the requirements for the degree of

Master of Science
in Maritime Technology

at the Delft University of Technology,
to be defended publicly on Thursday March 22, 2018 at 10:30 AM.

Student number:	4519310	
Thesis number:	SDPO.18.009.m	
MTI report number:	AO 155	
Thesis committee:	Ir. K. Visser,	TU Delft, Chairman
	Dr. ir. M. Godjevac,	TU Delft, Daily Supervisor
	Ir. B. T. W. Mestemaker,	IHC MTI, Daily Supervisor
	Prof. dr. ir. B. J. Boersma,	TU Delft, External Committee Member

An electronic version of this thesis is available at `http://repository.tudelft.nl/`.

PREFACE

With this project, I complete my incredible experience at the TU Delft, where I have been able to genuinely pursue all my academic interests with no limitations. Furthermore, the international dimension I gained is something that I will bring along in my future career.

My special thank is for IHC MTI B.V., where I spent the last year working on my graduation. Thank to Ir. Klaas Visser for having helped me finding an amazing thesis topic and, most importantly, for the first lecture on gas turbines for marine applications. At that moment I have felt the need to switch to the marine engineering track. I am also very grateful to my daily supervisors Milinko (TU Delft) and Benny (IHC MTI B.V.) who continuously helped me with technical and motivational support (and with many many many meetings). I also thank the external committee member Prof.dr.ir. B.J. Boersma for having found time to be part of the thesis committee. The last mention is for the whole marine engineering team and in particular to Lindert, Harsh and Rinze.

I wish to thank my parents and my brothers that brilliantly supported me since the beginning of this experience. Thanks to the "old" and "new" friends and to Suelo 2.0 for the amazing time spent together.

Finally, a special thank to Ale, who became a fundamental anchor in such a short period of time.

Federico Cattaneo
Delft, March 2018

SUMMARY

Environmental regulations are continuously raising the bar towards more advanced diesel engine designs capable of minimizing the emissions of polluting substances. The recent IMO Tier III legislation, entered into force in 2016, is forcing the engine manufacturers to meet a NOx reduction of more than 70% from Tier II for all the ships sailing in designated NOx Emission Control Areas (NECA). Although these zones are, up to now, limited to the North American and U.S. Caribbean Sea NECAs, future regions, such as the North Sea and Baltic NECA in 2021 as well as stricter national and port regulations, are increasing the uncertainty regarding the possible compliance methods.

The Selective Catalytic Reduction (SCR) represents a flexible, proven and commercially available technology capable of reducing more than 80% of the NOx in the exhaust gas. Its adoption started in the '70s and was aimed at the reduction of stationary source emissions. From early 2000, it has been extended to the automotive industry in order to meet the Euro and EPA legislation for heavy duty and light diesel engines. Despite the evident disadvantages of the high installation cost and the considerable space requirements, the application of the SCR is subjected to a number of operating limits such as the narrow optimal temperature window and the slip of byproducts originated from the chemical reactions. These limitations can be even more severe when the diesel engine undergoes transient and dynamic operations.

The main objective of this research is to gain insights into the behaviour of the SCR technology under steady-state and dynamic operations of the diesel engine. After an accurate literature review of the working principles, reaction kinetics and modeling approach, a first principle model of the SCR has been developed to fulfill the scope. A 1D single channel approach, discretized along the reactor length, has been adopted to simulate the heat exchange and the chemical reactions occurring in the catalyst. To facilitate the integration of the designed model with an existing diesel engine model available in the Maritime and Transport Technology Department of the 3me faculty, the resistance and volume approach has been selected. After the verification of the SCR model, the integrated system *"SCR+Engine"* has been tested under steady-state conditions, to analyze the effect that the added back pressure has on the engine performance, and under dynamic conditions, to simulate "real" load case scenarios that the SCR might experience.

The designed model, although limited from the chemical reaction point of view, is able to predict NOx reduction and ammonia slip under steady-state and transient operations. It can be further used in an early design phase to investigate the feasibility of the SCR inclusion in the drive trains of ships. Future studies are recommended to optimize the model, by taking into account the sulphur influence on the reduction efficiency and the catalyst aging, and to validate it with real experiments on marine SCR systems.

To Tina, Mario, Adriana and Pippo

CONTENTS

LIST OF FIGURES

LIST OF TABLES

1

INTRODUCTION

1.1. BACKGROUND

The future application of diesel engines is threatened by the raising concern regarding the emission of polluting substances in the exhaust flow. Besides the result of the complete combustion process, which forms carbon dioxide (CO_2), sulphur dioxide (SO_2), water (H_2O) and the nitrogen oxide originating from the fuel bound nitrogen; it is possible to further classify the diesel emissions in two subcategories belonging to the cylinder process:

- Incomplete combustion: carbon (C), carbon monoxide (CO), unburned hydrocarbons (UHC) and particulate matter (PM)
- Unintended combustion of the nitrogen contained in the air

Nitrogen oxides (NOx) belong to the latter category and are generally split into:

- Nitrogen oxide (NO)
- Nitrogen dioxide (NO_2)

Sometimes, the term is extended to include other oxides such as the nitrous oxide (N_2O). In this thesis, however, it is assumed that the combustion process generates only NO and NO_2.

1.1.1. NOX FORMATION

Nitrogen oxides are generally formed in (post) flame zones during the combustion process. NOx formation is a combined result of chain reactions at high pressure, high peak temperature and long residence time. From figure 1.1 it can be seen that local high temperatures and kinetics play a major role in NOx emissions.
The formation of NO from nitrogen and oxygen is described by the extended Zeldovich mechanism (Stapersma, 2010*c*):

$$\begin{aligned} O + N_2 &\Leftrightarrow NO + N \\ N + O_2 &\Leftrightarrow NO + O \\ N + OH &\Leftrightarrow NO + H \end{aligned} \tag{1.1}$$

NO_2 is formed via the following reaction:

$$NO + HO_2 \rightarrow NO_2 + OH \tag{1.2}$$

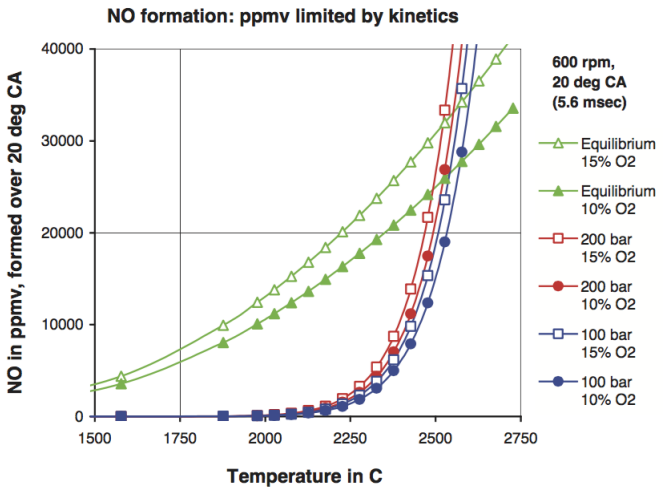

Figure 1.1: NO formation in a typical medium speed diesel engine (Stapersma, 2010*c*)

Because NOx emissions are for the largest part an air based emission, only a small part of the produced NOx is fuel based and its content can range up to 2% on a mass basis, depending on the fuel (Stapersma, 2010*c*) .
To summarise, the dominating parameters in the formation of NOx are temperature and oxygen concentration: the higher the temperature and the residence time at high temperature in the cylinder, the greater the amount of thermal NOx that will be created (Woodyard, 2003).

1.1.2. HEALTH AND ENVIRONMENTAL IMPACT

NO and NO_2 do not have the same environmental impact. While the first one is odourless, colourless and somehow non-toxic, the second one is pungent and toxic and is present not only in the engine but also, in the atmosphere, from the oxidation of NO.
NOx and volatile organic compounds (VOCs) react, in the presence of sunlight, to form photochemical smog, which is the cause of formation of ozone in the troposphere; the so-called ground level ozone.
Nitrogen oxides become nitric acid when dissolved in atmospheric moisture, forming a component of acid rain. This contributes to the acidification of the aquatic and terrestrial ecosystems. Furthermore, excess nitrogen inputs from the atmosphere promote the increased growth of phytoplankton and other marine plants which, in turn, may cause more frequent harmful algal blooms and eutrophication (the creation of oxygen-depleted dead zones) in some parts of the ocean. Last but not least, short-term NOx exposures, ranging from 30 minutes to 24 hours are linked with adverse respiratory effects, including airway inflammation in healthy people and increased respiratory symptoms in people with asthma. This latter effect is mostly due to the NO_2 which is detrimental to health at concentrations as low as one ppm (Eastwood, 2000).

1.1.3. IMO LEGISLATION

Annex VI of the International Convention for the Prevention of Pollution From Ships (MARPOL 73/78), had introduced a stepwise approach to the reduction of emissions of NOx and SOx.
The NOx control requirements apply to marine diesel engines of over 130 kW and is, at the moment, constructed with three Tiers, based on the ship construction date and the engine rated speed. Each Tier requires

further reductions of emissions compared to the previous one. To quantify the emission limit that each ship must comply with, the specific pollutant emission ratio (spe):

$$spe = \frac{\dot{m}_{pe}}{P_B} \tag{1.3}$$

in g/kWh is used; where $\dot{m}_{pe}$ is the mass flow of polluting substance and P_B is the engine brake power. The three levels of control are shown below:

Tier	Date	NOx Limit, g/kWh		
		n < 130	130 ≤ n < 2000	n ≥ 2000
Tier I	2000	17.0	$45 \cdot n^{-0.2}$	9.8
Tier II	2011	14.4	$44 \cdot n^{-0.23}$	7.7
Tier III	2016†	3.4	$9 \cdot n^{-0.2}$	1.96
† In NOx Emission Control Areas (Tier II standards apply outside ECAs).				

Figure 1.2: IMO Tier Controls (*https://www.dieselnet.com/standards/inter/imo*, 2018)

Tier III control applies only to the specified ships operating in NOx Emission Control Areas (NECA) established to limit NOx emissions. Outside such areas, the Tier II control applies. For example, a marine diesel engine that has been installed on a ship constructed after the 1^{st} January 2016 and operating in the North American NECA and/or the United States Caribbean Sea NECA, must comply with the Tier III NOx standards. When sailing far from these regions, Tier II applies. Slow speed diesel engines feature a more tolerant limit (figure 1.3) since their emissions are in general, even in specific terms, higher than the emissions of medium and high speed engines.

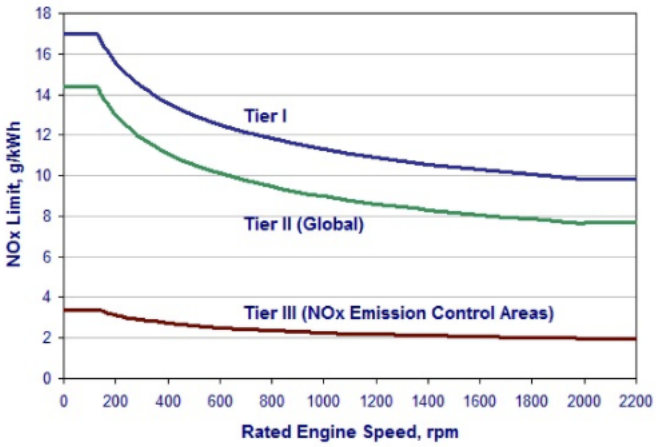

Figure 1.3: NOx emission requirements in g/kWh (*https://www.dieselnet.com/standards/inter/imo*, 2018)

These zones are, up to now, limited to the US and Canadian coastline and the gulf of Mexico. However, the discussion of future NECAs, such as the North Sea and Baltic NECA, which will enter into force in 2021 and the different national and port regulation are causing great uncertainty regarding the adoptable compliance methods (Döring et al., 2016).

1.1.4. NOx ABATEMENT TECHNOLOGIES

Marine diesel engines have faced, over the years, several challenges that led to outstanding and continuous improvements of the performances. In the '70s and '80s (fig.1.4), the biggest concern was represented by the

increasing price of fuel oil, which forced the engine manufacturers to reduce the specific fuel consumption by increasing the efficiency chain (mechanical, combustion, heat loss). In the last decade, engine builders have been focusing their efforts on the minimization of the engine polluting emissions, which has become the major challenge to the application of marine diesel engines.

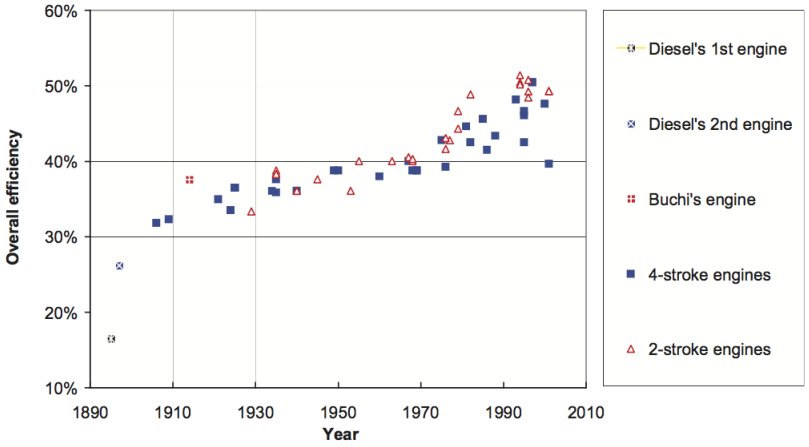

Figure 1.4: Trend of overall diesel engine efficiency over the years (Stapersma, 2010*a*)

Tier II NOx limits; i.e. 15-20% reduction from Tier I levels, have been largely achieved by means of modifications of the internal combustion process. However, to reach the Tier III control; i.e almost 80% reduction from Tier I, much bigger efforts are needed. In this section, the main methods that can be used to meet Tier III are introduced.
The three classes of reduction methods are:

- **Pre-treatment of fuel**
- **Engine modifications (Primary Methods)**
- **Exhaust gas aftertreatment (Secondary Methods)**

PRE-TREATMENT OF FUEL

Fuel can be pre-treated in order to reduce the sulphur and the nitrogen contents. While the first measure is indispensable to meet the IMO regulation on SOx emission limits, the denitration of fuel can't effectively affect the NOx emission since, as stated before, the majority of NOx formation is due to the combustion of the nitrogen content in the air. Another solution, which substantially harvests the nitrogen oxides emissions, is the adoption of alternative fuels such as LNG. Fuel conversion and dual fuel operations can achieve up to 80% of NOx reduction and represents one of the best alternatives to meet the current regulations on the NOx limit and sulphur cap.
However, the lack of infrastructures and worldwide availability, together with possible stricter limits in NOx emissions, still represent a challenge in the maritime sector.

PRIMARY METHODS

Primary methods are intended to lower the peak temperature in order to prevent NOx from forming. The main measures are now briefly introduced and described.
By **charge air-cooling**, cooler air is introduced in the cylinder. This allows for lower peak combustion temperatures and reduced fuel consumption by cutting down the heat losses however, the thermodynamic efficiency

may be negatively affected due the heat release at a lower temperature level. **Ignition delay**, delays the SOI (Start Of Ignition), resulting in a lower peak pressure and temperature during the combustion. Drawbacks are the increase in *sfc* and in PM emissions (in line with the so-called "diesel dilemma"). With **homogeneous charge**, an improved distribution of the air-fuel mixture inside the combustion chamber is obtained. This can be achieved through: a higher injection pressure, use of multiple injectors, which lead to a bigger nozzle volume, or an accurate design of the spray angles. **Rate shaping** consists of adjusting the fuel injection time profile in order to get a longer diffusion combustion at the expense of the premixed combustion. **Advanced Miller timing + 2-Stage Turbocharging + VIC** (Variable Inlet Closing) system has been designed to overcome the effect of non-optimal combustion at low loads. Its functioning principle, based on the delayed inlet valve closing, determines a better air filling in the combustion chamber and an increased compression pressure prior to injection, which results in an optimized combustion. Another measure is the introduction of **water in the cylinder**. It can be performed either through humidification of air at the inlet or by injection of a mixture of fuel and water or directly by different water injectors. The main aim is, again, the reduction of the peak temperature during the combustion process. The **Exhaust Gas Recirculation** (EGR), although is not sufficient to meet the Tier III regulation alone, may be used in combination with other techniques. Its functioning is based on the recirculation in the cylinder of part of the exhaust gas mixtures, which features a higher specific heat coefficient. As a main consequence the heat release, and so the peak temperature, is reduced. The high pressure EGR takes unfiltered exhaust gas before the turbocharger and introduces it after it is being cooled in the compressed airflow. On the contrary, in the low pressure EGR, the exhaust gas is firstly expanded and filtered and then cooled down before mixing with the fresh air entering the cylinder. The main advantage of the latter method is represented by the filtering of the particulates which have a positive effect on the wear of the engine. In this sense, the low pressure EGR is preferred in the marine sector, given the demand of durable and reliable engine. Slight increase in *sfc* is a drawback.

SECONDARY METHODS

The last group of measures are the "end of pipe" solutions, aimed at removing the NOx from the exhaust gas by treatments downstream of the engine. In contrast to the primary methods, these measures tend to have much higher installation costs and space requirements, but are also capable of the highest NOx reduction levels. **Non thermal plasma** and **wet scrubbing** belong to this category but is still questionable their viability for the marine sector (Stapersma, 2010*c*).

Selective Catalytic Reduction represents, however, the most promising aftertreatment system nowadays. The system reduces the level of nitrogen oxides in the exhaust gas by means of the following reaction with ammonia (reducing agent) occurring on the catalyst surface:

$$4NH_3 + 4NO + O_2 \rightarrow 6H_2O + 4N_2 \tag{1.4}$$

Major advantages of the SCR are:

- Proven technology: it has been extensively used in land based power plants and in the automotive sector with optimum results (Euro VI and EPA Tier II compliant)
- High efficiency: up to 90% of NOx removal potential, which means that no combination of other methods is required
- Allowing the engine to run at higher engine-out NOx can bring substantial fuel consumption benefits, which are valuable in terms of CO_2 production

1.1.5. SUMMARY

The potential of the described reduction methods is depicted in figure 1.5.

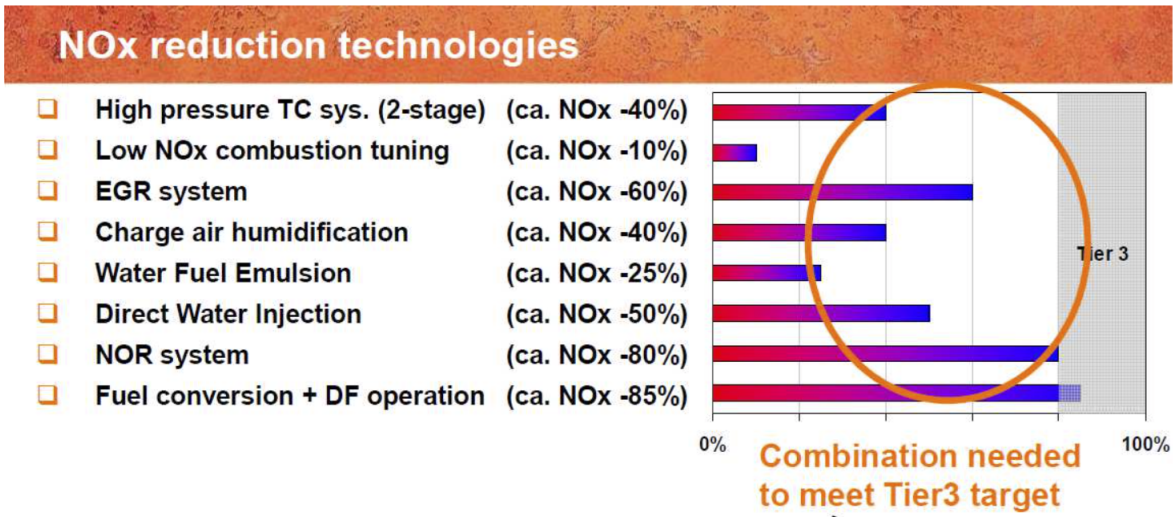

Figure 1.5: Reduction potential of the principal de-NOx measures (Wik, 2012)

The adoption of LNG as a primary fuel or the installation of the selective catalytic reduction (NOR system (Wik, 2012)) are the only options capable of meeting the IMO Tier III. The combination of EGR with other primary methods can achieve comparable reduction potentials at the expense of a more complicated engine design. Overall, the great uncertainty caused by national and international regulations on future stricter emission limits, makes the SCR an optimal compliance method which guarantees maximum flexibility and efficiency.

1.2. PROBLEM STATEMENT

From the reduction potential point of view, the SCR represents the best solution available in the market. Despite its application in the land based power generation has been successful, the dynamic operating profile that mobile applications experience, consistently reduces its adoption potential in the marine sector. Besides evident disadvantages such as the high installation cost, higher operational cost (due to the reducing agent consumption) and increased space requirements, the SCR main disadvantages are represented by:

- Limited optimal temperature range
- Catalyst deactivation
- Ammonia slip
- Sulphur influence
- Handling of the reducing agent

1.3. RESEARCH OBJECTIVES

The main objective of this thesis is to gain insight into the working principles of the SCR system, in order to study the influence that dynamic loading conditions have on its operation. The approach adopted to solve this main research topic is made of three sub-goals:

1. Literature review on the SCR working principles, chemical kinetics and modeling approach
2. Development of a SCR model capable of predicting NOx reduction, ammonia slip and urea consumption
3. Integration with a diesel engine model to investigate the performance and behaviour during steady-state and transient conditions

1.4. THESIS OUTLINE

This thesis is structured into 8 chapters. Chapter **2** describes the selective catalytic reduction technology with a focus on the marine sector. The literature review on the main chemical reactions and kinetic relations is further included. In chapter **3**, the SCR governing phenomena and the adopted reactor modelling approach are described. Chapter **4** deals with the model implementation in Matlab/Simulink. Chapter **5** is intended for the verification of the designed model. Chapter **6** describes the integration process with the diesel engine model and the required controller for the urea injection. Chapter **7** is focused on the simulations of the integrated system under both static and dynamic conditions. Finally, in chapter **8**. the main conclusions are drawn together with recommendation for future works.

2

SELECTIVE CATALYTIC REDUCTION: THE TECHNOLOGY

2.1. INTRODUCTION

The selective catalytic reduction of NOx by ammonia was patented in the United States by the Engelhard Corporation in 1957. It has been largely used to control nitrogen oxides emissions of fossil fuel power plants and chemical processes only from the 1970s, when the development of more cost-effective base metal catalyst allowed this technology to widespread in the market.
Mobile applications, on the other hand, had to overcome diverse operating challenges before being seen as valid aftertreatment systems. These obstacles are transient operating conditions, broad temperature windows, handling of the reducing agent, improvement of the low-temperature activity and high-temperature stability. These requirements, together with more stringent legislation, has led to continuous improvement of both catalyst materials and process design over the last twenty years.
In this chapter, the urea-SCR technology is thoroughly described with a focus on the challenges that its application involves in the maritime sector. The SCR reactions kinetics are further investigated, in order to set the basis for the modelling approach of chapter 3.

2.2. SYSTEM OVERVIEW

A typical scope of supply for a marine SCR unit consists of (fig.2.1):

- SCR honeycomb catalyst
- Reactor housing
- Urea tank
- Pumping system
- Dosing unit
- Injection system of the reducing agent
- Mixing devices

- Control unit

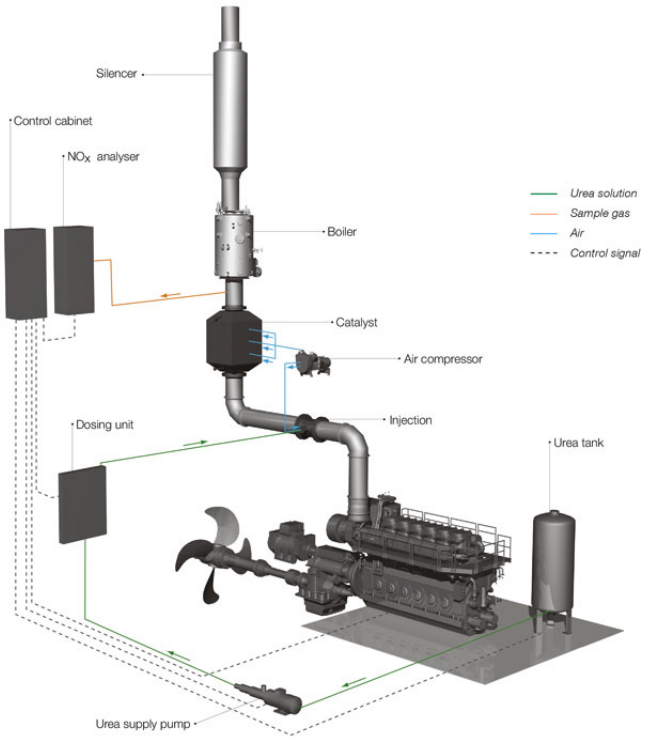

Figure 2.1: SCR unit (Struckmeier, 2015)

Depending on whether a medium speed or low speed diesel engine is adopted, the reactor is placed after or before the turbine, respectively. Since low speed engines features very low temperatures downstream of the turbine, the "pre-turbo" configuration is essential to guarantee an optimal behaviour of the system.

2.2.1. WORKING PRINCIPLES

The SCR process starts with the injection of the reducing agent, **urea**, which occurs through the pumping system and the injection system and is ruled by the dosing unit. Compared to pure ammonia injection, urea is non-toxic, non-combustible and its storage and injection operations are much easier and safer. Those reasons make it perfect for mobile applications. However, the drawback of such reactant is that it needs to decompose to ammonia through thermolysis and hydrolysis (an incomplete process might slow down the reduction efficiency of the SCR system). For this reason, a mixing duct upstream of the reactor, made up of static mixers, is used to enhance the ammonia formation. The solution used in the marine field is 40% urea in water or, alternatively, *AdBlue* (32.5% urea in water). The latter one is commonly adopted in the automotive sector.

Once ammonia is formed, it undergoes several reactions, mainly with nitrogen oxide, which contributes to the total reduction of NOx and the consequent formation of water and diatomic nitrogen. Despite the high selectivity, i.e. rate of desired product formation, urea-SCR inevitably leads to the formation of byproducts which either consume the reactants or directly poison the catalyst. To boost the wanted reactions and to limit the byproducts formation, the aftertreatment structure might be divided in three subsystems (fig.2.2), each of which plays a crucial role:

- Diesel Oxidation Catalyst (DOC): is used upstream of the urea injection to adjust the NO_2/NOx ratio

in order to increase the NOx conversion rate. The drawback of its application, when high sulphur fuels are used, is the enhancement of the SO_2 oxidation.

- SCR catalyst: is the core part of the system where the conversion of ammonia and NOx to nitrogen and water takes place.

- Ammonia Slip Catalyst (ASC): is an oxidation catalyst used after the SCR catalyst layers to convert the slipped byproducts, formed in the SCR catalyst, into less harmful compounds. As the DOC, it should be avoided when operating with high sulphur contents.

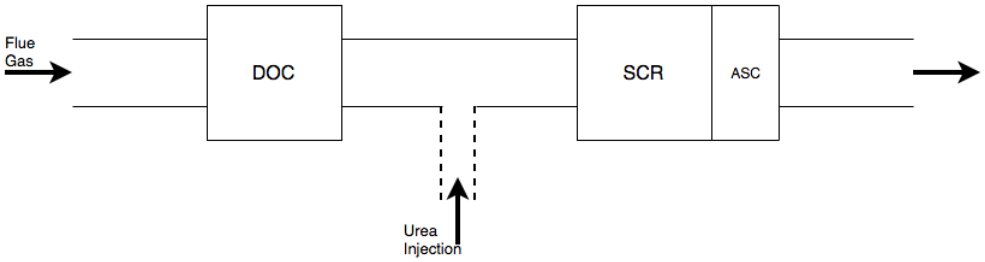

Figure 2.2: Possible integration of DOC, SCR and ASC

Once the exhaust gas exit the reactor, its content of nitrogen oxides and ammonia is measured through designated sensors and sent to the dosing unit which concordantly adjusts the injection of urea in order to meet the emission requirements.

2.2.2. SCR CATALYST

As addressed in the previous section, the SCR catalyst (or, equivalently, reactor) is the system's core part. It has a monolith structure which is sometimes referred to as a "honeycomb", made of several interconnected repeating cells or channels through which the exhaust gas passes (Nova and Tronconi, 2014). The honeycomb is generally inside a steel housing and is physically fixed in the exhaust duct. The main reason for its wide adoption in land based and mobile emission control devices, is its large open frontal area, which results in a very little resistance to flow and, hence, a low pressure drop. The lower the pressure drop the lower the resistance to flow or back pressure on the system. This is why, monolith supports, compared to packed bed reactors, are predominant in applications that require high flow rates and low pressure drops (Heck et al., 2009).
From the design point of view, the catalyst can be of two types: washcoated and extruded. The former consists of an inert structure, generally consisting of cordierite (ceramic) or steel (metal) which is coated with a porous material (the washcoat), which is used to further increases the surface area. The washcoat is made of the active elements, which enable the chemical reactions. In the latter, the entire catalyst structure incorporates the catalytic material, i.e. no inert material is used. Whichever the choice is, the monolith material needs to have enough mechanical strength and integrity to withstand the forces and vibrations the SCR catalyst will be exposed to (Nova and Tronconi, 2014). A square geometry example of both configurations is reported in fig.2.3a.

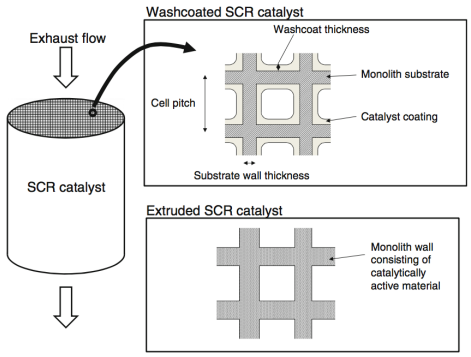

(a) Catalyst structure (Nova and Tronconi, 2014)

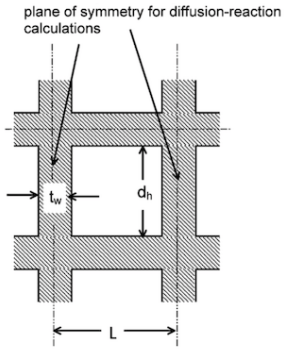

(b) Schematic diagram of monolith's square channel

Figure 2.3: Catalyst Monolith

MARINE SCR CATALYST

The most common catalyst materials used in the environmental industry are metals or metal oxides that are dispersed on high surface carriers. For marine applications, the predominant component in such catalysts is vanadium pentoxide (vanadia), V_2O_5, supported on titanium dioxide, TiO_2 (Magnusson et al., 2012).
Typical SCR configurations consist of TiO_2, WO_3 and V_2O_5 acting as the carrier, the promoter and the active component, respectively. Ordinary compositions are 1-3% V_2O_5 and ~10% WO_3 on the TiO_2 support (Nova and Tronconi, 2014). Vanadium is chosen both because of its lower cost, compared to iron and copper zeolites, and its higher efficiency and resistance to sulphur over the usual operating temperature range (250-400°C) of the diesel engine's exhausts. Tungsten trioxide (WO_3) acts as chemical and structural promoter by enlarging the temperature window of the SCR reaction and by improving the mechanical and structural properties of the catalyst (Lietti et al., 2000). Lastly, titanium dioxide is adopted because of its inertness to sulfate formation. The activity window of the catalysts can be changed by modifying the vanadia concentration: increasing the vanadia concentration will increase the low-temperature activity of the SCR catalyst. However, when incremented more than ~3.5%, it may lead to a loss in selectivity, an increased formation of N_2O and a higher SOx conversion.(Nova and Tronconi, 2014).
Channels properties of monoliths, such as geometric surface area to volume ratio (G_a), void fraction/open frontal area (ϵ) and hydraulic diameter (d_h) can be defined in terms of the cell density (n) and wall thickness (τ_w) (Williams, 2001). The cell density, often in cpsi (cells per square inch), is related to the cell pitch L via the following:

$$n = \frac{1}{L^2} \tag{2.1}$$

Consequently, void fraction and hydraulic parameter are given by:

$$\begin{aligned} \epsilon &= n \cdot (L - \tau_w)^2 \\ d_h &= L - \tau_w \end{aligned} \tag{2.2}$$

Finally, the geometric surface area to volume ratio for square ducts is a function of the above parameters:

$$G_a = 4\frac{\epsilon}{d_h} \tag{2.3}$$

A direct influence of the cell density and wall thickness on the G_a and the pressure loss is shown below.

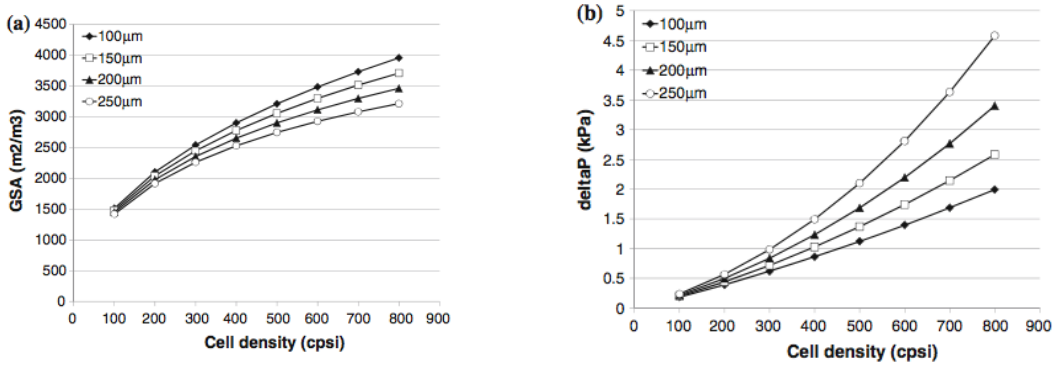

(a) G_a as a function of cell density and wall thickness

(b) Pressure loss at ambient temperature

Figure 2.4: Influence of cell density and wall thickness (Nova and Tronconi, 2014)

2.3. CHEMICAL REACTIONS

In this section, the set of the most important chemical reactions are addressed. These, are dived into three categories: urea conversion, desired reactions and undesired reactions. Unlike the last two, urea decomposition occurs upstream the SCR catalyst and is therefore treated first.

2.3.1. UREA DECOMPOSITION

It is broadly accepted that if urea, as an aqueous solution, is atomized into the hot exhaust gas stream, it decomposes in three steps (Guan et al., 2014): *evaporation* of the solution where the water is evaporated and the remaining urea melts and starts to decompose, *thermal decomposition* of sprayed urea into ammonia (NH_3) and isocyanic acid (HNCO) and *hydrolysis* of isocyanic acid, which occur just before the catalyst surface.
Step 1: Evaporation

$$(NH_2)_2CO_{liquid} \rightarrow (NH_2)_2CO_{molten} + H_2O_{gas} \tag{2.4}$$

Step 2: Thermal Decomposition

$$(NH_2)_2CO_{molten} \rightarrow NH_3 + HNCO \tag{2.5}$$

Step 3: Hydrolysis

$$HNCO + H_2O \rightarrow NH_3 + CO_2 \tag{2.6}$$

The most critical step is the thermal decomposition (reaction 2.5) which is an endothermic process. If the heating of the urea is slow, it might lead to the production of undesirable byproducts such as biuret, triuret and cyanuric acid. On the other hand, the hydrolysis reaction (2.6) is exothermic and its impact on the heat requested by reaction 2.5 can reduce to less than half the heat required by the thermal decomposition (Nova and Tronconi, 2014). Overall, the global process is slightly endothermic (89.6 kJ required per mole) and involves the generation of two moles of ammonia and one mole of carbon dioxide per each mole of urea. This information is crucial when designing the system dosing strategy. Given the small amount of required ammonia, between 500 and 2000 parts per million depending on the NOx content, the CO_2 production is negligible. As urea cannot be injected at temperatures less than 180°C (Nova and Tronconi, 2014), it is important to properly manage the ammonia storage in the catalyst (i.e. the amount of ammonia adsorbed onto the catalyst surface) for low-load applications.

2.3.2. DESIRED REACTIONS

In all heterogeneous catalytic processes, the first step, after the reactants transport to the boundary layer gas-surface, involves the activation of a reactant molecule by adsorption (chemisorption) onto the catalyst surface (Schmidt, 1998). The activation step implies that a rather strong chemical bond is formed with the catalyst surface. Once the available surface sites are occupied, no additional molecules can be chemisorbed (Davis and Davis, 2012). This process is in equilibrium with its contrary, named desorption, and depends on the surface temperature and the catalyst storage capacity:

$$NH_{3_{gas}} + \theta_{free} \longleftrightarrow NH_3^* \tag{2.7}$$

Where θ_{free} represents the free substrate active site of the SCR catalyst and NH_3^* represents the ammonia which has been adsorbed.

NOx reduction is the result of three distinct pathways, which have a different influence on the reduction efficiency based on the temperature and the NOx content in the flue gas. The three reactions are:

Standard SCR

$$4NH_3^* + 4NO + O_2 \rightarrow 4N_2 + 6H_2O \tag{2.8}$$

Fast SCR

$$2NH_3^* + NO + NO_2 \rightarrow 2N_2 + 3H_2O \tag{2.9}$$

Slow SCR

$$8NH_3^* + 6NO_2 \rightarrow 7N_2 + 12H_2O \tag{2.10}$$

The standard SCR converts nitrogen oxide, but no nitrogen dioxide. The consumption of ammonia is one mole per mole of NO. Reaction 2.9 is much faster and converts as much NO as NO_2. Again, one mole of NH_3 is consumed per mole of NO_x ($NO + NO_2$). Since the NO_2/NO_x ratio is generally low in diesel exhaust gas (around 5-10% (Woodyard, 2003)), the standard SCR represents the main reaction path. As already introduced, one way to support the fast SCR would be to use an upstream DOC which would bring the NO_2/NO_x close to 0.5 enabling a much faster reduction. Lastly, the slow SCR, as the name might suggest, is not of much importance in lean exhaust gas because of its slower rate and its requirement of NO_2/NO_x close to 1 (Nova and Tronconi, 2014).

The summary of these considerations are shown in figure 2.5 for an iron zeolite catalyst. Compared to zeolites, vanadia catalysts feature different reduction potential over the examined temperatures.

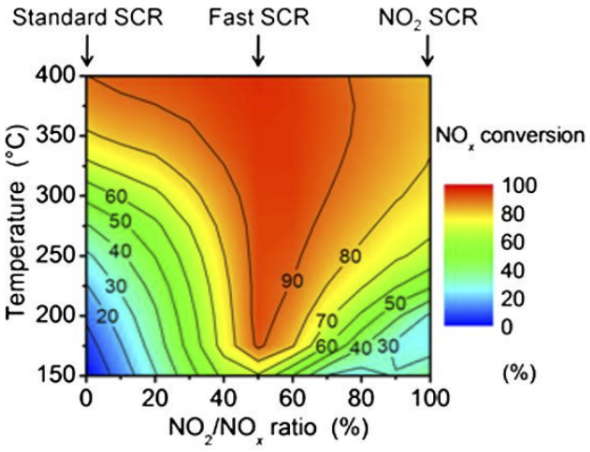

Figure 2.5: Different NOx conversion mechanism potential based on NO_2/NOx ratio over Fe/zeolite catalyst (Iwasaki and Shinjoh, 2010)

From the figure above, it is clear that low temperature operations hardly reach a satisfying NOx conversion when only the Standard SCR is exploited.

2.3.3. UNDESIRED REACTIONS

Despite the high selectivity, urea-SCR inevitably leads to the formation of byproducts which either consume the reactants or poison the catalyst.
The first group of side reactions are a result of operations outside the temperature range of the SCR catalyst:
Formation of nitrous oxide (T>400° C)

$$4NH_3^* + 4NO + 3O_2 \rightarrow 4N_2O + 6H_2O \tag{2.11}$$

Ammonia oxidation (T>400° C)

$$4NH_3^* + 5O_2 \rightarrow 4NO + 6H_2O \tag{2.12}$$

Formation of ammonium nitrate (T<200° C)

$$2NH_3^* + 2NO_2 \rightarrow NH_4NO_3 + N_2 + H_2O \tag{2.13}$$

These reactions play a large role as soon as the engine exhibits a peak in the exhaust gas temperature. The consumption of the key reactant is increased and, as a result, the NOx conversion slows down. Additionally, ammonia oxidation also leads to an increase in nitrogen oxides. Further drawbacks consist in the deposition of ammonium nitrate and deactivation and blockage of the catalyst pores. Finally, nitrous oxide formation must be limited since it is a powerful greenhouse gas with a GWP (Global Warming Potential) 265-298 times that of CO_2 for a 100-year timescale (*https://www.epa.gov/ghgemissions/understanding-global-warming-potentials*, 2018).

The second group of side reactions is associated with the sulphur content of the fuel oil. This is a sensitive issue in the maritime industry due to the widespread use of high sulphur fuels which are cheap and can be easily adopted until the new sulphur cap regulation will come to force. Although vanadia based catalysts are used because of their lower sensitivity to sulphur poisoning, a high percentage of SOx in the exhaust still might significantly affect the SCR efficiency.
Sulphur dioxide can be adsorbed, likewise ammonia in reaction 2.7, at the surface of a noble metal, when reacting with gaseous oxygen to form SO_3 (Lietti et al., 2000):

$$SO_{2_{gas}} + \frac{1}{2}O_2 + \theta_{free} \longleftrightarrow SO_3^* \tag{2.14}$$

The adsorption of the sulphur compounds at the catalytic layer surface blocks the access of the ammonia gas to the layer, slowing down the NOx reduction process. Moreover, when extreme temperature conditions occur (fig.2.6), the adsorbed sulphur may further react according to the following reactions:
SO_3 formation

$$SO_3^* \rightarrow SO_{3_{gas}} + \theta_{free} \tag{2.15}$$

Ammonium sulfate formation (AS)

$$2NH_3 + SO_3^* + H_2O \rightarrow (NH_4)_2SO_4 \tag{2.16}$$

Ammonium bisulfate formation (ABS)

$$NH_3 + SO_3^* + H_2O \rightarrow (NH_4)HSO_4 \tag{2.17}$$

Reaction 2.15 takes place above 400-450°C, depending on the fuel sulphur content. When operating with high sulphur fuels it is wise not to integrate the SCR with an ASC in order to avoid such conversion, which can lead to the formation of sulphuric acid, H_2SO_4, which inevitably affects the operation of the downstream systems. Reactions 2.16 and 2.17 occur in the SCR catalyst in combination with low temperatures and give rise to deactivation of the catalyst and blockage of the system, which may lead to a further drawback represented by an increased back pressure. The temperature range at which the poisoning mechanisms take place, as a function of the ammonia and SO_3 contents, is shown in figure 2.7.

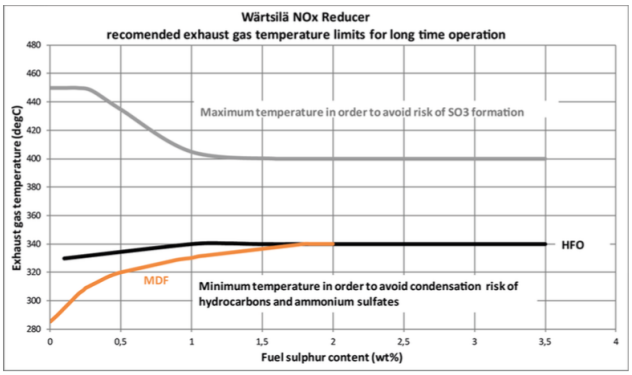

Figure 2.6: Average minimum/maximum exhaust gas temperature depending on sulphur content fuel (Wärtsilä, 2013)

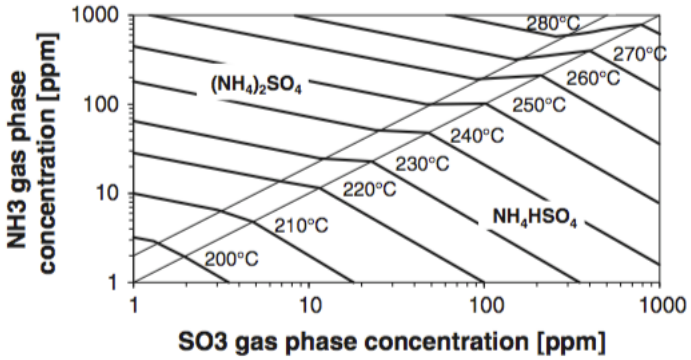

Figure 2.7: AS and ABS formation as a function of NH_3 and SO_3 (Nova and Tronconi, 2014)

An exhaustive investigation conducted by Magnusson et al. (2012), regarding the influence of sulphur dioxide and water on the performance of a marine SCR catalyst, shows important results which are in line with the presented theory. In general, the addition of SO_2, in absence of water, promotes the NOx reduction and the NH_3 conversion along with an increased formation of N_2O. On the contrary, the addition of H_2O, in absence of SO_2, results in a decreased NOx reduction and an inhibition of the N_2O formation. These trends are shown in figure 2.8. The experiment started with the cooling process, reducing from 400°C to 100°C, followed by a heating process. This was done for several sulphur concentrations, starting and finishing with 0 ppm sulphur. The sample was then oxidized in 8% O_2 at 550°C for 1 hour, to ensure removal of sulphurur compounds from the sample, followed by the equivalent cooling/heating process in the presence of 4% H_2O.
When both sulphur dioxide and water are present in the flue gas, the activity for NOx reduction decreases, in particular at high concentrations of SO_2, low temperatures, and high space velocities (SV), i.e. the quotient of the entering volumetric flow rate of the reactants divided by the reactor volume. This tendency might be

caused by an increased deposition of ammonium sulfate salts which reduce the NOx conversion, possibly by pore plunging.

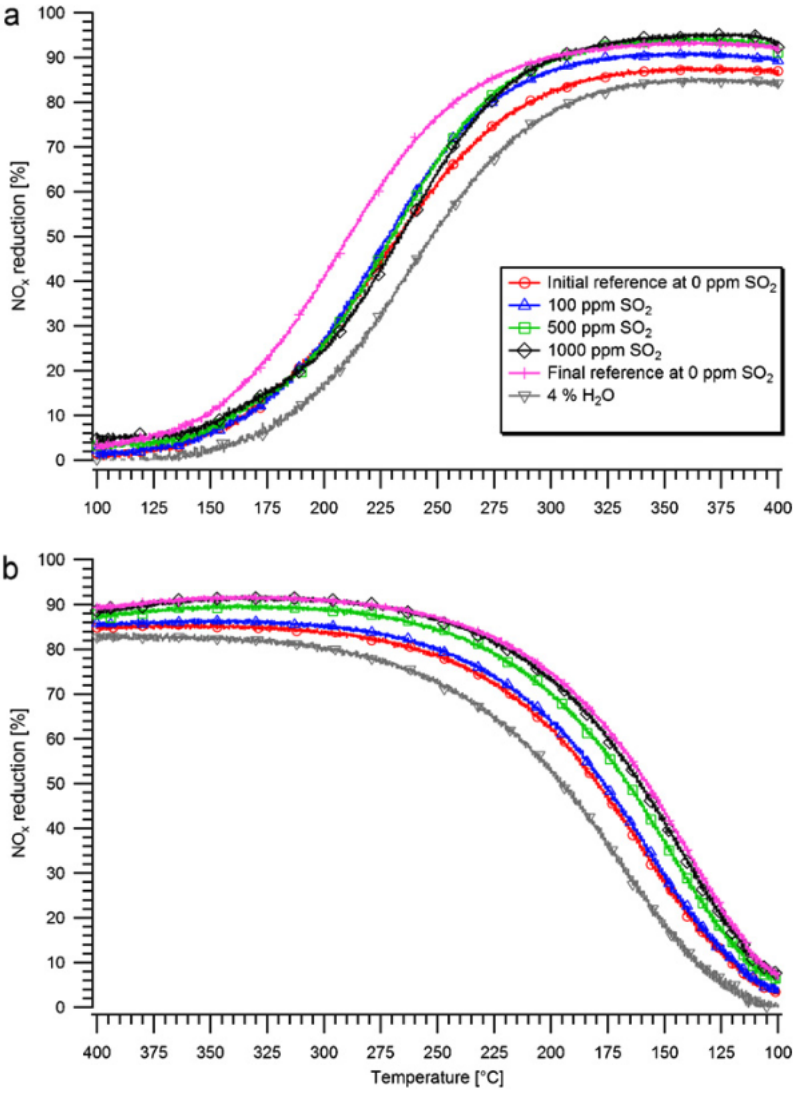

Fig. 3. Catalytic activity for lean NO_x reduction as a function of temperature (a) 100–400 °C and (b) 400–100 °C).

Figure 2.8: Catalytic activity for lean NOx reduction as a function of temperature (Magnusson et al., 2012)

Overall (fig.2.9), in presence of water, high percentages of sulphur at low temperatures result in a sharp decrease in NOx reduction. On the other hand, as long as the steady-state temperature is held above 300°C (depending on the fuel sulphur content), the NOx reduction seems to be not appreciably affected by the sulphur dioxide present in the flue gas.

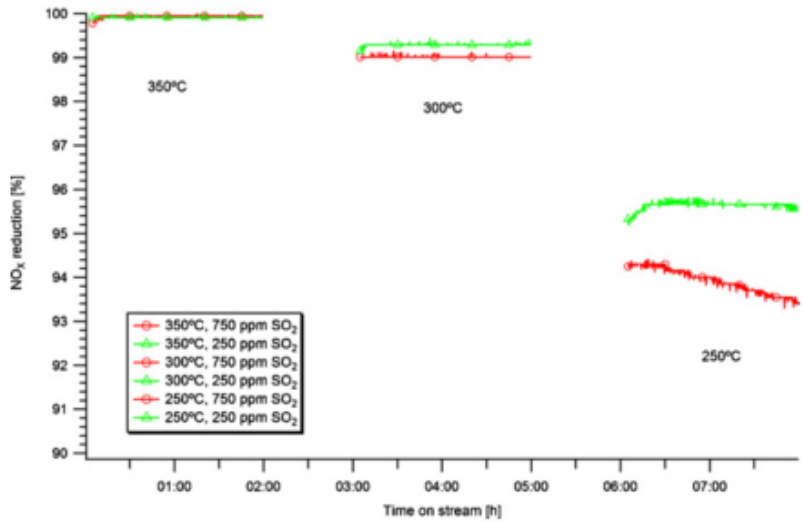

Figure 2.9: NOx reduction as a function of time at 350, 300 and 250°C Feed gas composition: 500 ppm NO, 500 ppm NH_3, 8% O_2, 250 and 750 ppm SO_2 and 4% H_2O (Magnusson et al., 2012)

2.4. REACTION KINETICS OVER VANADIA CATALYSTS

2.4.1. INTRODUCTION

Reaction kinetics, or chemical kinetics, is the study of the rates of chemical processes. Chemical kinetics includes the investigation of how different process conditions can influence the speed of a chemical reaction and yield information about the reaction's mechanism and transition states, as well as the construction of mathematical models that can describe the characteristics of a chemical reaction.

Before introducing the term reaction rate, it is important to set some definitions.
As presented in Vannice and Joyce (2005), a balanced chemical reaction can be expressed as:

$$0 = \sum_j \sigma_j \cdot B_j \tag{2.18}$$

where σ_j is the stoichiometric coefficient (positive for products and negative for reactants) of any product or reactant B_j.
The extent of a reaction is used to keep track of the number of times a certain reaction occurs and it is defined as:

$$\xi(mol) = (n_j - n_{j_0})/\sigma_j \tag{2.19}$$

where n_{j_0} and n_j are the moles of substance B_j, at time zero and at any other time, respectively.
The **reaction rate**, r, is defined as the number of times this reaction takes place per unit of time. From the definition of ξ, the reaction rate of a given reaction is:

$$r = \frac{d\xi}{dt} \tag{2.20}$$

When one is interested in the rate of **production** or **destruction** of species i, it is simply given by the product or r by its stoichiometric coefficient:

$$r_j = \sigma_j \cdot r \tag{2.21}$$

In order to make r an intrinsic property, it is usually normalized to unit catalyst volume (V).

$$r_V = r = \frac{d\xi}{V \cdot dt} \qquad \left[\frac{mol}{m^3 s}\right] \tag{2.22}$$

The number of moles per unit volume of species j is normally referred to as concentration, C_j. This term is relevant when defining the **rate law** of a reaction, which is simply an expression relating the rate of a reaction to the concentrations (or partial pressures) of the chemical reactants. For example, given the following:

$$aA + bB \rightarrow cC + dD \tag{2.23}$$

the elementary rate law which describes the reaction rate of the above reaction would be:

$$r = k \cdot C_A^a \cdot C_B^b \tag{2.24}$$

The rate law is said to be of order a with respect to A and of order b with respect to B. When a reaction is not elementary, the concentrations are not raised to the power of their stoichiometric coefficients but, instead, to some α and β coefficients which are partial reaction orders and should be determined experimentally. The vast majority of kinetic expressions reported in the literature are based on mechanistic approaches like Langmuir-Hinshelwood or Eley-Rideal models and/or empirical expressions like power-law kinetics (equation 2.24) (Pace, 2013). Whichever the model is used, the **rate constant** k is described by the Arrhenius expression:

$$k = k^0 \cdot exp(-E_a/(\tilde{R} \cdot T_s)) \tag{2.25}$$

where

- k^0 is the pre-exponential factor (unit depends on the reaction)
- E_a is the activation energy of the reaction in [J/mol]
- $\tilde{R}$ is the universal gas constant [J/mol/K]
- T_s is the surface temperature of the catalyst layer in [K]

The Arrhenius equation gives a direct indication of the catalyst purpose: by reducing the activation energy the rate constant is increased and, as a consequence, the reaction rate increases (2.24).

2.4.2. GLOBAL REACTION SCHEME

In this section, the governing chemical kinetic mechanisms of the SCR process is addressed with a focus only on the vanadium-based catalyst, which is the kind used in this work.
According to a considerable number of authors Guzzella and Onder (2009); Lietti et al. (2000); Nova and Tronconi (2014); Schär (2003); Song (2013), an Eley-Rideal mechanism may be assumed for the catalyst reactions over a wide range of temperatures. This means that only ammonia is being strongly adsorbed while the other species react in the gas phase according to the "simple" scheme:

$$\begin{aligned} A(g) + S(s) &\longleftrightarrow AS(s) \\ AS(s) + B(g) &\rightarrow Products \end{aligned} \tag{2.26}$$

where s and g stands for surface and gas, respectively.
In most cases, a reaction that looks straightforward can be subdivided into several elementary steps, each having its own rate law. Accordingly, a global reaction scheme is widely adopted. In such mechanism, several microkinetic adsorption, reaction, and desorption steps are "lumped" together, reducing the overall number of kinetic parameters (Güthenke et al., 2007).
From the above considerations, it follows that the characterization of the main reaction rates must be based on empirical formula and experimental data.
In the current work, the adopted reaction schemes are the ones investigated by the University of Milan over more than 20 years on vanadia SCR catalysts (Güthenke et al., 2007; Lietti et al., 2000; Nova and Tronconi, 2014).

2.4.3. ADSORPTION-DESORPTION

From the adsorption/desorption reaction (eq.2.7), a variable θ_{free} has been introduced to represent the *free* surface coverage of the catalyst. Instead of NH_3^*, the *adsorbed* surface coverage can be expressed with θ_{NH_3} such that

$$\theta_{free} + \theta_{NH_3} = 1 \tag{2.27}$$

It follows that, at time $t = 0$, when the catalyst is still unoccupied from the flue gas, the maximum surface coverage correspond to the free surface coverage and $\theta_{free} = 1$. When the fluid enters the reactor, an equilibrium value of θ_{free} and θ_{NH_3} is reached through the adsorption and desorption onto the catalyst,.
The dynamic adsorption and desorption of ammonia have been extensively investigated and the results of the step feed experiments, performed at different temperatures, have been analyzed according to a dynamic 1-D heterogeneous plug flow reactor model and fitted by nonlinear regression, to provide estimates of the relevant kinetic parameters. In Nova and Tronconi (2014), it is reported that a single site adsorption is used and the ammonia adsorption rate can be described by:

$$r_{ads} = k_{ads} \cdot C_{NH_3} \cdot \theta_{free} \tag{2.28}$$

where

$$k_{ads} = k^0_{ads} \cdot exp\left(-\frac{E_{ads}}{R \cdot T_s}\right) \tag{2.29}$$

Ammonia adsorption depends on the surface temperature (via the Arrhenius equation), the incoming ammonia concentration and the free surface coverage.
On the other hand, the desorption action solely depends on the ammonia surface coverage and it is described by:

$$r_{des} = k_{des} \cdot \theta_{NH3} \tag{2.30}$$

with a Temkin-type expression for the rate constant:

$$k_{des} = k^0_{des} \cdot exp\left(-\frac{E^0_{des}}{R \cdot T_s}(1 - \alpha \cdot \theta_{NH_3})\right) \tag{2.31}$$

Besides the single-site approach, a dual-site approach consisting of Bronsted acid sites, where ammonia is strongly bonded, and Lewis acid sites, where ammonia is weakly adsorbed can be also adopted. However, its description (Nova and Tronconi, 2014) is limited to zeolites catalysts and is therefore not treated in this thesis. The comparison between experimental results and simulation of the adsorption/desorption process described by the rates 2.28- 2.30 is given in figure 2.10.

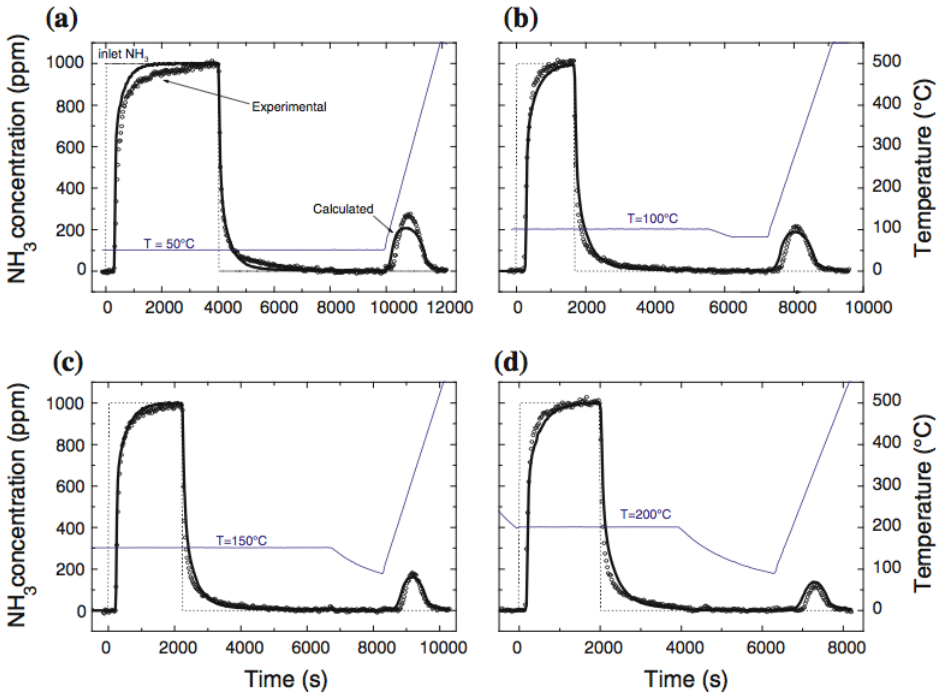

Figure 2.10: Adsorption/Desorption + Temperature Programmed Desorption (TPD) runs: SV= 92000h^{-1}; NH_3=1000 ppm, H_2O=1%, O_2 =2%. **(a)**T=50°C; **(b)**T=100°C; **(c)**T=150°C; **(d)**T=200°C. *Symbols*: experimental; *solid lines*: model fit (Nova and Tronconi, 2014)

2.4.4. STANDARD SCR

Transient experiments in a wide range of temperatures (50-550°C) were performed in order to develop a suitable kinetic model of the NH_3/NO/O2 reacting system, i.e. no NO_2 in the exhaust. The study of the standard SCR kinetics was particularly focused on the characteristics that are critical for mobile applications, namely the behaviour during transient operation and the reactivity in the low-temperature region (Güthenke et al., 2007; Nova and Tronconi, 2014). A simple Eley-Rideal rate law (ER), in line with several authors (Güthenke et al., 2007; Guzzella and Onder, 2009; Janssen, 1987; Nova and Tronconi, 2014), based on the equation:

$$r_{std} = k_{std} \cdot C_{NO} \cdot \theta_{NH_3} \tag{2.32}$$

was found to work well with temperatures above 250°C, when the inhibiting effect of gaseous ammonia does not play a valuable role. However, the NH_3 startup and shutdown transients at the lowest investigated temperatures were not reproduced by the model. A modified Eley-Rideal mechanism (Mθ), which estimates that r_{std} becomes independent of the ammonia surface coverage above a critical NH_3 coverage named $\theta^*_{NH_3}$, was also proposed:

$$r_{std} = k_{std} \cdot C_{NO} \cdot \theta^*_{NH_3} \cdot (1 - e^{-\theta_{NH_3}/\theta^*_{NH_3}}) \tag{2.33}$$

This expression afforded a good agreement between experimental and calculated data, again with the exception of the outlet concentrations of NO and N_2 during the NH_3 startup and shutdown transients at the lower temperatures. As for equation 2.32, the ammonia inhibiting effect was not taken into account.
A third kinetic model (MR) capable of capturing this effect was then derived. It features a dual site adsorption mechanism (contrary to the simple single site approach), which result in a reaction rate for the standard SCR equal to:

$$r_{std} = \frac{k_{std} \cdot C_{NO} \cdot \theta_{NH_3}}{\left(1 + K_{NH_3} \cdot \frac{\theta_{NH_3}}{1-\theta_{NH_3}}\right)\left(1 + k_{O_2} \cdot \frac{C_{NO} \cdot \theta_{NH_3}}{p_{O_2}^{1/4}}\right)} \tag{2.34}$$

Rate expression 2.34 differs from the Eley-Rideal rate 2.32 only in its denominator, which accounts both for the inhibiting effect of ammonia and for the favorable dependence of oxygen: at low ammonia coverage, i.e at high temperatures (above 250°C), the denominator tends to unity and rate 2.34 reduces to rate 2.32 (Nova and Tronconi, 2014).

Whichever the rate law assumed, the corresponding rate constant is again described by the Arrhenius equation:

$$k_{std} = k^0_{std} \cdot exp\left(-\frac{E_{std}}{R \cdot T_s}\right) \tag{2.35}$$

The comparison between experimental results and simulation of the Standard SCR reaction, described by the rates 2.32-2.33-2.34, is given in figure 2.11.

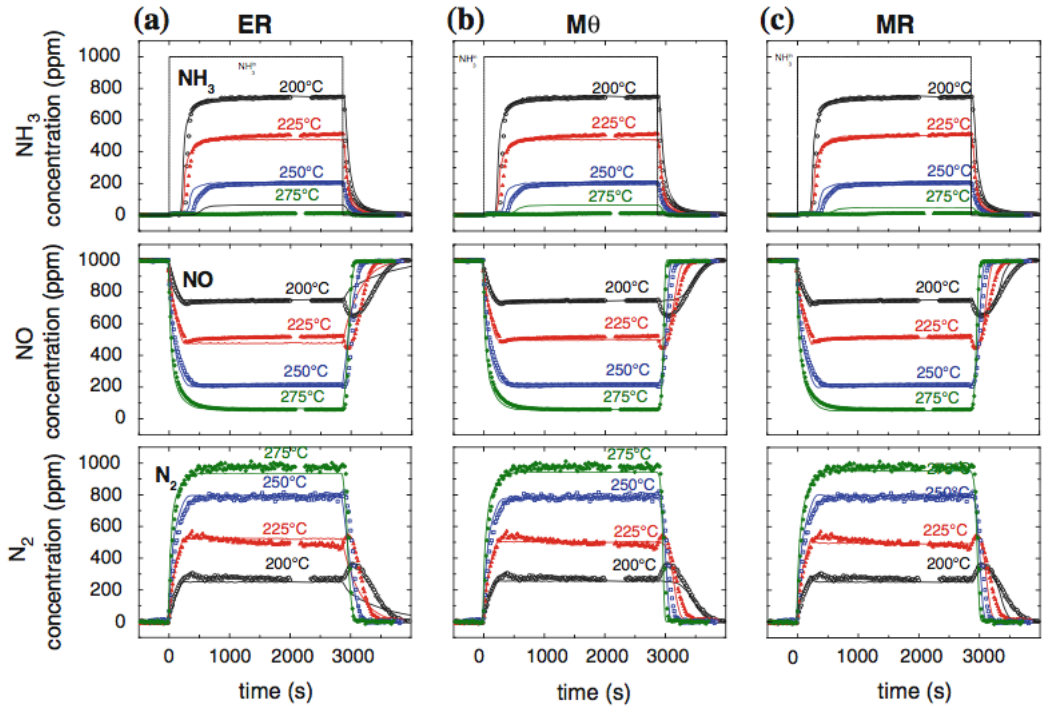

Figure 2.11: Transient SCR experiments at different temperatures: SV = 92000 h^{-1}; NH_3 = 0→1000→0 ppm, NO = 1000 ppm, H_2O = 1%, O_2 = 2%. *Symbols*: experimental; *solid lines*: model fit using **a** the Eley RIdeal rate mode 2.32, **b** the Mθ rate law 2.33, **c** the MR rate law 2.34 (Nova and Tronconi, 2014)

3

MODELLING APPROACH

3.1. INTRODUCTION

Due to the multitude of parameters influencing the SCR, experimental analysis of its performance are time-consuming and require large experimental setups. In this regard, mathematical models and simulations are necessary "cheap and fast" tools to determine the system response to process disturbances such as variable feed compositions and temperature. In the SCR technology, it is important to study the effects of load variations on the adsorption capacity of the catalyst in order to optimize the urea injection system and the overall reduction efficiency.

Over the years, catalyst modelling have been extensively investigated and numerous models have been presented for stationary applications and, in a second moment, for the automotive industry. Despite the consistent piece of literature, there is a great diversification in the approach of the available models. This is due to the following reasons (Pontikakis et al., 2004):

- Modeling objectives and application range
- Problem complexity
- Fast development of washcoat technology
- Performance assessment difficulty

Although the catalyst modeling approach development has been mainly focusing on the simulation of the three way catalyst (3WC), adopted in gasoline engines, the physics can actually be used for a wide number of devices (Depcik and Assanis, 2005). Since all monolithic catalysts have the same flow pattern, there are only a few differences between the diverse types of devices:

- Species thermodynamic properties
- Species transport properties
- Reaction mechanism

In the specific case of the SCR technology, the most different feature is the reaction mechanism: the 3WC technology strives for the simultaneous reduction of NO_x, HC and CO while the SCR focuses its selectivity towards the NO_x minimization.

3.2. MODEL REQUIREMENTS

The main objective of this thesis is to investigate the influence of dynamic loading conditions on the operation of a marine SCR system. To achieve this, a dynamic model of the SCR should be built and integrated with a complete diesel engine model that predicts exhaust gas composition, temperature and mass flow, which are the input of the SCR.
In consideration of the above, the SCR model should meet the following requirements:

- Sufficiently accurate to predict urea consumption, NO_x reduction and ammonia slip
- Low computational time

An important assumption of the model is the absence of reactions involving the negative influence of SO_2 on the formation of sulphates. Unfortunately, not much evidence was found in the literature about the kinetic data of such reactions. A limited number of reactions have been selected in order to guarantee consistency and to avoid mixing data coming from different papers.

3.3. GOVERNING PHENOMENA AND MAIN ASSUMPTIONS

As described in section 2.2.2, the SCR is a "flow through" reactor device, consisting of multiple parallel channels. For this reason, it should ideally be simulated with a 3-D model, which takes into account the unfair distribution of the inlet flow and temperature at the entrance of all the channels and the ambient heat transfer, to properly define the surface temperature of every channel (indispensable to determine the reaction kinetics). However, the amount of information needed, together with the high computation time that it would suffer, makes it more practical and convenient, for reactor performance evaluation and control, to adopt a **single channel approach**. This method has been mostly used in fixed system and, later, in mobile applications for both the 3WC and the SCR (as thoroughly described in Depcik and Assanis (2005); Pontikakis et al. (2004)). If uniform flow, temperature, and concentrations distribution at the entrance of all channels is assumed, it is possible to consider each channel to be identical and consisting of:

- Bulk Phase
- Solid Phase (Washcoat + Substrate)

A "film" layer approach is used between the two phases. It employs mean bulk values for the gas phase and solid-gas interface values for the solid phase species concentrations (Depcik and Assanis, 2005; Güthenke et al., 2007; Guzzella and Onder, 2009; Pontikakis et al., 2004). At this point, the model can be seen as a 2-D described by cylindrical coordinates; axial and radial. When the radial heat conduction is neglected, it is possible to further reduce the whole system to a 1-D single channel model.
For the one dimensional channel (fig.3.1), the following phenomena are important (Depcik and Assanis, 2005):

1. Bulk flow (gas phase)
2. Interphase transfer (gas-surface phase)
3. Chemical reactions (surface)
4. Heat generation (surface)
5. Diffusion through washcoat (surface)

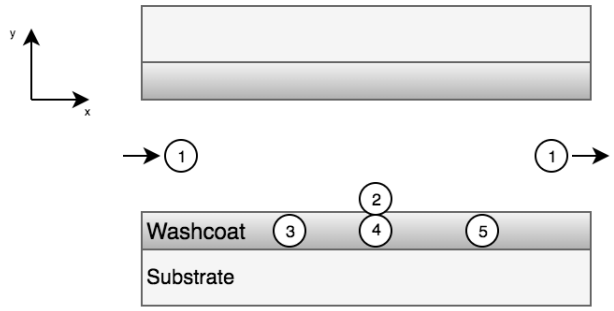

Figure 3.1: Governing phenomena

At this point, further assumptions are necessary. The influence of these phenomena is not of the same order of magnitude. According to Depcik and Assanis (2005); Guzzella and Onder (2009); Koltsakis and Stamatelos (1997); Nova and Tronconi (2014), the influence of internal diffusion (No. 5) is negligible and it can be lumped into the chemical reactions (No. 3), especially when dealing with washcoated catalyst. The surface reaction model approximates the washcoat with a solid-gas interface where it is assumed that all reactions take place. In this case, there is no concentration gradient in the washcoat. Furthermore, in addition to the negligible radial heat conduction, nearly the entire examined literature considers the SCR reactor to be adiabatic, since the external heat transfer is essentially absent(Heck et al., 2009). To sum up, the **main assumptions** adopted to model the SCR catalyst are the following:

- Uniform inlet flow, temperature, and concentrations distribution at the entrance of all channels (1-D single channel approach)
- Negligible radial heat conduction (1-D single channel approach)
- Plug flow
- Adiabatic reactor
- Ideal gas
- Laminar flow
- Negligible diffusion through washcoat (coated catalyst)
- Square channel shape
- Modelled reactions:
  - NH_3 Adsorption/Desorption

$$NH_{3_{gas}} + \theta_{free} \longleftrightarrow NH_3^*$$

  - Standard SCR

$$4NH_3^* + 4NO + O_2 \rightarrow 4N_2 + 6H_2O$$

  - Fast SCR

$$2NH_3^* + NO + NO_2 \rightarrow 2N_2 + 3H_2O$$

* NH_3 Oxidation

$$4NH_3^* + 5O_2 \rightarrow 4NO + 6H_2O$$

The absence of experimental data, led to the adoption of available kinetic data from the literature to fit the reaction rates equations. The choice has fallen upon Åberg et al. (2017), mainly because of two reasons:

1. The model equations and kinetic relations of Åberg et al. (2017) are in accordance with the main literature investigated in the present work (Depcik and Assanis, 2005; Güthenke et al., 2007; Lietti et al., 2000).

2. Compared to Güthenke et al. (2007); Lietti et al. (2000), a simple formulation of both the Fast SCR and the Oxidation is given (eq. A.4, A.5), together with the respective kinetic data (A.1).

3.4. GOVERNING EQUATIONS

After having defined the main phenomena and assumptions, the whole catalyst can be modelled by means of a first principle approach based on mass and energy balances (fig.3.2). These equations are written for the two existing phases; bulk and solid and are in accordance with the theory presented in Depcik and Assanis (2005) and Güthenke et al. (2007).

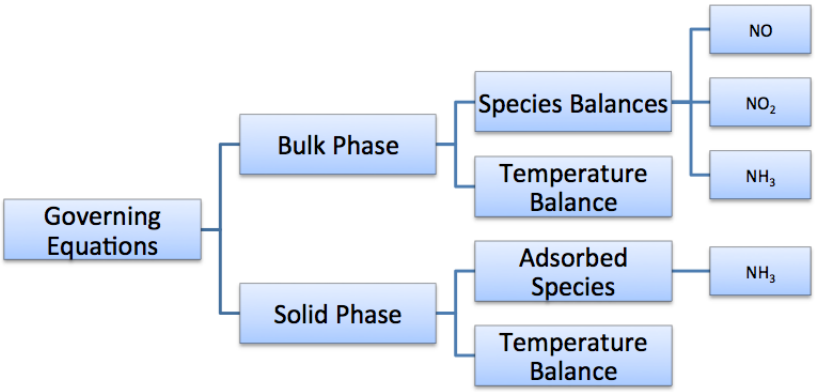

Figure 3.2: Overview of the model governing equations

The mass equations are used to describe the variation of the concentrations in time along the catalyst length, while the temperature balances describe the change of gas (T_g) and monolith (T_m) temperature, which influences the reaction rates through the Arrhenius equation. An equation which describes the ammonia surface coverage, i.e. the adsorbed ammonia in the washcoat, is further introduced to complete the set.
The accurate description of the set of equations can be found in appendix C.

4

MODEL DEVELOPMENT

4.1. INTRODUCTION

In this chapter, an extensive description of the model's structure is addressed. Firstly, the volume/resistance method is introduced with the characterization of the customization for the SCR system. The accurate explanation of the resistance and the volume element's modelling is then showed in two separated subsections, where a more specific approach to each block is demanded.

4.2. RESISTANCE AND VOLUME ELEMENTS

A typical SCR reactor's design is based on a multi-layer concept; it is made of either two or three catalysts layers separated by volumes which allow for the soot blowing system (fig.4.1a). Each layer is obtained by the packing together of several simple catalyst units (fig.4.1b).

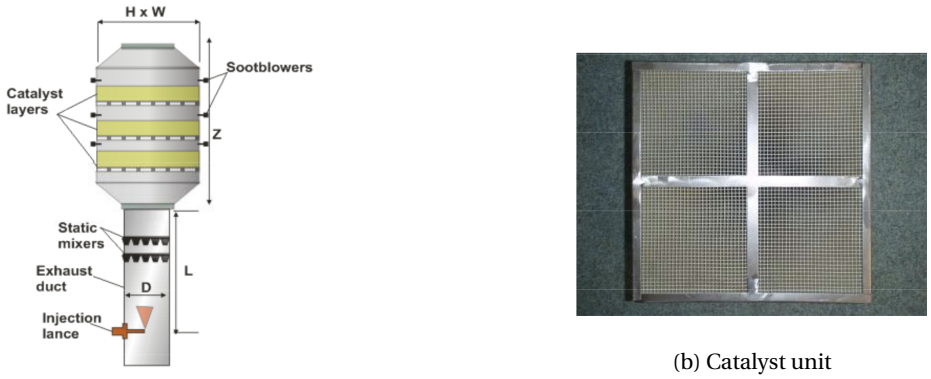

(a) SCR reactor

(b) Catalyst unit

Figure 4.1: Marine SCR system

For an accurate representation of the physical system, the different segments inside the reactor are all classified as either volume or resistance elements. A resistance element must always be connected to two volumes, whilst a volume can be connected with any number of resistance elements.
The intra-catalyst volumes are modelled as volume elements (fig.4.2). In the control volumes, the immediate

mass is calculated by integrating the net mass flow (coming from the resistance elements). Integrating the net energy flow connected with the mass flows results in the instantaneous temperature. The incoming mass flows have their own temperature, the outgoing mass flow has a temperature equal to the instantaneous temperature of the element. Finally, the instantaneous pressure of the element can be calculated using the ideal gas law.

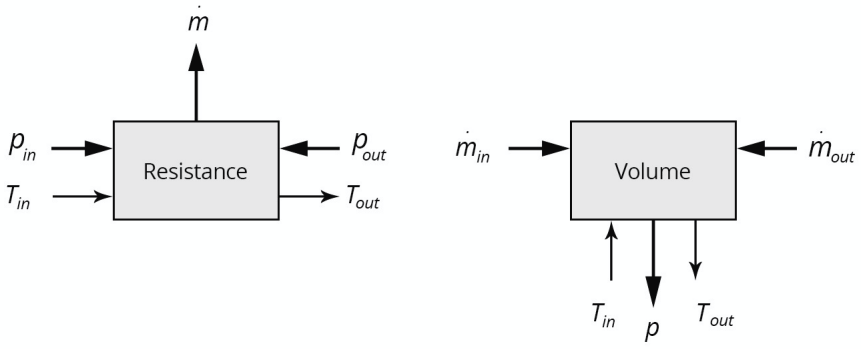

Figure 4.2: Standard volume and resistance blocks

The catalyst layers are modelled as resistance elements. The mass flow through the element is calculated as a function of pressure difference (of the upstream and downstream volumes) using the momentum equation (Schulten, 2005). The derivation of those equations can be found in appendix D.

4.2.1. SCR MODEL

In the special case of the SCR, an indispensable information which comes as an input, and is fed through the whole system, is the composition vector y, which contains the mole fraction of the species entering the SCR:

$$y = [y_{N_2} \quad y_{O_2} \quad y_{Ar} \quad y_{CO_2} \quad y_{H_2O} \quad y_{SO_2} \quad y_{CO} \quad y_{NO} \quad y_{NO_2} \quad y_{NH_3}] \tag{4.1}$$

The mole fraction of a generic species "j" is defined as:

$$y_j = \frac{n_j}{n} \tag{4.2}$$

where n_j is the number of moles of component j and n is the mixture's total number of moles:

$$n = \sum_{j=1}^{nc} n_j \tag{4.3}$$

from which it follows:

$$\sum_{j=1}^{nc} y_j = 1 \tag{4.4}$$

Since the mole fraction of NO, NO_2 and NH_3 is below 0,01% (NOx is around 500-1500 ppm (Stapersma, 2010*c*)), the parts per million (ppm) notation is adopted:

$$ppm_j = y_j \cdot 10^6 \tag{4.5}$$

In real applications, the exhaust mixture also contain traces of soot, hydrocarbons and particulate matter. Although they might be cause of fouling and poisoning of the catalyst, in this thesis it is assumed that their influence on the SCR is negligible, since the main focus of the model lies more on the NO_x reduction potential rather than the catalyst deactivation. Other assumptions are:

- Sulphur oxides in the exhaust gas are all present as sulphur dioxides

- Once urea is injected, full conversion to gaseous ammonia takes place

The model's sketch, consisting of a dual layer concept, is given in fig.4.3.

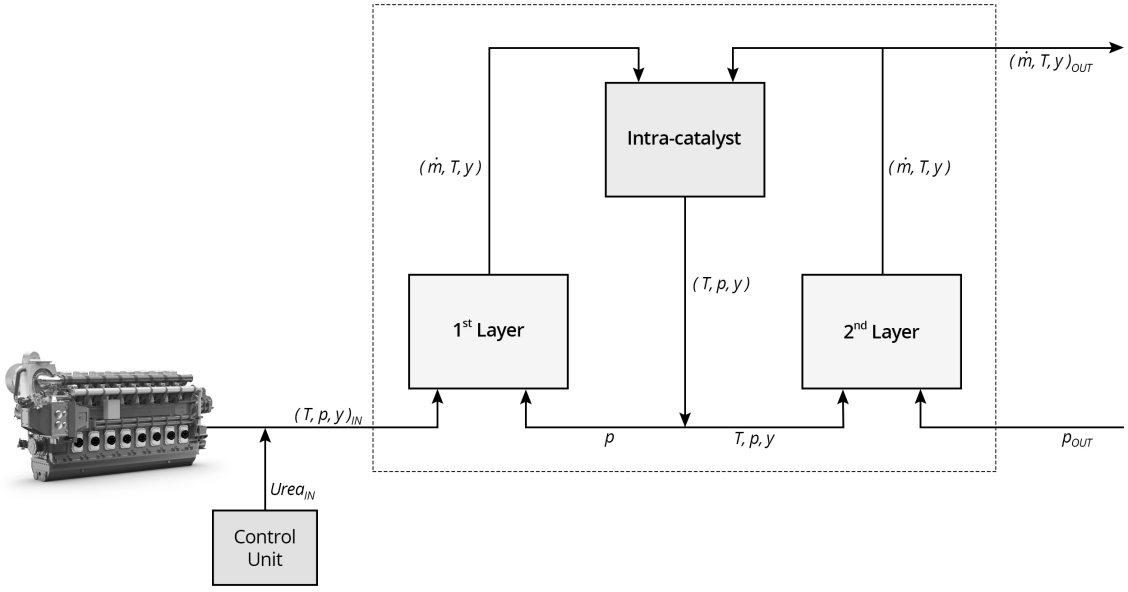

Figure 4.3: SCR model's main blocks

The inputs of the SCR model are the pressures upstream and downstream, while one of the output is the mass flow. From figure 4.2, it follows that the SCR acts as a resistance block (internally divided in volumes and resistances). This information will be used when it comes to integrating the reactor with the diesel engine model (section 6.3). Moreover, through this approach, one can adapt the model to any real reactor design. For example, by simply adding a resistance element and by changing the reaction mechanisms, the ammonia slip catalyst layer can be integrated.
A thorough description of the two main blocks and their relatives sub-blocks is given in the following sections.

4.3. CATALYST LAYER

The catalyst layer model, in figure 4.4, takes as input all the information (temperature, pressure and composition vector) coming from the inlet volume and the pressure of the downstream volume, which, in case of the 1^{st} layer, is the intra-catalyst. The output is represented by the mass flow through the layer and the outlet gas composition and temperature.

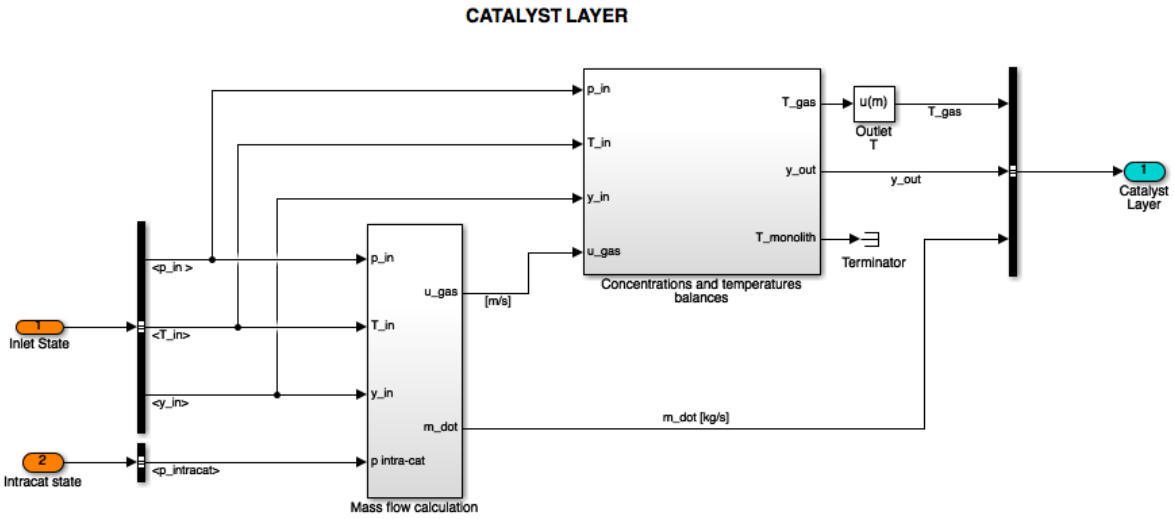

Figure 4.4: Inside of the catalyst layer

The outlet information are calculated via two main sub-blocks:

- **Mass flow calculation**, evaluates the mass flow using the pressure difference of the upstream and downstream volumes. The gas channel velocity is further obtained as it is needed for the balance equations.
- **Concentrations and temperatures balances**, is the core part of the catalyst layer. The entire set of governing equations described in chapter 3 are solved and, as a result, the change in gas temperature and composition is evaluated.

4.3.1. MASS FLOW CALCULATION

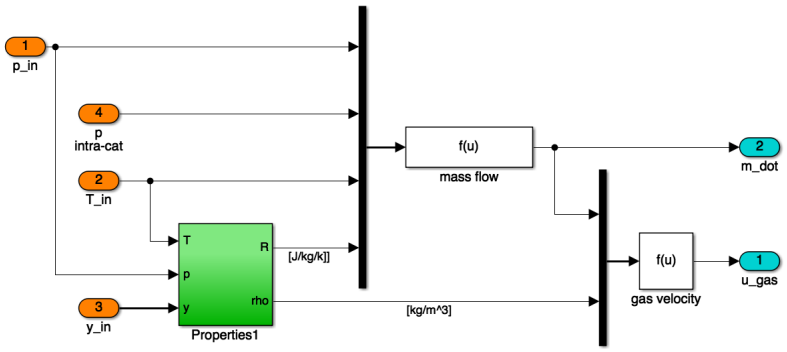

Figure 4.5: Mass flow calculation sub-block

By means of the pressure difference between the layer's inlet and outlet, the mass flow in the resistance is calculated using:

$$\dot{m} = (\mu \cdot \phi) \cdot A \cdot \epsilon \cdot \frac{p_{in}}{\sqrt{R_{in} \cdot T_{in}}} \cdot \sqrt{2} \cdot \sqrt{1 - \frac{p_{out}}{p_{in}}} \tag{4.6}$$

where: μ and ϕ are the contraction and resistance factors, respectively, and the product between the reactor cross-sectional area and the void fraction (ϵ) represent the effective open area where the gas flows.

The velocity in the channel is calculated as follows:

$$u_{gas} = \frac{\dot{m}}{\rho \cdot A \cdot \epsilon} \tag{4.7}$$

Since the key reactants' concentration is low, it is feasible to calculate the mass flow and the gas speed across the layer using the composition vector at the inlet. The impact on the calculation of the mixture gas constant (R) and density is not appreciably affected, since the composition's variation is below 1%. The specific gas constant, in $[\frac{J}{kg \cdot K}]$ is related to the universal gas constant ($\tilde{R}$) via the following:

$$R = \frac{\tilde{R}}{M_{gas}} \tag{4.8}$$

where M_{gas} is the molar mass of the gas mixture given by:

$$M_{gas} = \sum_{j=1}^{nc} M_j \cdot y_j \tag{4.9}$$

Finally, the mixture density is easily calculated using the ideal gas law:

$$\rho = \frac{p}{R \cdot T} \tag{4.10}$$

4.3.2. CONCENTRATIONS & TEMPERATURE BALANCES

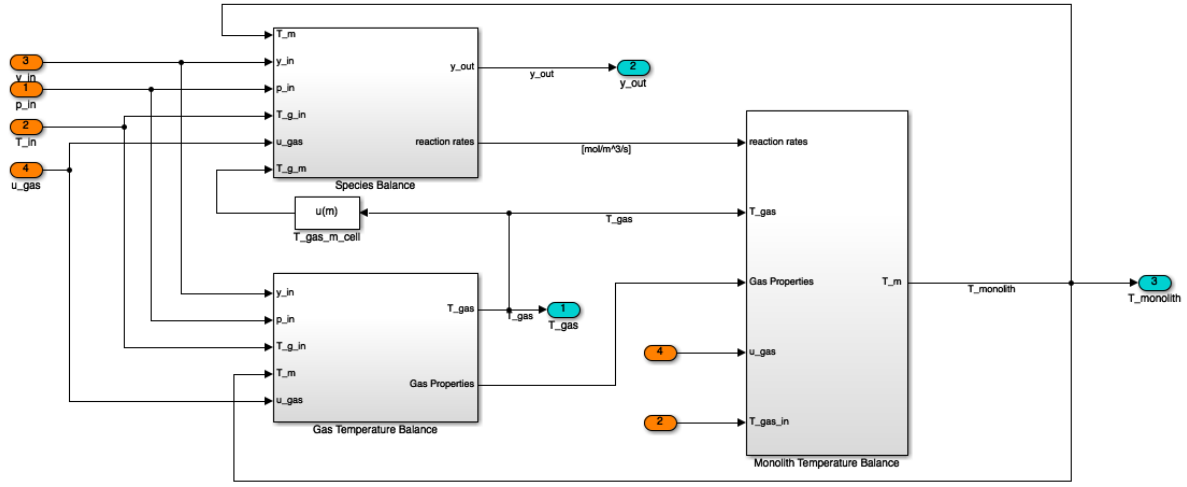

Figure 4.6: Balances sub-block

This section is the core part of the SCR model. The incoming exhaust flow, with its temperature, pressure, composition and speed, reacts according to the mechanisms presented in chapter 2. Since a one dimensional model has been adopted, only axial gradients of the reactants' concentrations and the gas/solid temperatures are evaluated. The set of mass and temperature balances, presented in section 3.4, are therefore formulated as partial differential equations and, in order to solve them, the catalyst layer's length has been discretized into "m" cells. The space derivatives are discretized according to the backward differences method (Anderson and Wendt, 1995):

$$\frac{\partial f}{\partial x} = \frac{f_i - f_{i-1}}{\Delta x} \tag{4.11}$$

where f is a general fluid's property and Δx is the length of segment i. Index i is used to keep track of the cells' number and it belongs to the interval $\{1....m\}$, where $i = 0$ represents the inlet boundary conditions, i.e.

the model's inlet values. By applying such method, the set of PDEs reduces to a set of ordinary differential equations in time which are solved using the "*Level 2 S-Function*" of Matlab®/Simulink®. Such function, allows the user to build custom blocks with multiple input and output ports and capable of handling any type of signal produced by a Simulink® model, including matrix and frame signals of any data type. For the discretized model, the continuous states are solved in the "derivatives" block.
From above, it follows that the block's key signals are classified as follows:

Table 4.1: Key signals of block in fig.4.6

Signal	Dimension	Description
T_{gas}	1xm	Gas temperature in each cell
$T_{monolith}$	1xm	Surface temperature in each cell
Rates	5xm	Reaction rates of the 5 modelled reactions in each cell
C_j	1xm	Concentration of species j in each cell

The concentration vectors of NO, NO_2 and NH_3 are calculated in the "Species Balance" sub-block, but their m^{th} value is the most relevant information, as it is converted to mole fractions, by means of the m^{th} value of T_g, enabling the update of the mole fraction vector from y_{in} to y_{out}. At this point, a deeper description of the three sub-blocks in fig.4.6 is needed.

SPECIES BALANCES

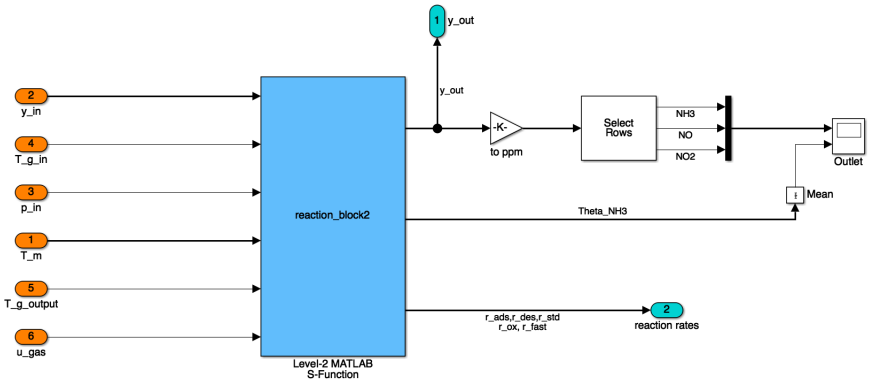

Figure 4.7: Species balance block

The complete species balance equations (appendix C) are rewritten, after having discretized the spatial derivatives and having introduced the proper reaction rates per each species:

$$\begin{aligned}
\epsilon \cdot \frac{\partial C_{NO,i}}{\partial t} &= -u_{gas} \cdot \epsilon \cdot \frac{C_{NO,i} - C_{NO,i-1}}{\Delta x} + (-r_{std,i} - \frac{r_{fast,i}}{2} + r_{ox,i}) \\
\epsilon \cdot \frac{\partial C_{NO_2,i}}{\partial t} &= -u_{gas} \cdot \epsilon \cdot \frac{C_{NO_2,i} - C_{NO_2,i-1}}{\Delta x} + (-\frac{r_{fast,i}}{2}) \\
\epsilon \cdot \frac{\partial C_{NH_3,i}}{\partial t} &= -u_{gas} \cdot \epsilon \cdot \frac{C_{NH_3,i} - C_{NH_3,i-1}}{\Delta x} + (-r_{ads,i} + r_{des,i}) \\
\frac{d\theta_{NH_3,i}}{dt} &= \frac{1}{\Omega}(r_{ads,i} - r_{des,i} - r_{std,i} - r_{ox,i} - r_{fast,i})
\end{aligned} \tag{4.12}$$

The positive reaction rates belongs to the products while the negative ones represent the reactants. The kinetic data used to calculate the reaction rates can be found in the appendix A.1.
At any time t, the boundary conditions are:

$$C_{NO,0} = C_{NO,in} \quad , \quad C_{NO_2,0} = C_{NO_2,in} \quad , \quad C_{NH_3,0} = C_{NH_3,in} \tag{4.13}$$

As described in table 4.1, the reaction rates are calculated, and updated, for each cell, contributing for a more accurate description of the concentrations variation along the catalyst in time. Concentrations are obtained from mole fractions via the following:

$$C_j = y_j \cdot C_{tot} \tag{4.14}$$

where the mixture total concentration in $[\frac{mol}{m^3}]$ is obtained via:

$$C_{tot} = \frac{n}{V} = \frac{p}{\tilde{R} \cdot T} \tag{4.15}$$

While the temperature is calculated for each cell, constant pressure and velocity are assumed through the layer.

GAS TEMPERATURE BALANCE

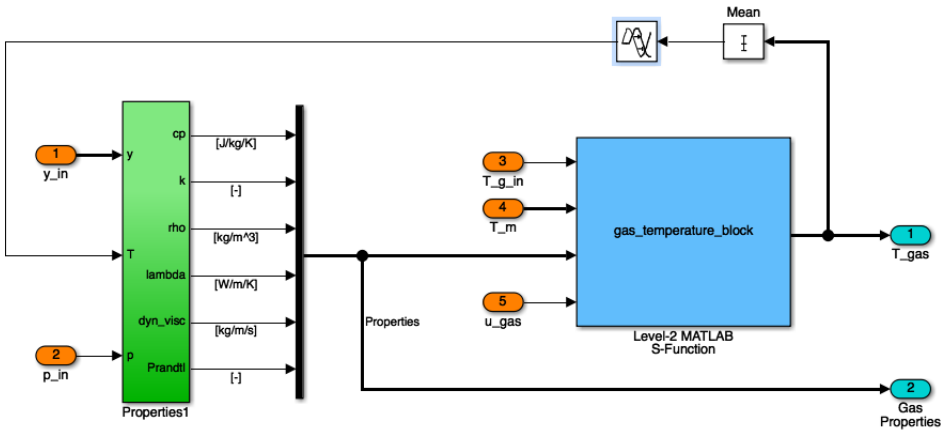

Figure 4.8: Gas temperature balance block

As for the species balances, also the gas temperature balance is discretized along the catalyst length, in order to keep track of the variation in time in each cell:

$$\epsilon \cdot \rho_g \cdot c_{p_g} \cdot \frac{\partial T_{g,i}}{\partial t} = k \left[-u_{gas} \cdot \epsilon \cdot \frac{T_{g,i} - T_{g,i-1}}{\Delta x} - h_{g \to m} \cdot G_a \cdot (T_{g,i} - T_{m,i}) \right] \tag{4.16}$$

The boundary condition at the layer inlet is:

$$T_{g,0} = T_{g,in} \tag{4.17}$$

In the honeycomb, the convective heat transfer between the solid phase and the bulk phase, is ruled by the heat transfer coefficient:

$$h_{g\to m} = \frac{Nu \cdot \lambda}{d_h} \tag{4.18}$$

The Nusselt number in monoliths, according to Jacob et al. (1995), is given by:

$$Nu = Nu_{\infty}(1 + B_1 \cdot Re \cdot Pr \cdot \frac{d_h}{L})^{0.45} \tag{4.19}$$

with:

- Nu_{∞} = 2.976 for square channels
- B_1 = 0.095 for catalytic monoliths
- L = 0.3 (channel length)

The Prandtl number is calculated via:

$$Pr = \frac{c_p \cdot \eta}{\lambda} \tag{4.20}$$

with η being the dynamic viscosity and λ the thermal conductivity. Lastly, the Reynolds number is given by:

$$Re = \frac{\rho \cdot u_{gas} d_h}{\eta} \tag{4.21}$$

The complete description of the fluid properties calculation is given in the appendix B. The inlet composition is fed to the properties block because the reactants' composition is negligible compared to the amount of O_2, N_2, CO_2 and H_2O and, therefore, it is acceptable to use the y_{in} and not a mean value. On the other hand, for the gas temperature, its mean value across the layer's cells is used. This is done in order to simulate a more accurate change in fluid's properties due to a variation in the inlet gas temperature.

MONOLITH TEMPERATURE BALANCE

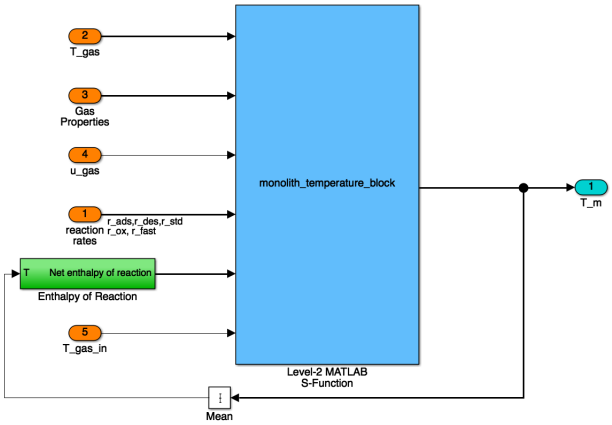

Figure 4.9: Monolith temperature balance block

The monolith temperature balance equation, in its discretized and extended form, is given by:

$$\rho_m \cdot c_{p_m} \cdot \frac{\partial T_{m,i}}{\partial t} = h_{g\to m} \cdot G_a \cdot \frac{(T_{g,i} - T_{m,i})}{1-\epsilon} + \lambda_m \cdot \frac{T_{m,i+1} - 2 \cdot T_{m,i} + T_{m,i-1}}{\Delta x^2} + \\ + \frac{\sum_{k=1}^{n_r} (-\Delta H_{r,k}) \cdot r_k}{1-\epsilon} \tag{4.22}$$

In addition to the convective heat transfer between gas and surface, the monolith temperature depends on: the monolith properties, the conduction in the axial direction and the enthalpy change due to the reactions. In the conduction term, the second partial derivative with respect to the axial direction is discretized using a finite difference method.

The standard enthalpy of formation (ΔH° or h^{ref}) is a measure of the energy released or consumed when one mole of a substance is created under standard pressure and temperature from its pure elements. This term must be included in the monolith balance due to the presence of multiple reactions, either exothermic or endothermic, which might help the monolith to cool down or heat up, especially during transients. The enthalpy change due to a reaction, takes into account the enthalpies of formation of products and reactants and their stoichiometric coefficients. An example of the standard enthalpy change due to the Standard SCR is:

$$\Delta H^\circ_{r,STD} = (\Delta H^\circ_{N2} + \frac{3}{2}\Delta H^\circ_{H_2O}) - (\Delta H^\circ_{NH_3} + \Delta H^\circ_{NO} + \frac{\Delta H^\circ_{O_2}}{4}) \tag{4.23}$$

However, the monolith temperature is far from being at standard temperature since it rapidly heats up to more than 300 C°. For this reason, the standard enthalpy of formation of each species j (table B.1) must be adjusted according to the current surface temperature T_m:

$$\Delta H_j(T_m) = \Delta H^\circ_j + \int_{STP}^{T_m} c_{p_j} dT \tag{4.24}$$

The knowledge of the specific heat at constant pressure comes from the properties block, which is illustrated in appendix B. The described procedure to calculate the enthalpy of formation at the new T_m is included in the "*Enthalpy of Reaction*" sub-block. In the 2 S-Function, the summation of the enthalpy of each reaction, multiplied by the respective rate, gives the net heat generation/destruction for each cell.

If one would avoid the conduction and the reaction enthalpy terms, the monolith temperature would, at most, be equal to the gas temperature. The effect of dynamics are better captured when those terms are included and the monolith temperature might reach values that are higher or lower than the inlet gas temperature, directly influencing the magnitude of the reaction rates. The analysis of the addition of the net enthalpy of reaction is performed in section 5.2.3.

4.4. INTRA-CATALYST LAYER

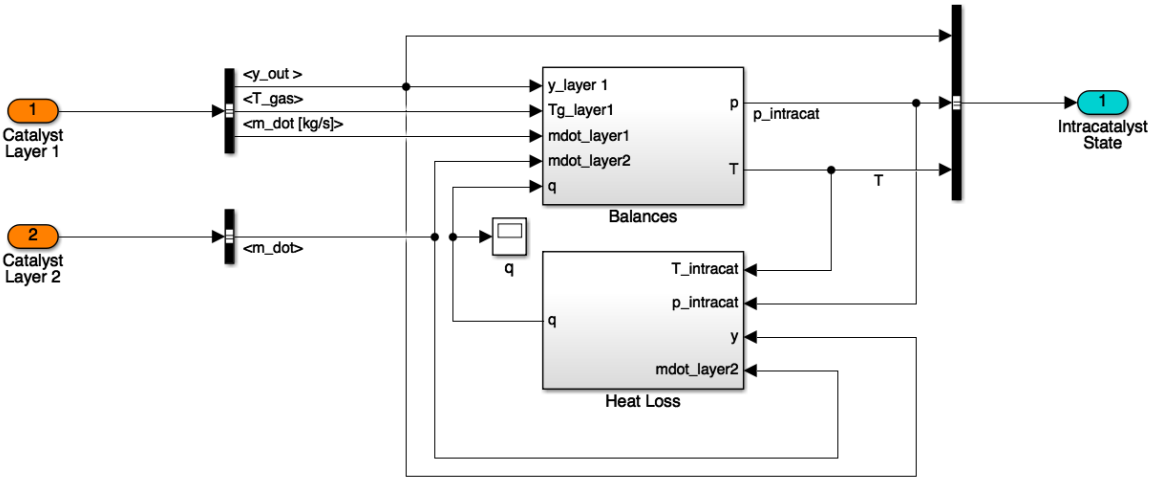

Figure 4.10: Volume element block

The intra-catalyst volume block in fig.4.10 is essentially a link between the upstream and downstream catalyst layers. It is used to calculate the pressure between the two resistances as a function of the instantaneous mass and temperature within the volume. The latter derivation occurs in the "Balances" sub-block whose internal description is given in fig.4.11.

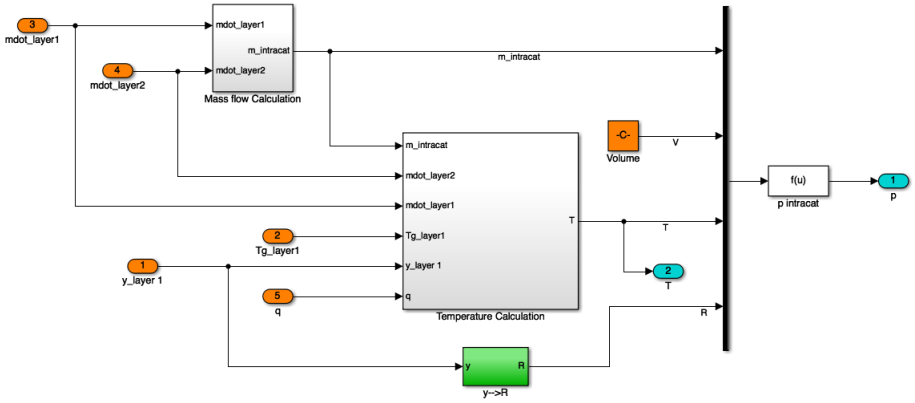

Figure 4.11: "Balances" sub-block

Here, by integrating the net mass flow coming from the two resistances, the instantaneous mass is obtained:

$$\frac{dm}{dt} = \dot{m}_{layer_1} - \dot{m}_{layer_2} = \dot{m}_{net} \tag{4.25}$$

The instantaneous temperature is calculated via the energy balance inside the volume element:

$$m \cdot c_v \cdot \frac{dT}{dt} = [(h_{layer_1} - u) \cdot \dot{m}_{layer_1}] - [(h_{layer_2} - u) \cdot \dot{m}_{layer_2}] + \dot{Q} \tag{4.26}$$

where h_{layer_i} is the enthalpy associated with the mass flow $\dot{m}_{layer_i}$ and u is the instantaneous internal energy of the volume element. While the upstream enthalpy is a function of the 1^{st} layer's temperature, the internal energy and the downstream enthalpy are both functions of the instantaneous volume's temperature. This can be better explained by looking at the "Temperature Calculation" sub-block in fig.4.12.

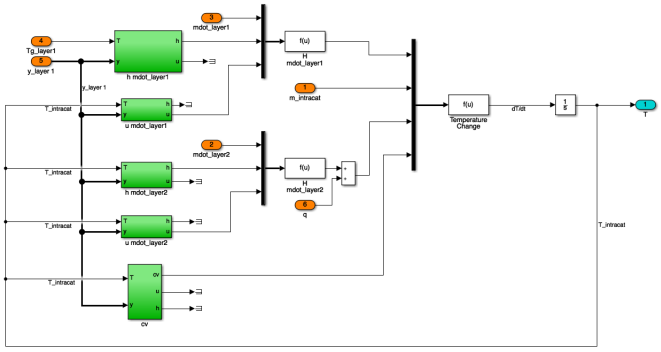

Figure 4.12: Temperature Calculation sub-block

Finally, a heat loss term (in the "Heat Loss" sub-block) is added to simulate the heat exchange between bulk phase and wall:

$$\dot{Q} = h_{g \to w} \cdot A \cdot (T_g - T_w) \tag{4.27}$$

where A is the wetted area and $h_{g\rightarrow w}$ stands for the heat transfer coefficient gas and wall.
Once the temperature and mass are known, the pressure simply comes from the ideal gas law:

$$p = \frac{m \cdot R \cdot T}{V} \tag{4.28}$$

If the entire reactor is considered to be adiabatic, the "Heat Loss" sub-block can be freely neglected.

5

MODEL VERIFICATION

5.1. INTRODUCTION

The designed model needs to be verified and/or validated. According to Glossary (2011), **verification** is defined as the process of determining that a model/simulation implementation accurately represents the developer's conceptual description and specification. Verification also evaluates the extent to which the model/simulation has been developed using sound and established software engineering techniques. On the other hand, **validation** is the process of determining the degree to which a model/simulation is an accurate representation of the real system from the perspective of the intended uses of the model/simulation. To put in simple words (Cook and Skinner, 2005), verification refers to the question *"Have we built the model right?"* while validation addresses the question *"Have we built the right model?"*.
In this thesis, although it would be ideal to perform both analyses, only the verification process is described. The main reasons are:

- The impossibility of performing real experiments on marine SCR systems.
- The lack of published data not only from the marine industry, where the adoption of the SCR is "new", but also from the automotive sector, where all the conducted experiments are connected with too many unknowns such as catalysts formulation, adopted kinetic data and engine maps.

The influence of process parameters such as temperature, feed composition and mass flow has already been mentioned in the previous pages. In this chapter, such effects are qualitatively shown and verified. The performed simulations, are divided into two categories: **static** and **transient**. As the names may suggest, the static analysis deals with the influence of constant input parameters on the system behaviour, while the dynamic analysis addresses the effect of varying input parameters. The combination of the two investigations is important to gain knowledge on how the SCR system works in terms of reduction efficiency and ammonia slip and what is the sensitivity of the input parameters.
To recapitulate, the model verification is structured in the following way:

- **Static response to:**
    1. Inlet gas temperature
    2. Ammonia to NOx ratio (ANR)

3. NOx composition (NO_2/NOx)
4. Heat of reaction
5. Mass flow

- **Transient response to:**
  1. Ammonia step feed
  2. Inlet gas temperature (step up/down)

Geometric parameters such as cell size, wall thickness, catalyst length and catalyst shape do influence the SCR behaviour, but their investigation is not included in this work, since the main aim is not the catalyst geometry optimisation, but the effect of dynamic input parameters.

5.1.1. SCR GEOMETRY

All the simulations have been performed according to the **two layer** model described in the previous chapters. The main physical parameters are given in table 5.1.

SCR Physical Parameters			
Parameter	**Value**	**Parameter**	**Value**
Layer length	0.3 m	Monolith cp	1050 J/kg/K
Layer height	1.2 m	Monolith density	1800 kg/m^3
Layer width	1.2 m	Monolith heat conduction coefficient	1.7 W/m/K
Cell density	100 cpsi	Intra-catalyst length	0.1 m
Wall thickness	0.012 in	Catalyst shape	"Square"

Table 5.1: SCR Physical Parameters

Other monolith features such as geometric surface to volume ratio and void fraction can be determined as described in section 2.2.2.

5.2. STATIC ANALYSIS

By simulating the stand alone model; i.e. the SCR model with arbitrary input variables, one can perform a thorough analysis of their influence on the steady-state behaviour of the SCR system. If not specified, the standard simulation features are $ANR = 1$ and $NO_2/NOx = 7{,}5\%$. This, for 1000 ppm of NOx, results in 925 ppm of NO, 75 ppm of NO_2 and 1000 ppm of NH_3. Furthermore, the effect of the total heat of reaction in each monolith cell is addressed in section 5.2.3 while, in all other analyses, the simple convection case is considered. The axial heat conduction in the solid phase is found to be negligible and its influence is not shown.

5.2.1. INLET GAS TEMPERATURE

The inlet temperature is the most limiting factor in the SCR process. If the light-off temperature is not reached, the catalytic reactions are not initiated and the major risk is to emit the total amount of injected ammonia, in addition to the other natural exhaust gas pollutants. In figure 5.1, the so called SCR characteristic is depicted. It shows the influence of the temperature on the reduction efficiency and the ammonia slip.

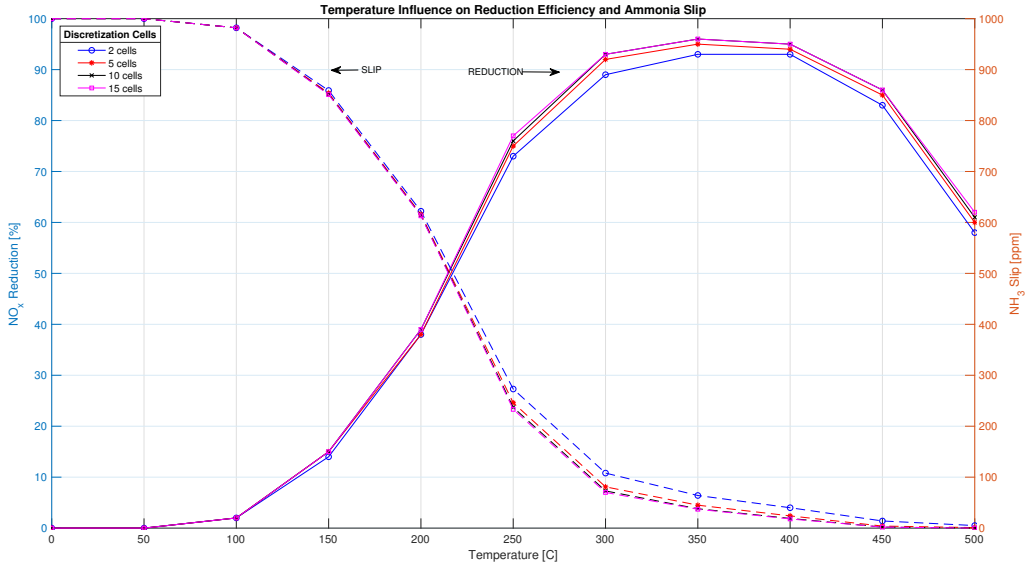

Figure 5.1: SCR static characteristic for different discretization cells ($\dot{m}_{gas}$= 12 kg/s)

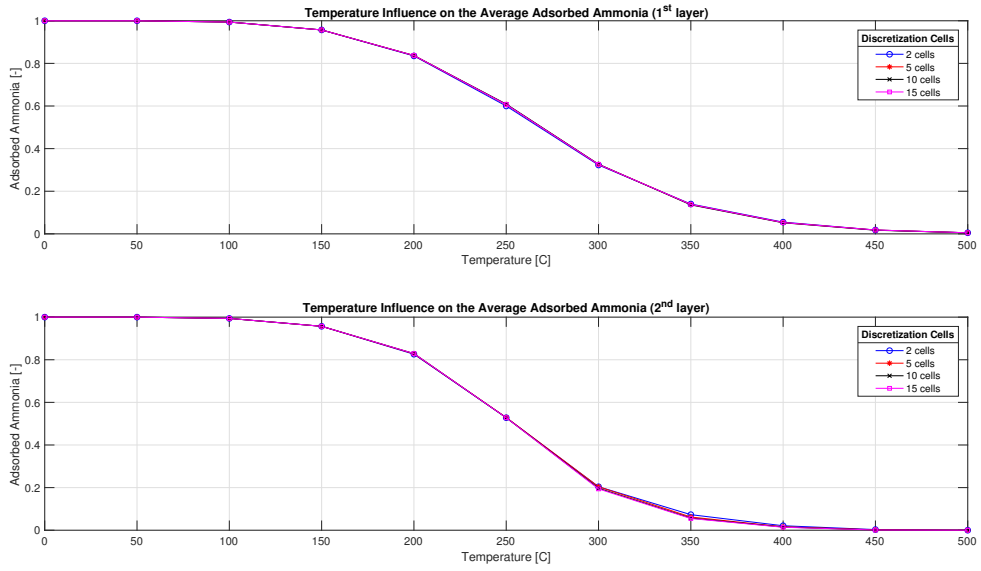

Figure 5.2: Adsorbed ammonia as a function of temperature for different discretization cells

Looking first at the reduction efficiency, it is evident that higher temperatures are beneficial. The maximum efficiency is around 350°C, although this number depends on the catalyst formulation. Below that value, the NOx reduction decreases almost exponentially. On the other hand, above 350°C, it shows a flat behaviour, after which it falls due to the increased action of the NH_3 oxidation reaction at high temperatures. Indeed, ammonia is consumed more in favour of NO formation rather than NO destruction with growing temperature already at 400°C (Ruggeri et al., 2012). This behaviour can also be noticed in the ammonia slip trend. Its minimum is not at 350°C but at 500°C, where the oxidation reaction is stronger than the standard reaction. As the temperature decreases, the slip increases and it reaches the inlet value (1000 ppm) when the

reduction efficiency is 0%. As described in chapter 4, the partial differential equations are discretized into m cells, therefore, also their sensitivity must be investigated. For 2 cells, the simulation is faster but the result might be underestimated, especially in the range of temperatures where the catalyst is more active. For higher cells numbers, the solution for both the reduction efficiency and ammonia slip seems more accurate at the expense of a higher computational time. Generally speaking, above 5 cells, the solutions for different temperatures are not affected by the number of discretizations. For this reason, the following simulations are performed with 10 discretization cells.
Finally, the ammonia adsorption for different temperatures in the two layers, is given in figure 5.2.
The trend is in line with the exothermicity of the NH_3 adsorption, as described in Ruggeri et al. (2012).

5.2.2. ANR

The goal of the SCR system should be the maximization of the NOx reduction and the minimization of the ammonia slip. In this regard, the ammonia to NOx ratio is a significant parameter. Intuitively, when more urea is injected, more ammonia is present in the catalyst and, as a main consequence, a higher NOx reduction is achieved. However, more ammonia at the inlet means also more ammonia slip. For this reason, the results of figure 5.1 can be further extended by looking at the effect that different ANR have on the reduction efficiency and the ammonia slip. In figure 5.3, the result for different ANR and temperature is shown.

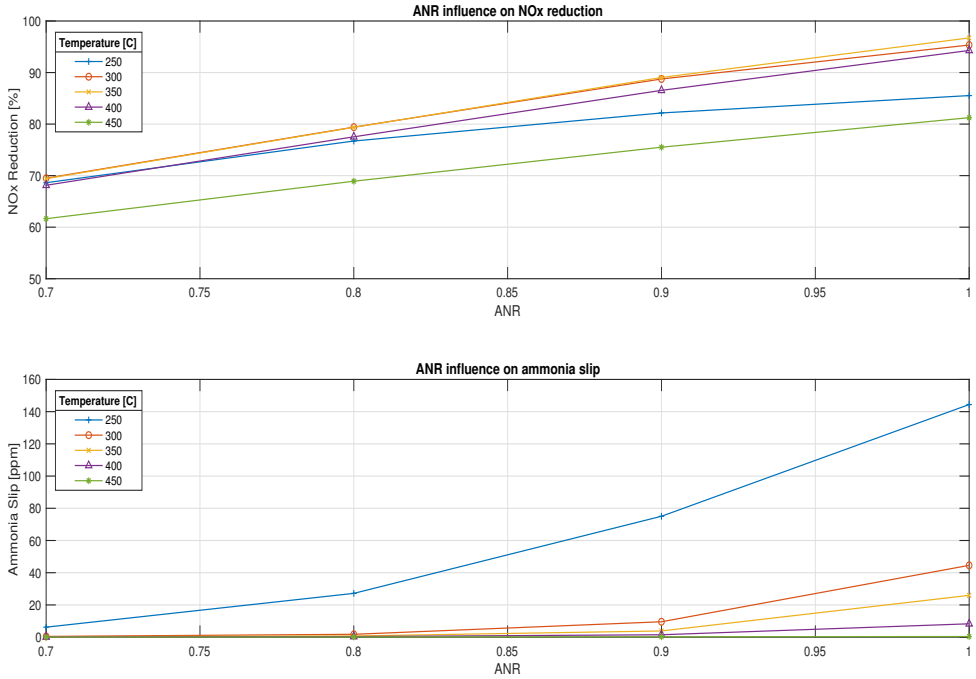

Figure 5.3: ANR influence on the reduction efficiency and ammonia slip ($\dot{m}_{gas}$= 12 kg/s)

When ANR=1, the trend is the same as figure 5.1. Outside the optimal temperature range, ammonia slip is higher for 250°C but the reduction efficiency has the lowest value for 450°C. Again, this is due to the stronger ammonia oxidation reaction, which occur at increasing temperatures. As the ANR is reduced, the slip of ammonia decreases exponentially while the NOx reduction follows a more linear trend, especially between 300°C and 400°C. It is in this range that the standard SCR is the main path and the ratio of conversion 1:1 between ammonia and NO seems to be achieved (ANR=0,7 results in a reduction efficiency of almost 70% and

this trend is confirmed for other ANRs too). This result is quite important when considering a control strategy consisting of a simple feedforward. If the operating conditions are stable and do not diverge from 350°C, one can simply adjust the urea injection by estimating the NOx amount at the engine outlet (see section 6.2).

5.2.3. ENTHALPY OF REACTION

The total enthalpy (or heat) of reaction is the net change in enthalpy due to the reactions occurring in the solid phase. When the net change is negative, the net reaction is exothermic and, thus, heat is released. On the contrary, heat is adsborbed as the net reaction is endothermic. In case of the SCR process the enthalpy of reaction heats up the monolith allowing for a slightly higher gas temperature at the outlet (fig.5.4)

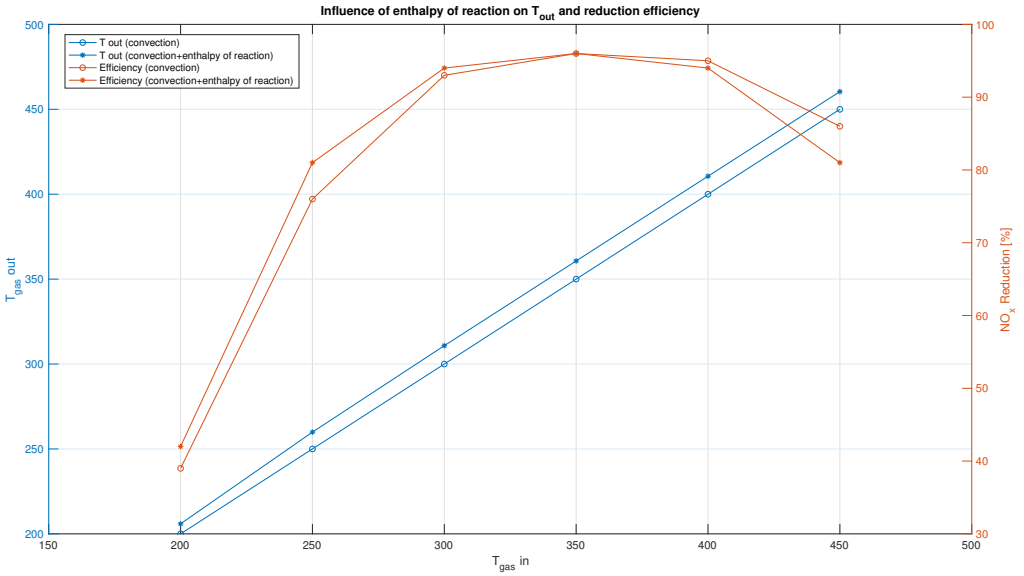

Figure 5.4: Influence of the total enthalpy of reaction

Compared to the simple convective case, where the temperature at the outlet and the inlet is equivalent, the net exothermicity of the reactions heats up the monolith which in turn, via convection, increases the gas temperature. The direct effect of such phenomena is a change in reduction efficiency. In figure 5.4, it can be seen that the major divergence from the convective case is outside the temperature range of 300-400°C. Below 300°C, the higher temperature helps the SCR to achieve higher NOx reduction, while above 400°C the oxidation reaction is enhanced by the increased gas temperature and, therefore, the reduction efficiency is negatively affected.

Overall, it can be concluded that the addition of the net enthalpy of reaction, in the monolith temperature balance (section 4.3.2), does influence the SCR behaviour when it operates outside its optimal temperature range. This difference does not depend on the discretization cells but only on the adopted kinetic data and the amount of key reactants. Furthermore, it is important to state that the magnitude of the heating phenomenon varies with the selected kinetic and monolith data.

5.2.4. NO_2/NOx

In section 2.2.1, it was mentioned the possible adoption of a DOC to increase the NO_2/NOx ratio to approximately 50%, in order to boost the reaction mechanisms via a stronger fast SCR. In figure 5.5, the static effect of different NO_2/NOx on the reduction efficiency is addressed.

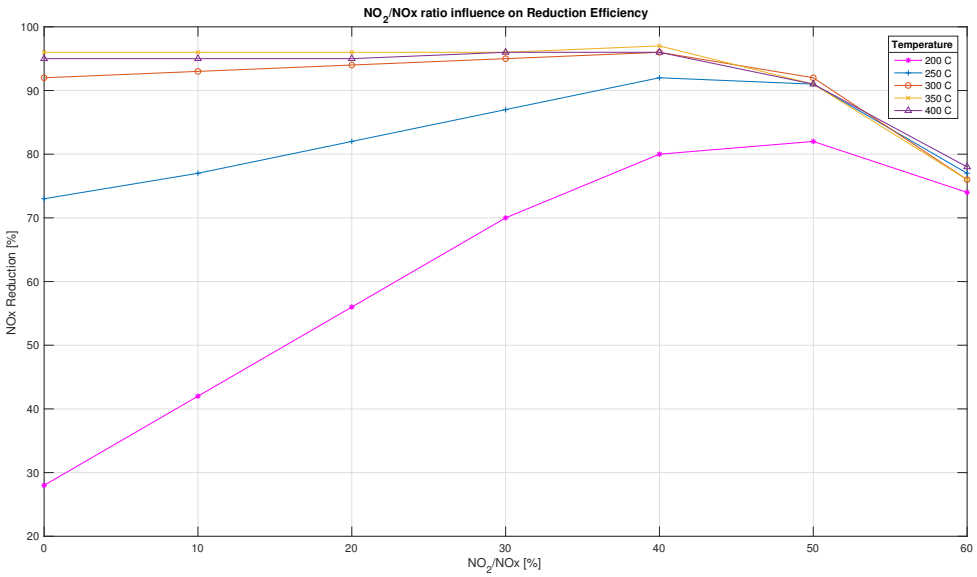

Figure 5.5: NO_2 influence on the NOx reduction ($\dot{m}_{gas}$= 12 kg/s)

The optimal operating range of the SCR (300-400°C) seems not affected by the change in the NOx balance. A slightly higher maximum of reduction efficiency is observable for NO_2/NOx=40%. After such value, the NOx reduction falls mainly due to an over-presence of NO_2. The trend is far more pronounced for the lower temperature region (200-300°C). Furthermore, the maximum reduction can achieve an astonishing peak of more than 80% for 200°C and 50% of NO_2. These trends confirm what found in the examined literature.
In figure 5.6, the investigation conducted by Magnusson et al. (2016) on the influence of varying NO_2/NOx ratios on the catalytic activity for lean NOx reduction with ammonia shows that, for low temperatures (250°C), the NOx reduction and ammonia conversion reach a peak of more than 80%. This confirms what predicted by the model in figure 5.5. In addition, it is possible to recognize the negative effect that the Slow SCR has on the NOx reduction when the NO_2/NOx ratio is closer to 1. The formation of N_2O, although relevant, is not treated in this thesis.
Magnusson et al. (2016) suggest that an improved low-temperature activity for the marine SCR system can be achieved by increasing the NO_2/NOx ratio to 50%, whereby utilizing the fast SCR reaction scheme. However, in order to withstand such low temperatures; i.e. to avoid catalytic deactivation, marine fuels with a maximum 0.10 wt% sulphur should be used in emission control areas. This combination seems reasonable once the new sulphur cap regulation will have entered into force.

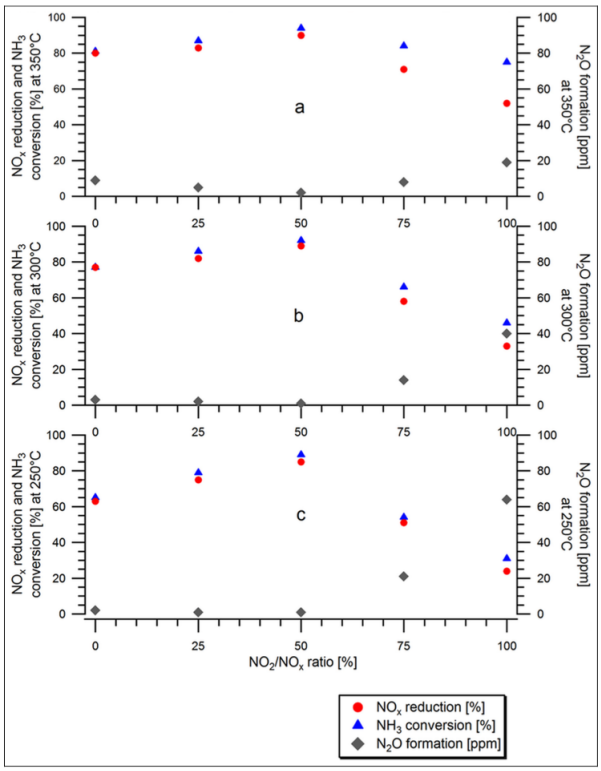

Figure 5.6: Influence of the NO_2/NOx ratio on the NOx reduction performance. Feed gas composition: 500 ppm NO, 500 ppm NO_2, 500 ppm NH_3 and 8% O_2 (SV 12200 h^{-1}). Steady-state measurement for 20 min for each NO_2/NOx ratio and temperature: (a) 350°C, (b) 300°C and (c) 250°C. (Magnusson et al., 2016)]

To complete the analysis, the slip of NO_2 and NH_3 for different temperatures and NO_2 are plotted in figure 5.7.

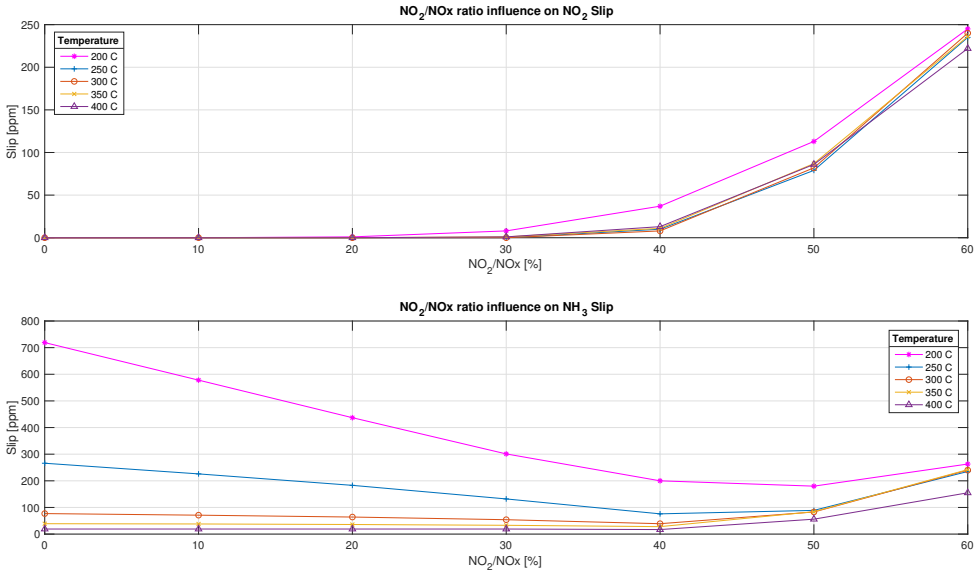

Figure 5.7: NH_3 and NO_2 slip for different NO_2/NOx ($\dot{m}_{gas}$= 12 kg/s)

It is worth noting that the minimum ammonia slip, for low temperature operations, can be obtained with

an equal amount of NO and NO_2. Although, this feed composition enables high reduction efficiency for the temperature window of 200-300°C, the adoption of an ammonia slip catalyst is an imperative due to the slip of more than 100 ppm. Again, this integration seems possible if ultra low sulphur fuels are used.

5.2.5. MASS FLOW

For sake of consistency, it must be mentioned that the SCR characteristics (fig.5.1-5.3) varies with the residence time within the reactor and, consequently, with the mass flow: a high space velocity means that the residence time in the SCR catalyst is shorter and the possible NOx conversion for the system is decreased. These considerations are summarized in figure 5.8.

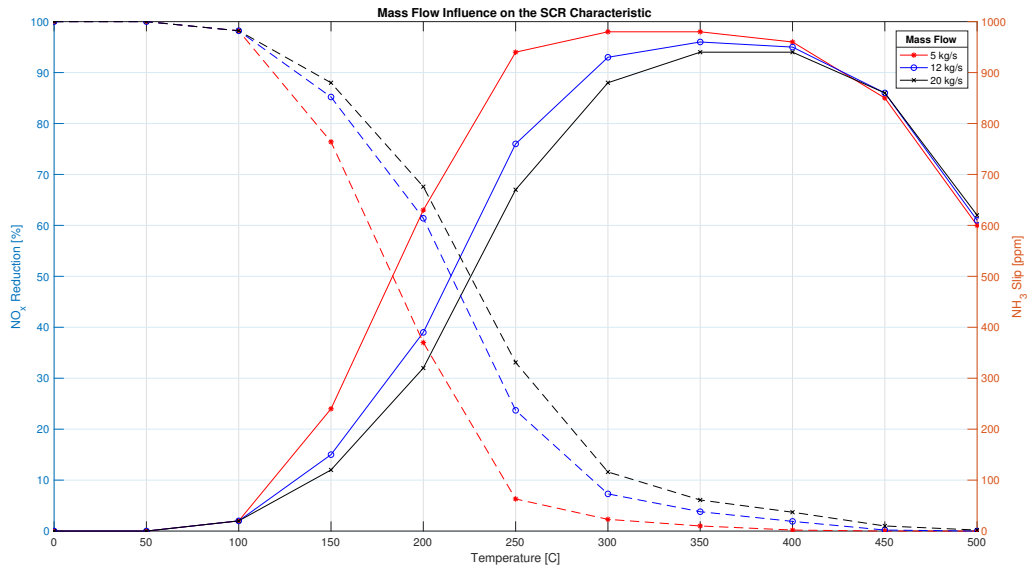

Figure 5.8: Mass flow influence on the SCR characteristic

It is clear that, especially in the low temperature region, smaller flows are beneficial for the reduction efficiency and, consequently, for the ammonia slip. For increasing temperatures, the influence of different mass flow values is reduced. The divergence between high and low temperatures is the result of the assumption made on the modelled reactions. While above 400°C, the oxidation competes with the standard SCR, at low temperatures, the standard and fast SCR are the only active reactions. For this reason, a smaller flow in the latter case brings much more benefits than in the former case where, a bigger flow may limit the influence of the oxidation.
Overall, a smaller flow is not always the best design solution, because there are reactions, not modelled in this thesis, which negatively affect the SCR behaviour also at low temperatures (see chapter 2). These might be limited by reducing the residence time within the reactor.

5.3. DYNAMIC ANALYSIS

The first principle modelling approach is selected because of the special attention to dynamic and transient loads. The response of the SCR system to dynamic loading is investigated in the following sections. Again, the standard simulations feature:

- ANR = 1

- NOx_{IN} = 1000 ppm
- NO_2/NOx = 7,5%
- m = 10 cells
- Only convection in the monolith temperature balance

5.3.1. STEP FEED OF AMMONIA

In figure 5.9, the typical effect of a step feed (at 3000s) and a shut-off (at 7000s) of ammonia is investigated.

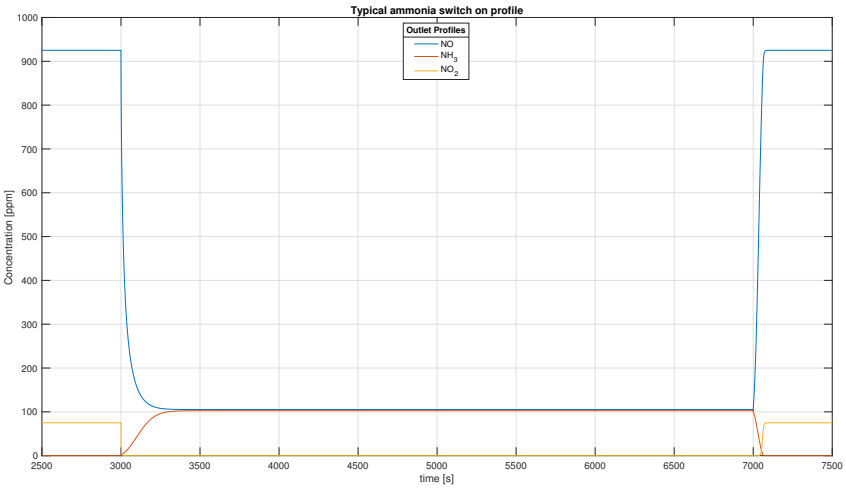

Figure 5.9: Ammonia addition (3000s) and shut-off (7000s) for 350°C and $\dot{m}_{gas}$= 12 kg/s

Upon ammonia step addition (fig.5.10a), the NO quickly decreases to its steady-state value due to the occurrence of the main reaction (standard SCR). On the other hand, the ammonia outlet concentration takes a little time to increase till the steady-state because of the adsorption/desorption process taking place in the two catalyst layers. Finally, the NO_2 concentration goes to zero almost instantaneously because of the fast SCR. When ammonia feed is shut off (fig.5.10b), the inverse process occurs: ammonia rapidly goes to zero while the NO concentration takes some time to reach the inlet value due to the residual presence of adsorbed ammonia in the catalyst.

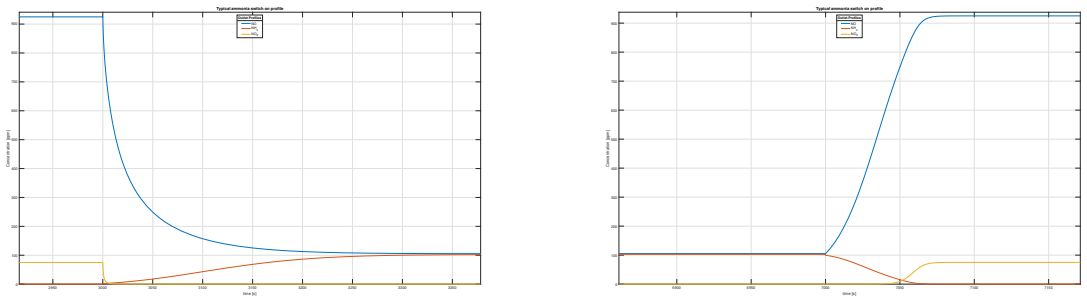

(a) Ammonia addition

(b) Ammonia shut-off

Figure 5.10: Details of ammonia step variation in fig.5.9

The dynamics, especially in case of the ammonia shut-off, are quite faster than Ciardelli et al. (2004); Lietti et al. (1998, 2000). This can be explained by multiple reasons: the adopted kinetic data are different, the effect of a critical NH_3 coverage above which the standard SCR becomes independent of the stored ammonia (see eq. 2.33-2.34) is not included in this thesis and that most of the performed analyses were conducted at lower temperatures.
Despite those discrepancies, an important result of Ciardelli et al. (2004); Lietti et al. (1998, 2000) is that, on increasing the reaction temperature:

- The steady-state NOx conversion is increased.
- The NH_3, NO and NO_2 steady-state concentration levels are more rapidly reached.
- The "dead time" in the variation of the NO concentration that is observed upon the ammonia shut-off is reduced.

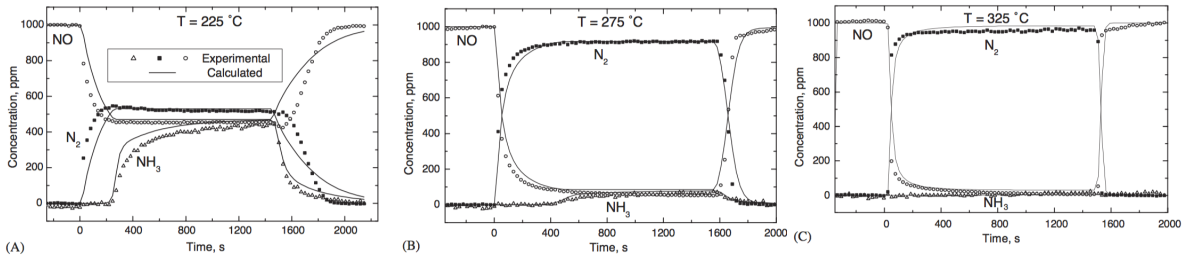

(a) T=225°C (b) T=275°C (c) T=325°C

Figure 5.11: NO + NH_3 TRM runs at different temperatures. Symbols: outlet concentration of ammonia (triangles), NO (circles) and N_2 (squares); solid lines: kinetic fit (Ciardelli et al., 2004).

Such temperature effects are in line with both the exothermicity of the NH3 adsorption and with the increased rate of reaction, which result in lower ammonia surface coverage (see fig.5.2). Accordingly, the rate of NO consumption becomes dependent on the ammonia surface concentration, so that the evolution of NO closely follows that of NH_3. Those results hold also for the model developed in this work (fig.5.12)

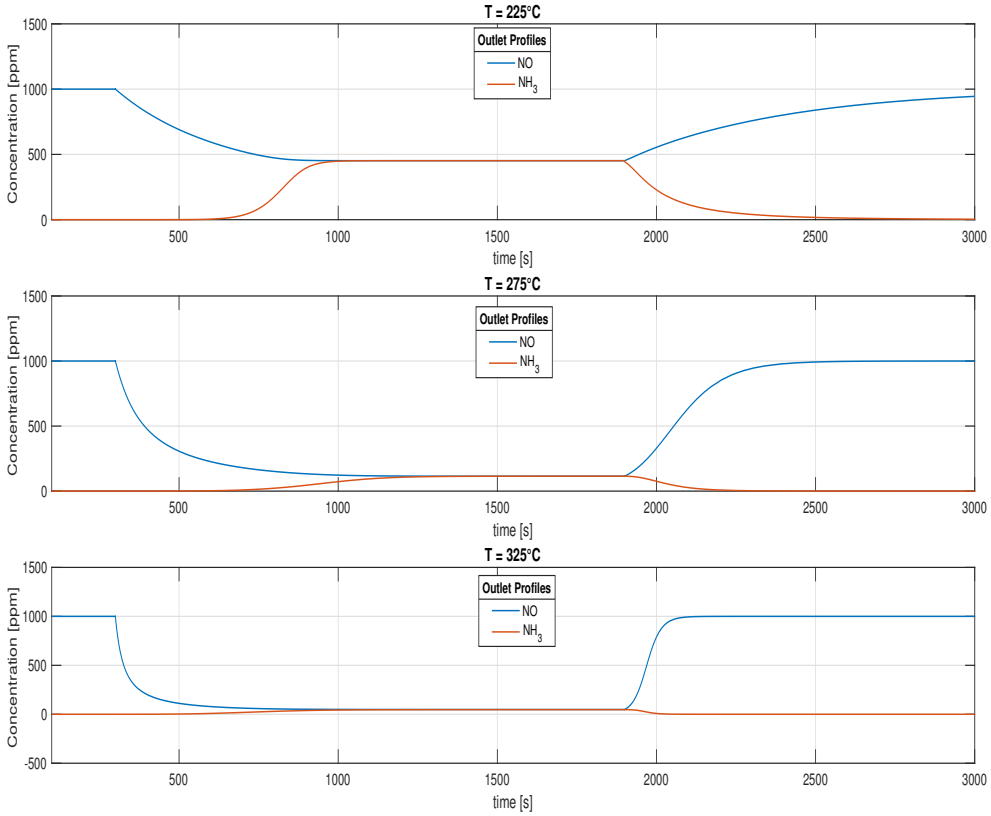

Figure 5.12: Step feed of ammonia for 225°C, 275°C and 325°C (NO = 1000ppm, NH_3 = 1000ppm)

5.3.2. TEMPERATURE STEPS

Sudden change in the inlet temperature might not only affect the NOx generation inside the cylinder, but also the amount of stored ammonia in the catalyst. As a main consequence, ammonia can be released in the gas phase or further trapped in the catalyst layers. In this section, the effect of step changes of the inlet temperature are investigated. For sake of simplicity, only the NO and NH_3 results are discussed, since the NO_2 is not appreciably affected by rapid temperature variations.

Temperature Step Up 330°C ⟶ 370°C

The result of a temperature step increase is plotted in figure 5.13.

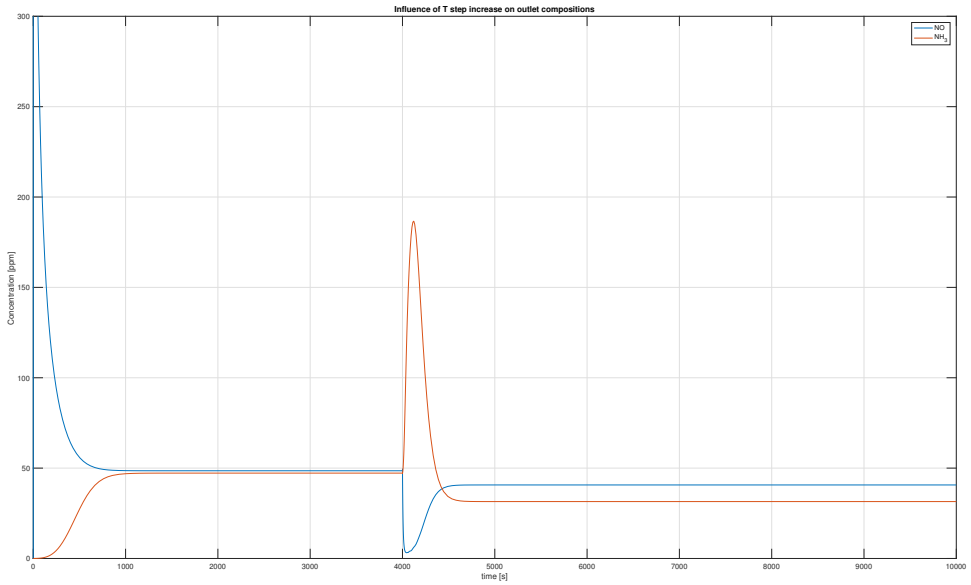

Figure 5.13: Influence of temperature transient (4000s) on NH_3 and NO profiles

The ammonia slip experiences a sudden peak, which is the result of to the reduction of the overall adsorbed ammonia (see section 5.2). After such peak, the slip decreases due to the higher activity of the standard SCR and the oxidation reactions. The higher reduction activity is beneficial for the NO profile too, which after a rapid drop, stabilizes around lower overall values. This trend, however, depends also on the temperature range at which the step variation occur; above 400°C indeed, the oxidation reaction is much stronger and the NO slip will overall rise. Moreover, the sharp peak is, to a much lesser extent, caused by the way the output signals are computed. In section 4.3.1, indeed, it was explained that the total concentration at the outlet, which is a function of the outlet temperature, is used to update the NO and NH_3 signals. When inlet temperature steps occur, the outlet temperature does not reach immediately the inlet value due to the reactor thermal inertia causing, thus, an amplification of the phenomena.
Figure 5.13 only looks at what comes out of the catalyst. To get a better picture of the process inside the layers, the NO, NH_3 and θ_{NH_3} profiles at different catalyst length are plotted against time.
Before 4000s, the steady-state for 330°C is reached. Values of NO, NH_3 and θ_{NH_3} near the entrance are obviously greater than those next to the catalyst end. The temperature transient occurs at 4000s. Shorter distances show quick spikes in the ammonia concentration, mainly due to a higher desorption process; ammonia adsorption, indeed, decreases as temperature increases. When approaching the layer outlet, the effect of the released ammonia is combined with the propagated ammonia from the prior catalyst segments. This result in longer transient as we move towards the catalyst exit. The ammonia trend is connected with the adsorbed NH_3 along the catalyst. When the temperature increases, θ_{NH_3} immediately reduces at the catalyst entrance (fig.5.14). Along the two layers, the trend changes because the ammonia released at the entrance passes through the catalyst, causing first an increase in the adsorbed ammonia and, secondly, a slowly reduction at lower values. The NO, in the end, experiences a fast drop caused by the simultaneous higher activity of the standard SCR (as soon as the temperature changes) and the previous higher values of adsorbed ammonia. In this regard, is important to recall the dependence of the standard SCR on both the temperature and the θ_{NH_3}.
After the quick depression, the NO reaches the new steady-state value as a result of the new temperature and adsorbed ammonia.

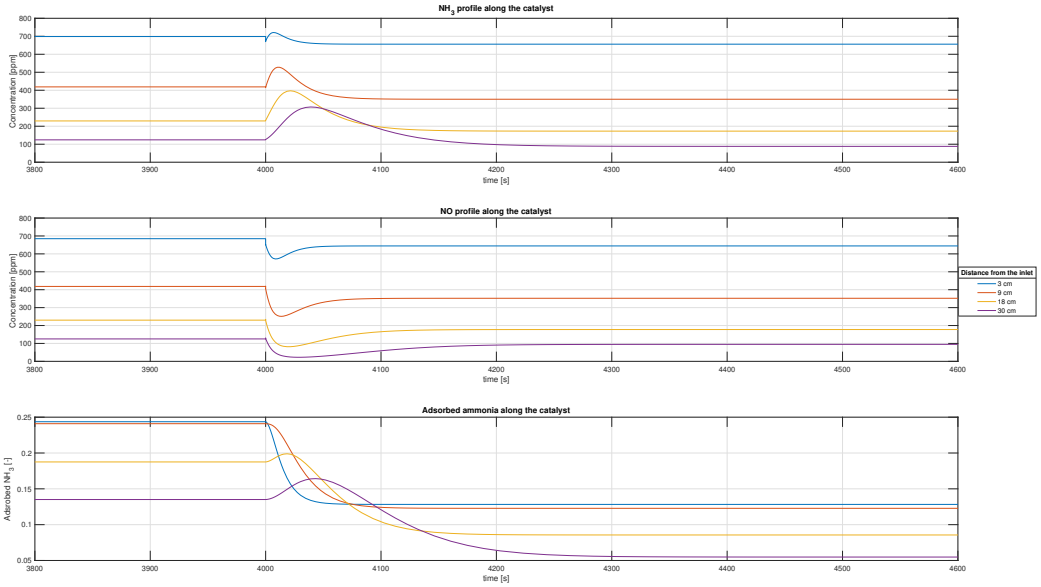

Figure 5.14: 1^{st} Layer (positive temperature transient)

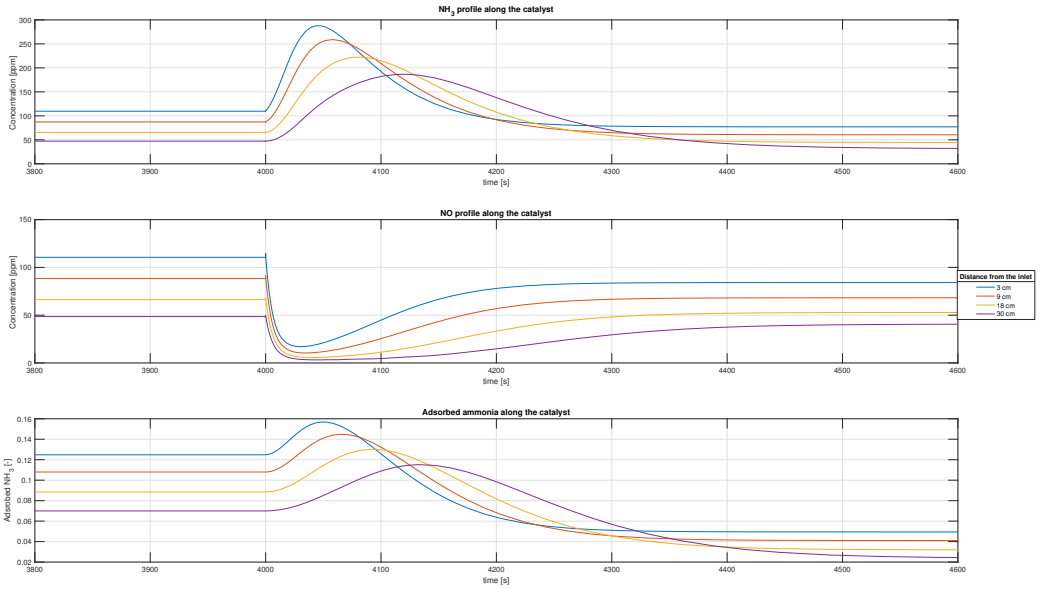

Figure 5.15: 2^{nd} Layer (positive temperature transient)

Temperature Step Down 370°C ⟶ 330°C

When the temperature is instantaneously reduced, the effects on the key reactants are found to be the opposite of a step increase. The result is shown in figure 5.16.

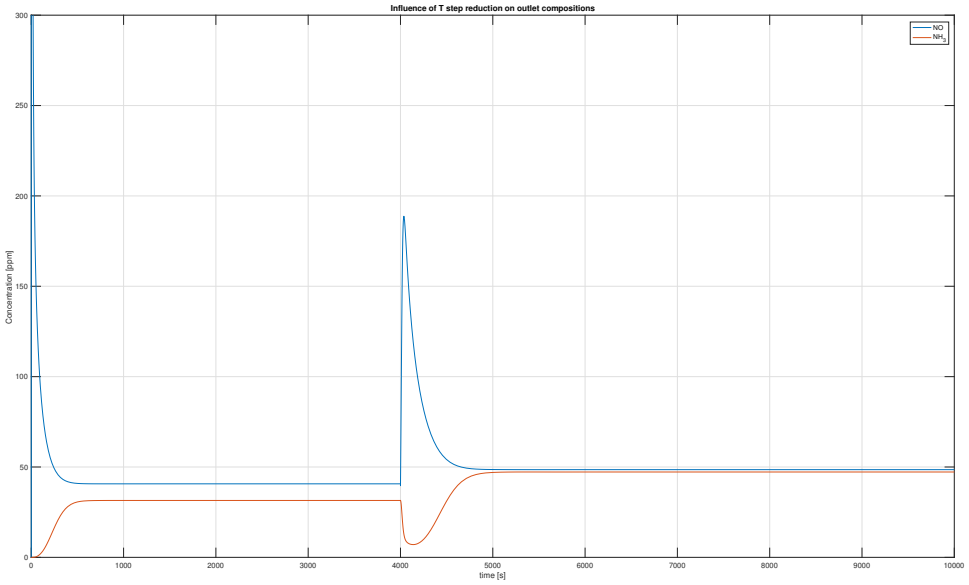

Figure 5.16: Influence of negative temperature transient (4000s) on NH_3 and NO profiles

As the temperature decreases, the adsorption process becomes more active and, as a main result, NH_3 shows an initial depression followed by the stabilization at higher values, due to the reduced activity of the standard SCR. The latter, is also the main cause of the NO sudden peak after which the new steady-state is reached. Again, to get a better understanding of the whole process, the profiles at different catalyst length are given in figure 5.17 and 5.18.

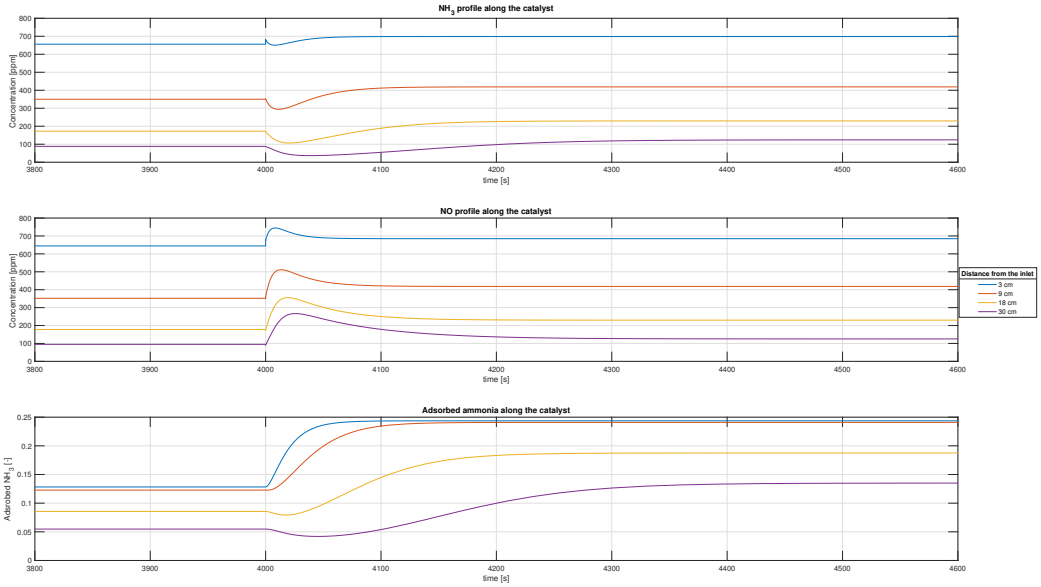

Figure 5.17: 1^{st} Layer (negative temperature transient)

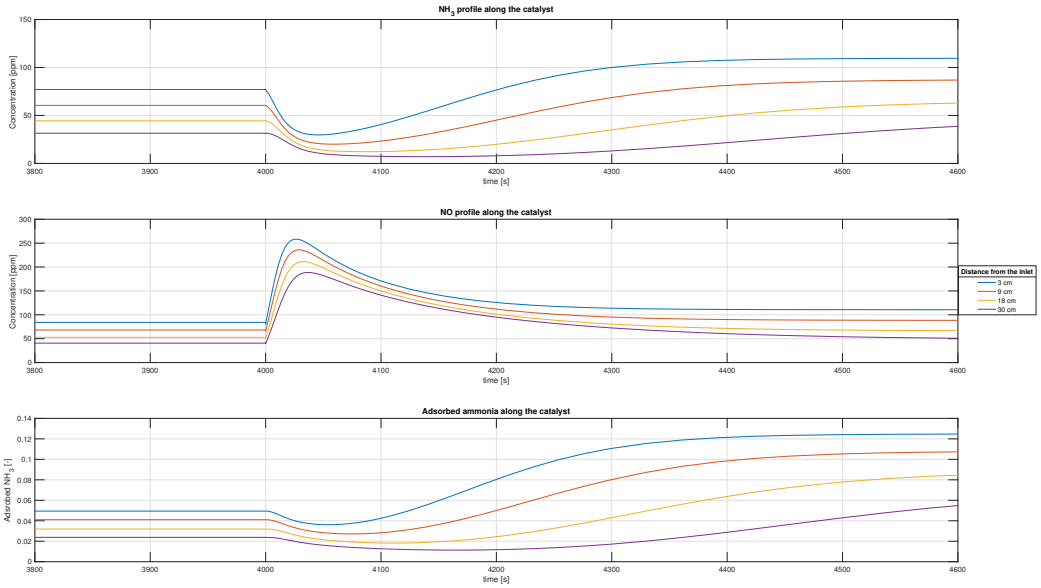

Figure 5.18: 2^{nd} Layer (negative temperature transient)

5.4. SUMMARY

The verification has been performed in order to gain confidence and knowledge in the designed model. The static and dynamic simulations confirmed, under the assumptions made, what found in the literature:

- The maximum reduction efficiency is around 350°C. Below that value, the NOx reduction decreases almost exponentially. On the other hand, above 350°C, it shows a flat behaviour, after which it falls

since ammonia is consumed more in favour of NO formation (ammonia oxidation) rather than NOx cut with growing temperature already at 400°C (Ruggeri et al., 2012).

- In the optimal temperature range (300-400°C) there is a quasi linear relation between ANR and NOx reduction. This behaviour is an indication of the strong influence of the Standard reaction which is always considered as the main reaction path in the SCR process (Yun and Kim, 2013)
- The net change in enthalpy due to the reactions occurring on the surface is negative. Heat is therefore released in the solid phase, allowing for a slightly higher outlet gas temperature (Nova and Tronconi, 2014)
- Below 300°C the Fast reaction becomes the main path once the ratio of NO_2/NOx ratio is set close to 50%. This trend is in line with the stoichiometry of the Fast reaction (Güthenke et al., 2007; Magnusson et al., 2016)
- Lower mass flows allow for higher reduction potentials (Depcik and Assanis, 2005; Yun and Kim, 2013). The direct advantage is a reduction of the reactor volume. A drawback might be the enhanced formation of byproducts when the SCR is operated outside the optimal temperature range
- On increasing the reaction temperature, the steady-state concentrations of outlet NH_3 and NO are lowered and more rapidly reached. Such aspects are in line with the increase in the SCR activity with temperature and the concurrent depletion of adsorbed NH_3 (Lietti et al., 1998).
- A step variation in temperature causes overshoots in the ammonia signal, when the temperature is increased, and in the NOx signal, when the temperature is decreased(Schmitt, 2010). These phenomena are connected with the great temperature dependence of both the desorption process and the standard reaction

6

CONTROL STRATEGY & INTEGRATION WITH DIESEL MODEL

6.1. INTRODUCTION

In the previous sections, the SCR model has been developed and verified. The remaining subgoal (see section 1.3) is the investigation of the integrated system *"SCR+ENGINE"*. Before the simulations, the following tasks are performed:

- Building a suitable control strategy for the urea injection
- Integration with an existing diesel engine model

Both tasks are described in the following sections. The control strategy is treated first, as it is directly connected to the SCR model. The different strategies are introduced and the selection of the most convenient, based on the system requirements, is addressed. The engine integration, on the other hand, is divided into two parts: the selection of the engine model and the integration process.

6.2. CONTROL STRATEGY

Two of the most important evaluating criteria for the SCR process are the **NOx reduction** and the **ammonia slip**. The main goal of the controller is to keep the NOx concentration at the output of the SCR as low as possible and, at the same time, to limit the emission of ammonia. Naturally, the set point for the desired outlet NOx represents a trade-off between the NOx legislation and the maximum permissible ammonia slip. If the catalyst is optimized for constant loads, which feature small fluctuations in exhaust temperature, mass flow and NOx amount, one can simply adopt a feedforward controller. The principle of the open loop control strategy is based on the calculation of the required amount of urea as a fraction of the estimated (engine map) or measured NOx content in the exhaust gas. As shown in section 5.2.2, the Standard SCR (eq. 2.8), which assumes that 1 mole of NOx reacts exactly with one mole of ammonia, plays the largest role in the NOx reduction process. This, in combination with the knowledge of the SCR characteristics as a function of temperature and ANR (fig. 5.3), allows for an easy estimation of the desired ammonia that must be injected to obtain the reference NOx reduction (Ref_{NO_x}):

$$NH_{3_{in}} = Ref_{NO_x} \cdot NOx_{in} \tag{6.1}$$

where $NH_{3_{in}}$ and NOx_{in} are the values in ppm and Ref_{NO_x} is the percentage of reference reduction. In simple words, if an optimal temperature range and perfect mixing conditions are considered, when the ANR is set to 0.8, it will lead to an overall conversion of approximately 80%.
Despite the evident benefits of this strategy, such as the system simplicity and the absence of a NOx sensor, the controller cannot effectively compensate for steady-state errors and highly varying loads. For this reason, a feedback loop, which brings information of the outlet NOx and ammonia slip, is added to provide a corrective action to the feedforward branch and to complete the control strategy. The NOx at the outlet is therefore looped back and subtracted to the reference NOx out, in order to estimate the error ($e(t)$) as follows:

$$e(t) = NOx_{out} - NOx_{out_{ref}} = NOx_{out} - (NO_{x_{in}} \cdot Ref_{NO_x}) \tag{6.2}$$

The error, is then fed to a PID controller, which estimates the corrective action that needs to be added to the feedforward ammonia prediction, to meet the reference reduction (fig.6.1).

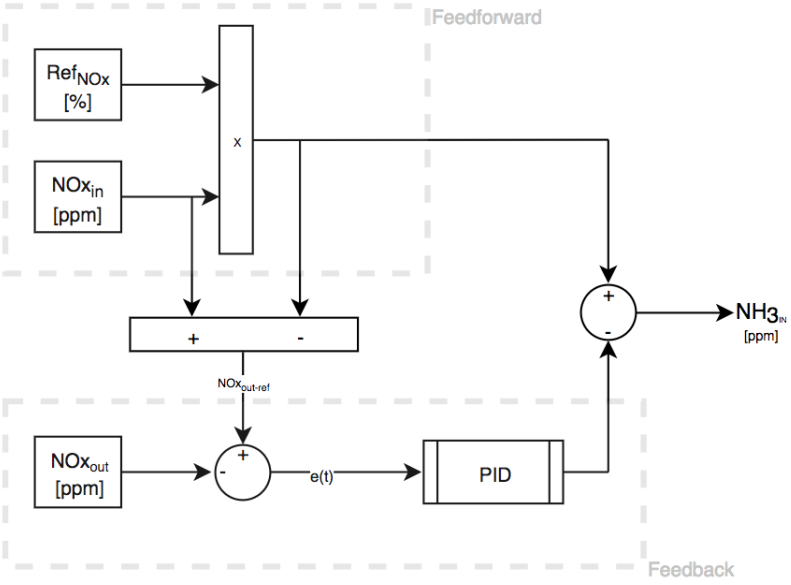

Figure 6.1: Control strategy for the required ammonia

Finally, the resulting urea consumption is obtained from the decomposition of the urea solution to ammonia, described in section 2.3.1, and the knowledge of the exhaust mass flow.
The performance of the described control strategy ensures fast responses to changes in the process parameters and a minimum low steady-state error. Main drawbacks of such solution, when compared with real time devices, are the measurement of the exhaust flow and the NOx concentration. The latter, in particular, can also lead to inaccurate readings from the NOx sensor due to the cross sensitivity to ammonia in case of slip. For these reasons, more accurate control strategies, such as *model based predictive control* (MPC) and *adaptive control*, based on the control of the ammonia storage (θ_{NH_3}) level, are widely adopted in the automotive sector and are, therefore, highly recommended for future studies on improved control strategies (Brandenberger et al., 2008; Dolanc et al., 2001).

6.3. DIESEL MODEL INTEGRATION

The purposes behind the integration of the SCR with an existing diesel engine model are twofold: firstly, to investigate how the diesel engine responds to an additional system downstream which increases the flow

resistance (additional back pressure) and secondly, to simulate "real" load cases that feature their own time constants and are utterly different from the load conditions generated by look-up tables (chapter 5).

6.3.1. SELECTION

The engine models investigated in this thesis belong to the category of the high order Mean Value First Principle (MVFP) models, developed in TUDelft. These, are further subdivided into the so called *Diesel B* and *Diesel A* models, which differ both in complexity and application. While the *B* version requires detailed data of the turbocharger groups (compressor and turbine maps), the *A* model does not use any operating map, but adopts a simplified equation for the charge pressure through (the *Büchi* equation) instead. Furthermore, the *B*'s higher complexity is due to additional components such as the air filter, the air cooler, the inlet/outlet receiver, the silencer and so on, which are interconnected through the resistance and volume elements strategy described in section 4.2.
The most important requirements that the engine model must fulfil, when integrated with the SCR, are:

- Accurate estimation of the temperature T_e after the turbine, which corresponds to the SCR inlet temperature, for a given matched engine.
- Relatively short computation time.

When the SCR block, which behaves as a resistance element, is added to the more complex *Diesel B* model, the result is an unusual slow simulation which does not allow for any prediction of the SCR behaviour under transients. This high running time is probably due to the presence of multiple *Level 2 S-Function* in combination with an already heavy model. For this reason, the choice has fallen upon the *Diesel A*, which couples a very short computation time with a fairly accurate estimation of the turbine outlet temperature. Indeed, the adopted *A* model (Geertsma et al., 2017), is the one featuring the most accurate turbocharger exit temperature, which is within 5% of actual measurements during Factory Acceptance Tests (FAT), except for the lower loads region (around 25% load), where a bigger discrepancy occurs.

6.3.2. INTEGRATION

The complete Simulink® view of the integrated system is given in fig.6.2.

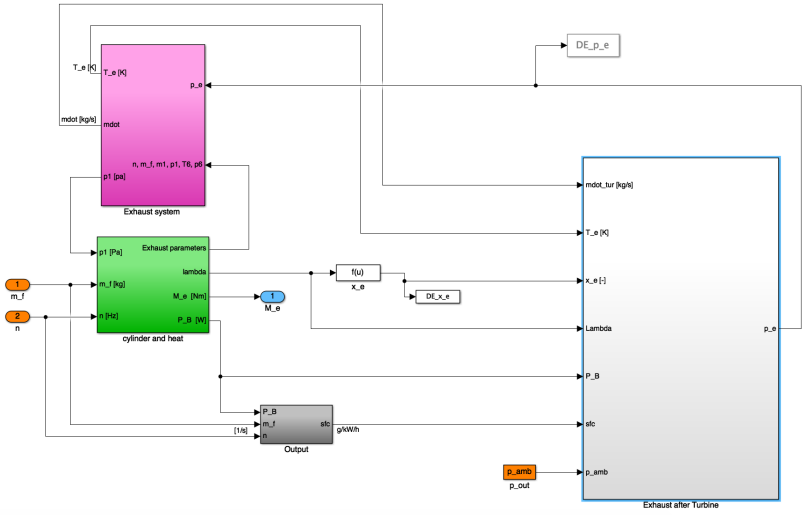

Figure 6.2: Integration with the engine model

The engine blocks (green and magenta) are connected to the SCR block via a volume element, which has been developed in order to estimate the pressure (p_e), at the turbine outlet, as a function of the mass flow upstream and downstream. The grey subsystem ("Exhaust after turbine"), consisting of the SCR, the silencer and the connecting pipes is depicted in figure 6.3.

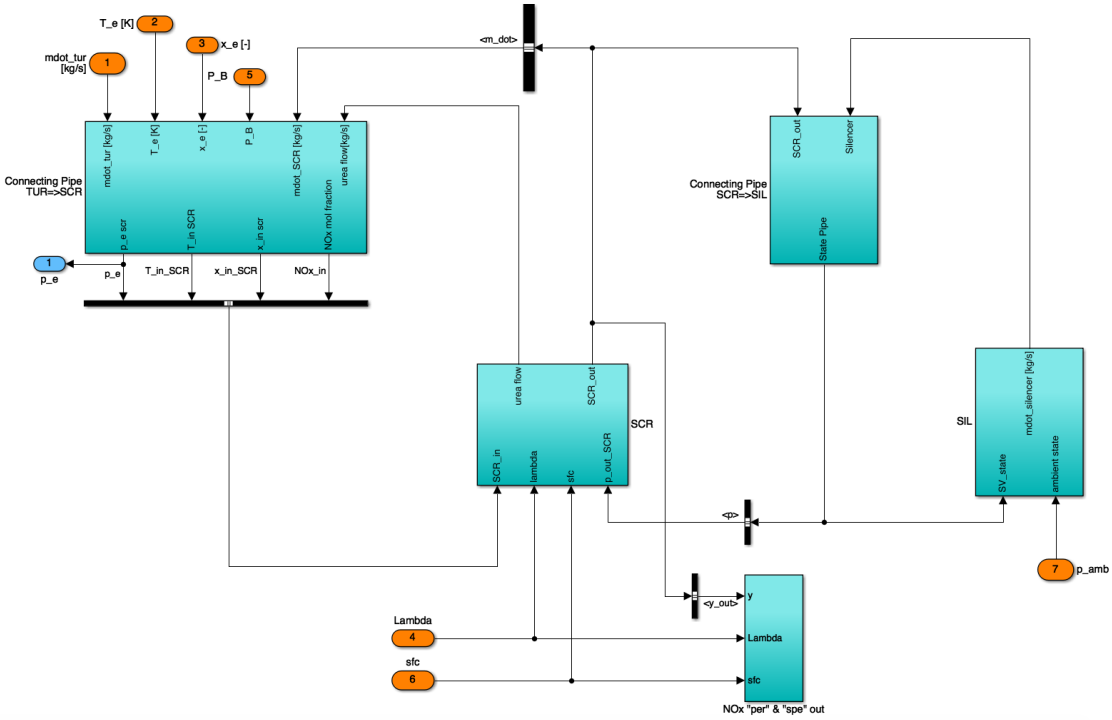

Figure 6.3: "Exhaust after turbine" sub-block

This modification is necessary due to the assumption of constant ambient pressure after the turbocharger of the basic model (Geertsma et al., 2017). By adding a series of two volumes (the connecting pipes) and two resistances (the SCR and the silencer), it is possible to simulate the added flow resistance due to the SCR addition. Furthermore, the pressure drop caused by the reactor, can be investigated thanks to the inclusion of the silencer block, which is connected to the ambient through the pressure p_{amb}.
In order to get the composition vector y, the first step is to calculate the air mass fraction (x_{air}) of the exhaust flow, as a function of the actual air excess ratio (λ) and the stoichiometric air/fuel ratio (σ):

$$x_{air} = \frac{(\lambda - 1) \cdot \sigma}{\lambda \cdot \sigma + 1} \tag{6.3}$$

The stoichiometric gas fraction is simply given by:

$$x_{sg} = 1 - x_{air} \tag{6.4}$$

The mass fraction of each component j in the stoichiometric gas ($x_{j_{sg}}$) is a function of the adopted fuel Stapersma (2010*b*). Once the $x_{j_{sg}}$ are calculated, the total mass fraction of component j is obtained via:

$$x_j = x_{sg} \cdot x_{j_{sg}} + x_{air} \cdot x_{j_{air}} \tag{6.5}$$

With this approach, one can derive the composition vector on a mass fraction basis. The conversion to a mole fraction basis (y_j) is achieved as follows:

$$y_j = \frac{x_j \cdot M_{gas}}{M_j} \tag{6.6}$$

with the gas molar weight equal to:

$$M_{gas} = x_{sg} \cdot M_{sg} + x_{air} \cdot M_{air} \tag{6.7}$$

Through the composition vector, one can keep track of the change in key products of the stoichiometric combustion process at any loads. However, the NOx prediction, as stated in Shi (2013), is determined not only by the fuel consumption and fuel composition, but also, and strongly, by the engine speed, local combustion temperature and local oxygen concentration. There are several approaches that can be adopted, which lead to different degrees of accuracy (Shi, 2013). The main aim of the integration is not the accurate modelling of the NOx values, but the combined effect that a variation in temperature, mass flow and NOx would have on the SCR behaviour. Thus, a simpler and straightforward look-up table approach, correlating the NOx prediction with the engine load, is selected (see appendix E). The available measurements belong to a Wärtsilä 34DF engine in diesel mode, which, for generator load, features a similar outlet turbine temperature trend as the adopted MAN engine. Given the strong interaction between temperature and NOx, the 4 measured points (at 100%, 75%, 50%, 25% of MCR) are used to build the look-up table which generates the NOx signal. Finally, the NO_2 amount is considered to be 7,5% of the total NOx.
For legislation purposes, the outlet specific pollutant emission ratio, introduced in chapter 1, is calculated:

$$spe_{NOx} = \frac{per_{NOx} \cdot sfc}{1000} \tag{6.8}$$

with *per* being the pollutant emission ratio in gram emission per kg fuel:

$$per_{NOx} = \frac{ppm_{NOx}}{1000} \cdot \frac{M_{NOx}}{M_{gas}} + [(1 + x_{H_2O}) \cdot \lambda \cdot \sigma + 1] \tag{6.9}$$

As anticipated, the selected engine is the MAN-12V28 (Geertsma et al., 2017). Again, a dual layer arrangement is adopted. The dimensions of the piping system and the SCR reactor are in accordance with engines of the same power output (fig.6.4).

Reactor Size	Engine power output (kW)	Reactor inlet DI Flange DN	Reactor outlet DO Flange DN	Weight (kg) (incl. catalyst elements)	L (mm) (incl. cones)	H (mm) (incl. 150 mm insulation)	W (mm) (incl. 150 mm insulation)	Mixing pipe, straight length (m) (bends are allowed after straight lenght)	Mixing pipe, total lenght (m) (includes straight lenght)
1	0...400	350	300	1100	3000	840	840	2.3	3
2	401...550	400	350	1200	3000	1000	840	2.4	3.2
3	551...700	450	400	1500	3116	1000	1000	2.5	3.4
4	701...900	500	400	1600	3116	1160	1000	2.6	3.6
5	901...1100	550	450	2000	3230	1160	1160	2.7	3.8
6	1101...1350	600	500	2100	3230	1320	1160	2.7	3.9
7	1351...1600	700	550	2500	3346	1320	1320	2.5	3.9
8	1601...1850	700	600	2600	3346	1480	1320	2.8	4.2
9	1851...2150	800	600	3000	3460	1480	1480	2.6	4.1
10	2151...2450	800	700	3100	3460	1640	1480	2.9	4.5
11	2451...2800	900	700	3500	3578	1640	1640	2.7	4.3
12	2801...3150	1000	800	3600	3578	1800	1640	2.6	4
13	3151...3600	1000	800	4100	3692	1800	1800	2.9	4.4
14	3601...4000	1100	900	4200	3692	1960	1800	2.7	4.2
15	4001...4400	1200	900	4700	3808	1960	1960	2.6	4
16	4401...4800	1200	1000	4800	3808	2120	1960	2.8	4.3
17	4801...5300	1300	1000	5300	3924	2120	2120	2.7	4.1
18	5301...5850	1300	1100	5400	3924	2280	2120	2.9	4.4
19	5851...6300	1400	1100	5900	4040	2280	2280	2.8	4.3
20	6301...6800	1400	1200	6000	4040	2440	2280	3	4.6
21	6801...7400	1500	1200	6600	4156	2440	2440	2.9	4.4
22	7401...8000	1500	1200	6800	4156	2600	2440	3.1	4.7
23	8001...8600	1600	1200	7300	4270	2600	2600	3	4.5
24	8601...9200	1600	1300	7500	4270	2760	2600	3.2	4.8
25	9201...9900	1700	1300	8300	4420	2760	2760	3.1	4.6
26	9901...10600	1700	1400	8500	4420	2920	2760	3.3	4.9
27	10601...11200	1800	1400	9400	4688	2920	2920	3.2	4.7
28	11201...11900	1900	1500	9600	4688	3080	2920	3.1	4.6
29	11901...12700	1900	1500	10500	4716	3080	3080	3.3	4.8
30	12701...13400	1900	1600	10700	4716	3240	3080	3.4	5.1
31	13401...14200	2000	1600	11700	4866	3240	3240	3.4	4.9
32	14201...15000	2000	1700	11900	4866	3400	3240	3.5	5.1
33	15001...15800	2000	1700	12800	5014	3400	3400	3.6	5.4
34	15801...16600	2200	1800	13000	5014	3560	3400	3.4	4.9
35	16601...17500	2200	1800	14000	5162	3560	3560	3.5	5.1
36	17501...18400	2200	1900	14300	5162	3720	3560	3.6	5.3

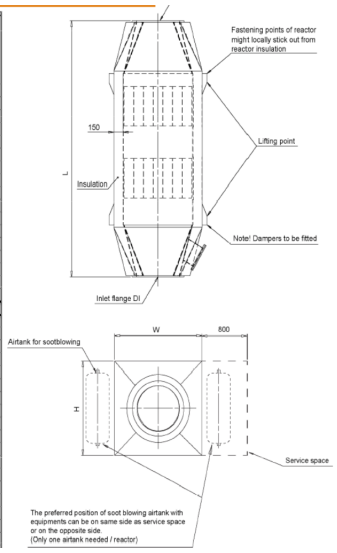

Figure 6.4: Reactor dimensions as a function of the engine power output (Wärtsilä, 2011)

In addition to this, the insulation of 150mm and a filling efficiency of 95% (due to the packing of multiple squared catalyst units (fig.4.1b) lead to the final dimensions of table 6.1

Table 6.1: Main dimensions of connecting pipe and SCR

Connecting pipes			
Parameter	**Value**	**Parameter**	**Value**
Length	5 m	Diameter	1.3 m
SCR			
Parameter	**Value**	**Parameter**	**Value**
Layer length	0.3 m	Layer width	1.73 m
Layer height	1.88 m	Intra-cat. length	0.5 m

For the other catalyst parameters, table 5.1 still holds.

7

SIMULATIONS AND RESULTS

7.1. INTRODUCTION

This section is divided in two parts. Firstly, the static influence of the SCR and silencer addition to the diesel model is analysed for different loads. Secondly, load ramps are simulated in order to understand what load variation, in terms of duration and magnitude, is the most demanding for the SCR with regard to the NOx reduction and ammonia slip.
When performing the simulations, it has been further assumed:

- Negligible temperature drop due to the urea injection
- 100% conversion of urea to ammonia
- Generator load for 1000 rpm
- No heat losses to the ambient in both the resistance and volume elements

7.2. STATIC ANALYSIS

When the SCR is added to the engine model, the turbine does no longer expand the fluid to ambient pressure. In this thesis, the term back pressure is referring to the difference between the turbine outlet pressure p_e and the ambient pressure. The static back pressure experienced by the engine for different loads is shown in figure 7.1.

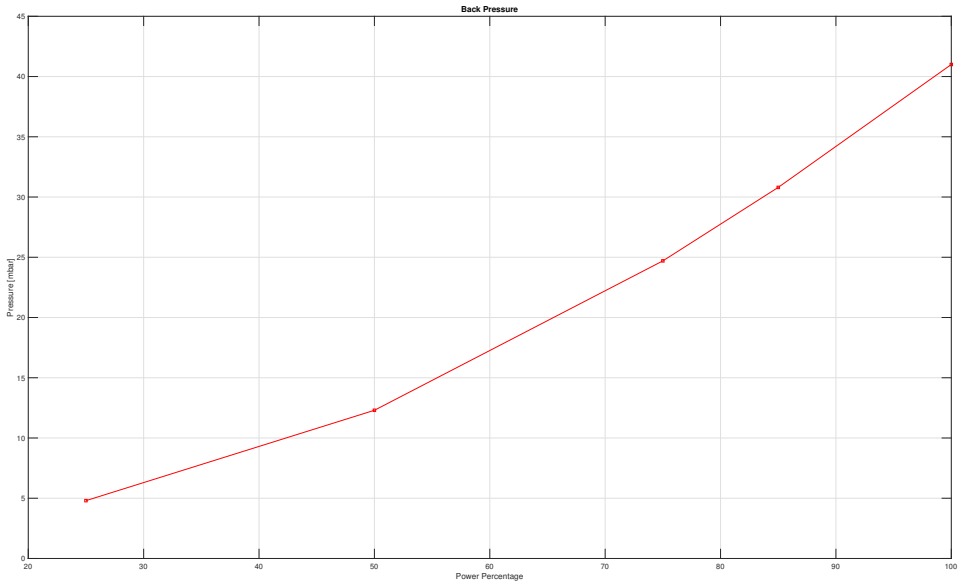

Figure 7.1: Back pressure in milibar

According to Sapra et al. (2017), an increase in back pressure means an increase in the turbine outlet pressure and so, a reduction in the turbine pressure ratio. This, causes the compressor pressure ratio to reduce. A drop in compressor pressure ratio leads to a decrease in the inlet receiver pressure and in the air flow through the engine, as shown in figures 7.2 and 7.3.

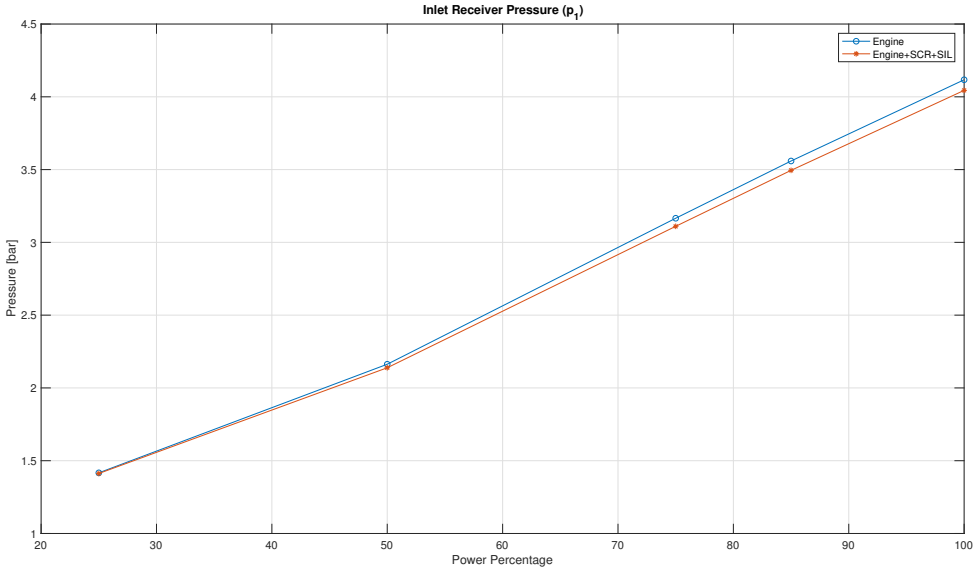

Figure 7.2: Inlet receiver pressure as a function of the engine load

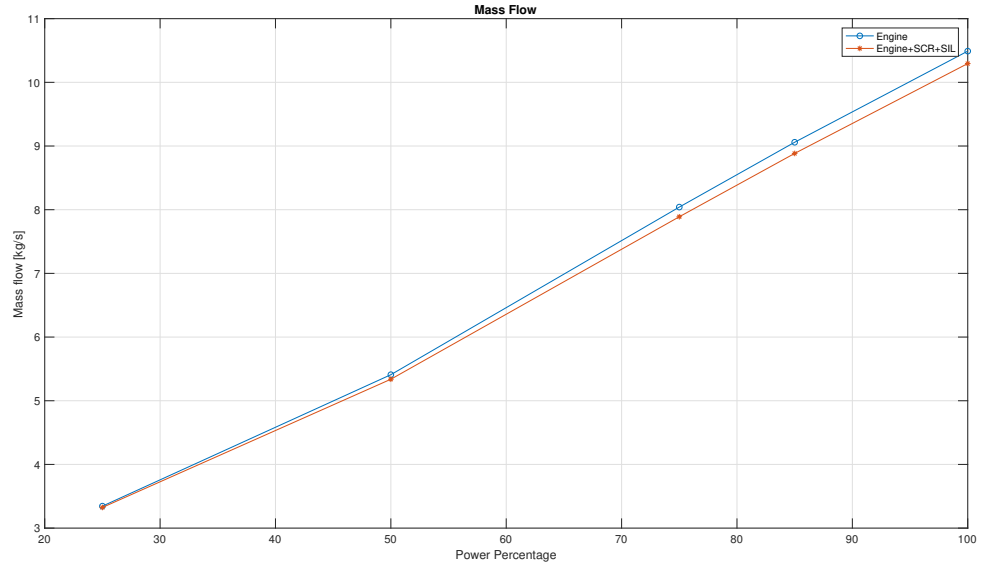

Figure 7.3: Engine mass flow as a function of the engine load

The difference between the integrated system and the stand alone engine predictions is less as the load reduces. This is caused by the reduction in back pressure which, for 25% load, is below 5 millibar. The maximum deviation in mass flow and inlet pressure is around 2%. In Sapra et al. (2017) it is further suggested that an increase in back pressure would result in a minor increase in the fuel consumption (fig.7.4). This is due to the action of the governor, which prevents the engine from decelerating in response to a higher work requested to pump out the exhaust gases.

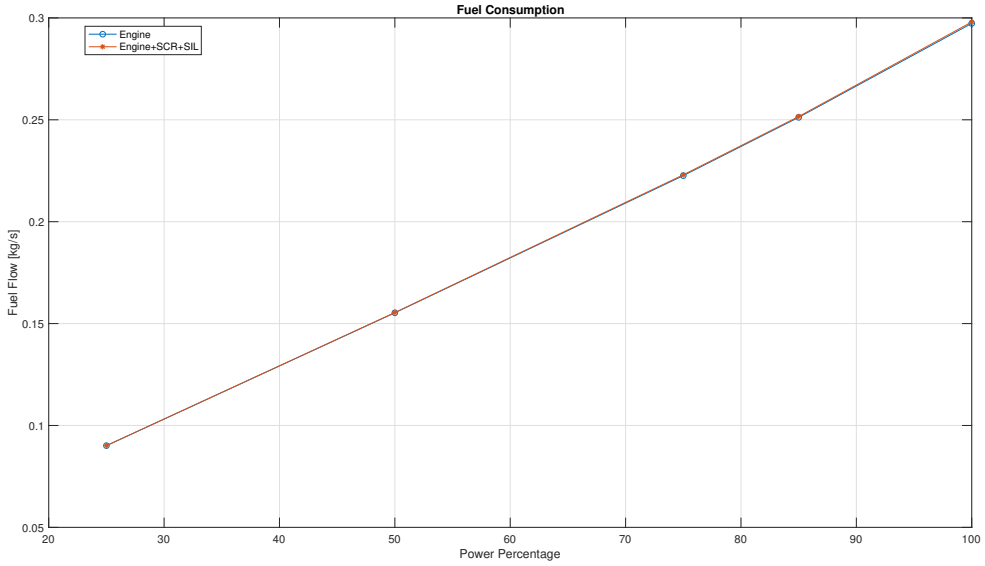

Figure 7.4: Specific fuel consumption as a function of the engine load

The added back pressure affects the SCR behaviour by increasing the turbine outlet temperature as shown in figure 7.5.

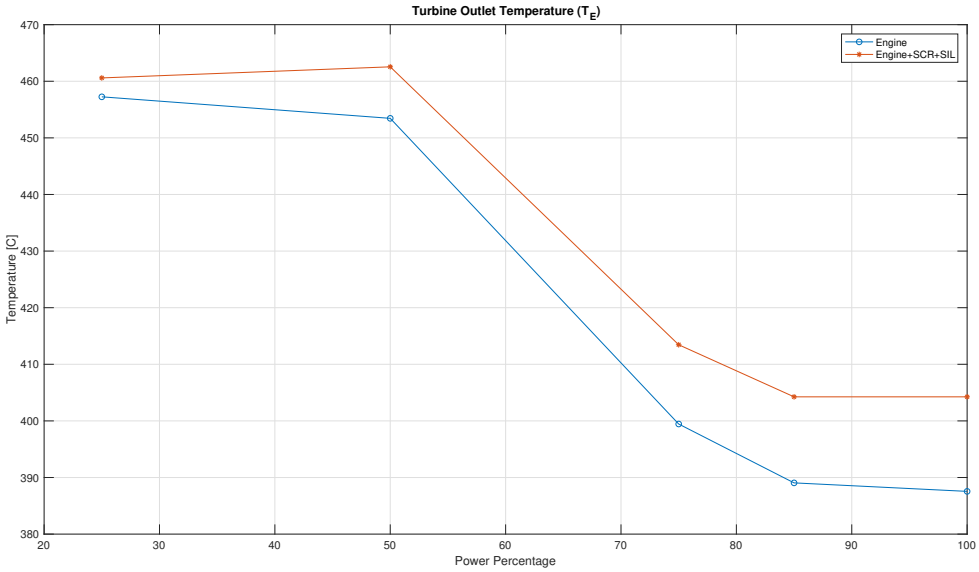

Figure 7.5: Turbine outlet temperature as a function of the engine load

The maximum deviation is, again, at full load and features an increase in the outlet temperature of 4%. This, as explained in chapter 5, negatively influences the NOx reduction due to a stronger action of the ammonia oxidation.
Finally, the pressure drop along the catalyst is depicted in figure 7.6.

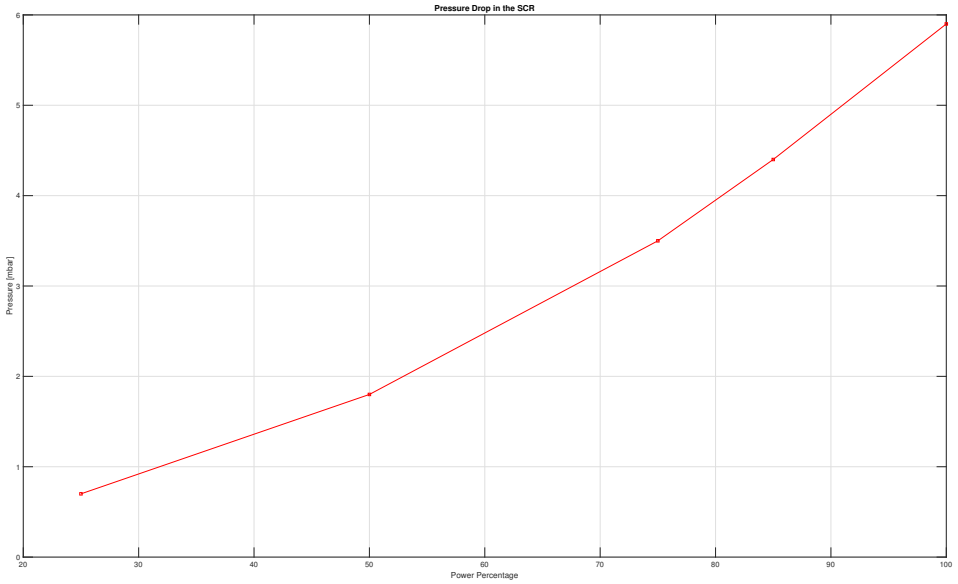

Figure 7.6: SCR pressure drop as a function of the engine load

The maximum pressure drop in the SCR is below 10 millibar. This value is probably underestimated due to the assumptions made throughout the modelling process. A better estimation of the back pressure caused by the presence of the reactor might be reached, if the following effects are taken into account:

- Sulphur action on the pores blockage and on the deposition of sulfates
- Catalyst aging
- Influence of the static mixers
- Maldistribution of the inlet flow (3D)

7.3. DYNAMIC ANALYSIS

The dynamic analysis is performed in order to understand what loading conditions are the most critical for the SCR behaviour, in terms of reduction stability, urea consumption and NH_3 slip.
Three scenarios, in increasing order of severity, are simulated with a desired reference reduction for the controller. The main results are discussed at the end of each subsection.

100% → 75% → 100%

The system undergoes a first load reduction, from 100% to 75% in 20 secs, a stabilisation period and finally, a load increase, again, in 20 secs. The power profile in combination with the NH_3, NO, overall reduction and ANR trends are depicted in figure 7.7

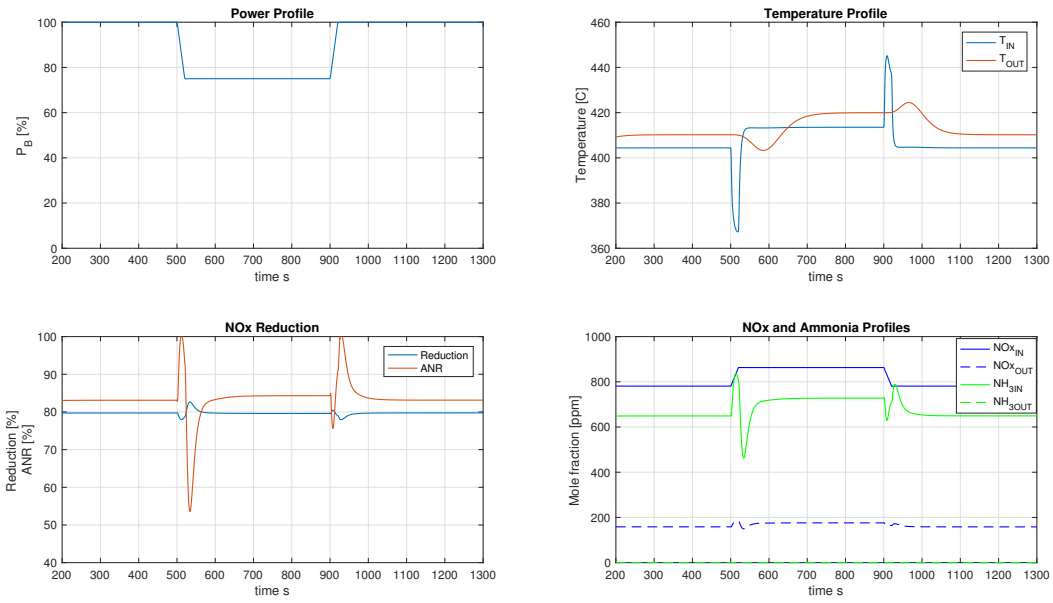

Figure 7.7: Reactants, temperatures and overal reduction trends for 100% → 75% → 100% (80% reduction)

Despite the sharp variations of the inlet temperature (T_{IN}) during the transients, the overall reduction deviates from the reference reduction (80%) by just 1-2%. The inlet ammonia is adjusted, at 500 secs, to compensate for the temperature drop and the subsequent rise to a higher steady-state level. In section 5.3.2, it was explained that, for constant inlet reactants, a temperature decrease makes the NO rise and the NH_3 fall. The opposite occurs if the temperature is rapidly increased. The NO_{IN}, however, does not accurately follow the temperature but it is subjected to a steady increase, when the load is dropped, and a steady decrease, when the load is raise. This limitation is due to the selection of the look-up table approach for the NOx inlet signal as a function of the engine load. The outlet gas temperature (T_{OUT}), due to the SCR thermal inertia, does

not experience any sudden peak but it shows a more gradual trend between the old and the new steady-state value, which, according to the net enthalpy of reaction, is slightly higher (~ 3-6°C) than the inlet temperature. The gram of NO emissions, per kWh, are reported in figure 7.8, together with the actual consumption of the urea solution (40% urea in water).

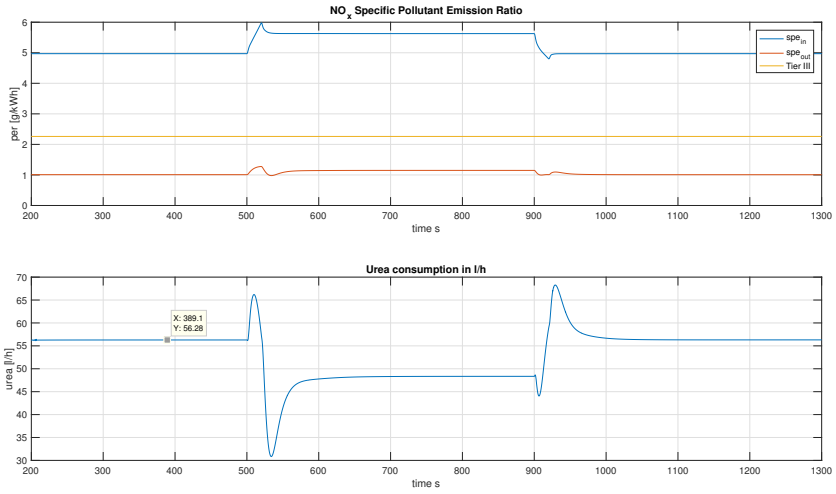

Figure 7.8: NOx spe and urea consumption for 100% → 75% → 100% (80% reduction)

The reference reduction of 80% could be even reduced to 70% (fig.7.9-7.10), if the Tier III is met with a less safer margin .

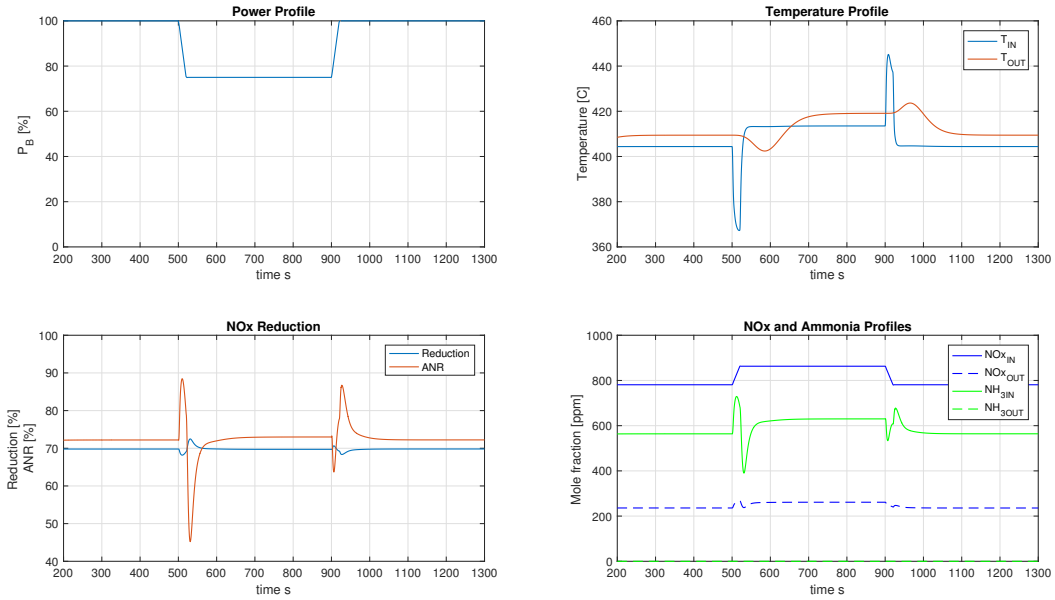

Figure 7.9: Reactants, temperatures and overal reduction trends for 100% → 75% → 100% (70% reduction)

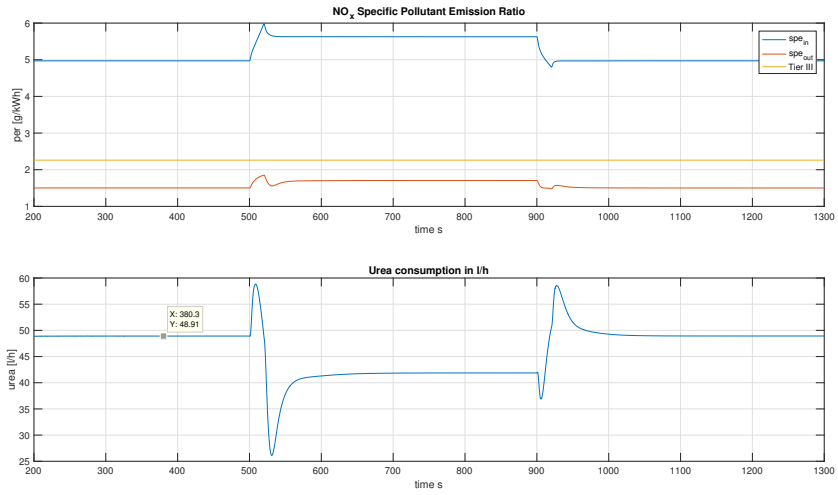

Figure 7.10: NOx spe and urea consumption for 100% → 75% → 100% (70% reduction)

In the latter scenario, for a 10% reduction in the reference value, the urea consumed at maximum load is reduced by 13%. In both cases, the ammonia slip does not represent an issue because of the combined effect of the high operating temperatures (strong ammonia oxidation) and the reference reduction value, which is below 100%.
Overall, even for shorter transients, it can be concluded that the loading condition between 100% and 75% can be easily handled by the SCR and that the main parameter affecting the urea injection is the temperature variation.

100% → 50% → 100%

Again, the engine is subjected to transients of 20 secs separated by a stabilisation period. Compared to the the 75% case, the inlet temperature experiences much bigger fluctuations (fig7.11). During the load rise, it first decreases till 310°C, then it sharply increases till almost 450°C. To compensate for the latter phenomenon, the inlet ammonia is hugely decreased (a saturation value of 0 ppm is set). The reaching of the steady-state is slower due to the more favourable oxidation of ammonia, which causes not only a higher outlet NO but also a larger inlet ammonia (compared to fig.7.7), computed by the controller to meet the reference reduction. When the load is increased, the temperature reaches a peak of approximately 545°C causing, therefore, a rising request of ammonia (limited to 1000 ppm) to withstand the increased NO production (again through oxidation), despite the decrease in inlet NO. The specific emission ratio is given, together with the consumed urea (fig.7.12), to complete the overall picture.

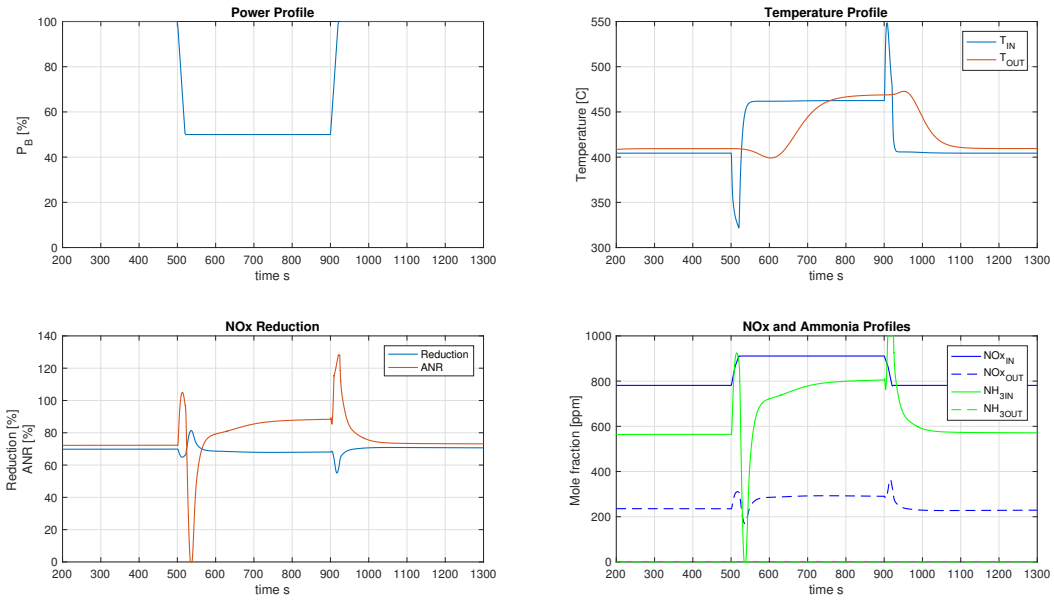

Figure 7.11: Reactants, temperatures and overall reduction trends for 100% → 50% → 100% (70% reduction)

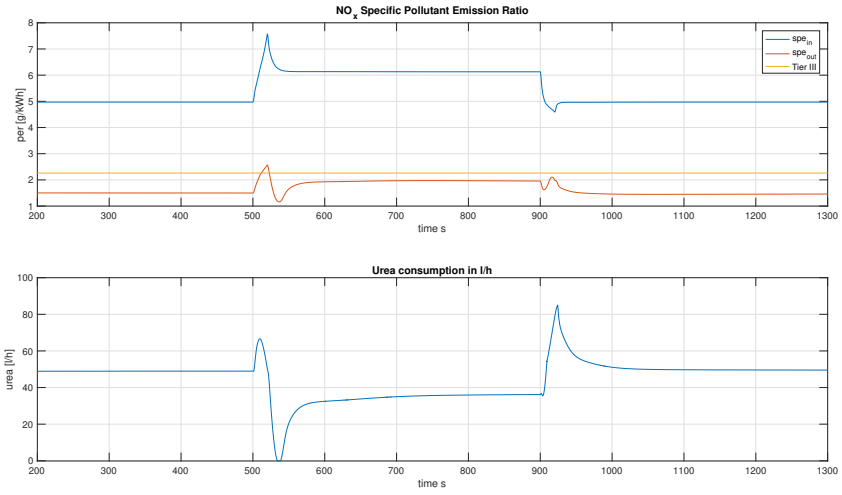

Figure 7.12: NOx per, spe and urea consumption for 100% → 50% → 100% (70% reduction)

The 50% load scenario allows for a quite satisfying reduction trend at the expense of a more aggressive controller, which is used to compensate for the effect of the inlet peak temperature. While during the load decrease, the long stabilisation period may cause, for more relaxed reference reduction values, an excessive NO slip, the load increase shows a sharp increase in the consumed urea, which is, however, necessary to simultaneously cope with the high peak temperature and the desired NOx reduction. Although the limit curve is exceeded for a short time, the Tier III is still met since the mean value of the NOx *spe* is taken over 4 load points.

As for the 75% scenario, the NH_3 slip is absent because of the strong ammonia oxidation.

100% → 25% → 100%

The last loading scenario is obviously the most unpleasant. The load is dropped and raise till 25% in only 20 secs. Although, as stated in section 6.3.1, the engine model features the worst temperature estimation, it is meaningful to investigate the behaviour of the integrated system under very low loads, since this is the most limiting condition for the adoption of the SCR.

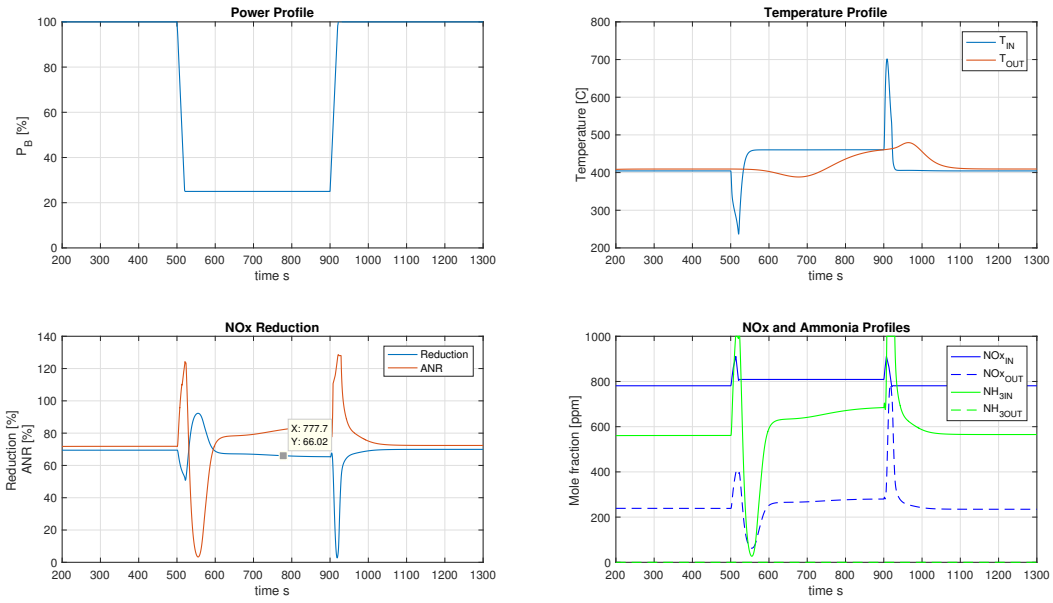

Figure 7.13: Reactants, temperatures and overal reduction trends for 100% → 25% → 100% (70% reduction)

When comparing the 25% scenario (fig.7.13) with the 50% and 75%, it immediately stands out the wider temperature window during the transients. Despite the similar trends, the extreme inlet temperatures at 500 and 900 secs, together with the variation in mass flow (see fig. 7.3), makes it difficult, for the controller, to meet the reference reduction during the stabilisation time (from 520 to 900 secs). It is, however, during the load rise, that the system truly struggles to reduce the NOx. The peak temperature reaches almost 700°C, enabling a strong NO production due to the ammonia oxidation reaction. Despite the increased inlet ammonia and the resulting depressed overall reduction, the higher mass flow helps the system to stabilise in a much shorter time compared to the load drop case. The described behaviour is negatively reflected on the NOx emission ratios (fig.7.14) , where the Tier III threshold is exceeded, and on the injected urea, which experience a huge overshoot when the load is increased.

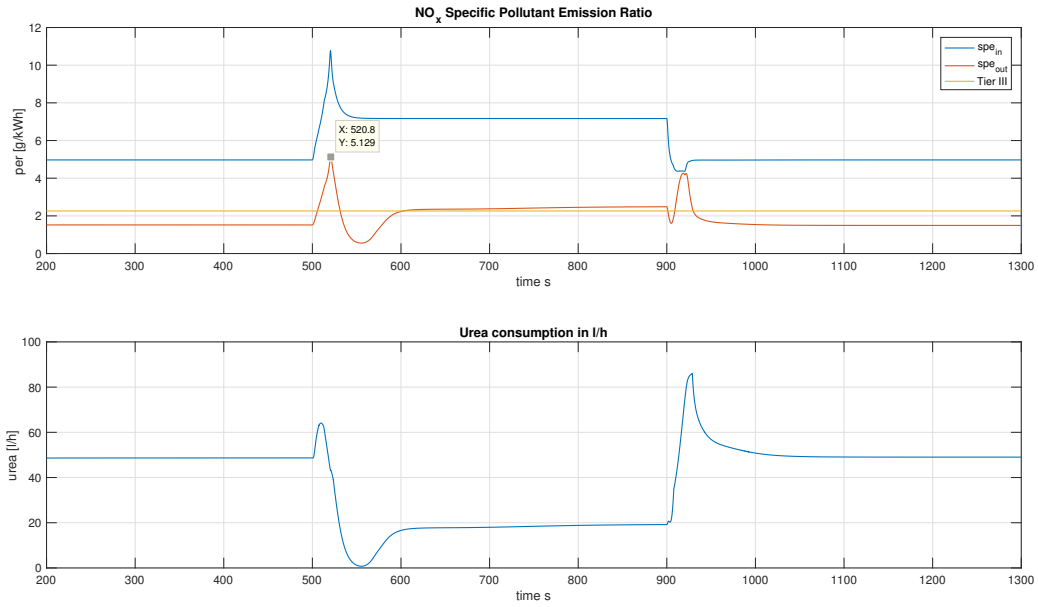

Figure 7.14: NOx per, spe and urea consumption for 100% → 25% → 100%

In this scenario, it is clear that a more accurate model, which takes into account the sulphur influence as well as the catalyst deterioration at high temperatures, would reproduce much more severe consequences.
A possible solution to this problem might be to lengthen the transients, allowing for lower peak values. The results for the 60 secs transient are depicted in figure 7.15 and 7.16.

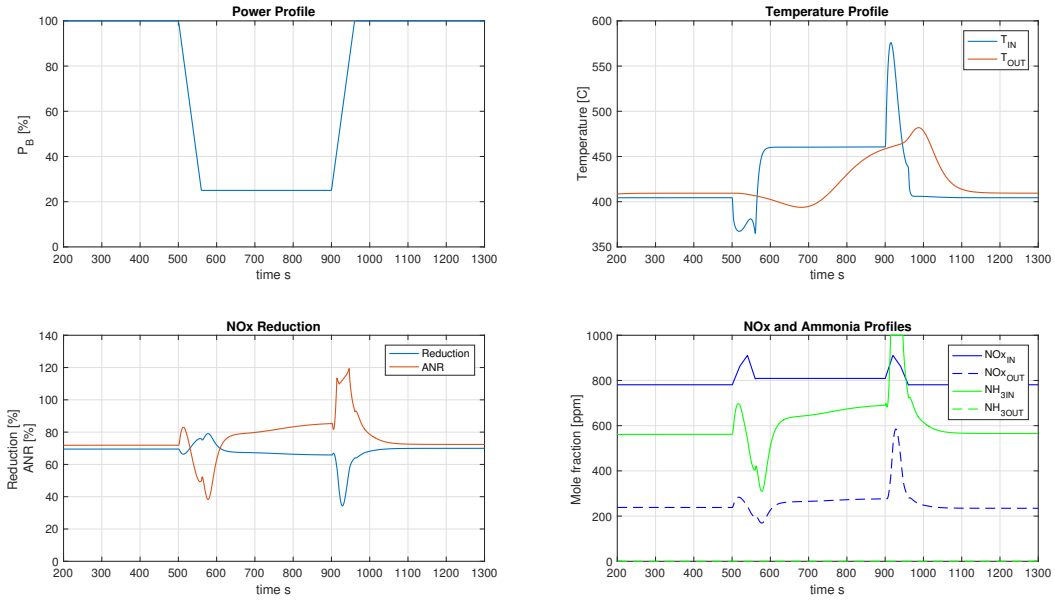

Figure 7.15: Reactants, temperatures and overal reduction trends for 100% → 25% → 100% (60 secs)

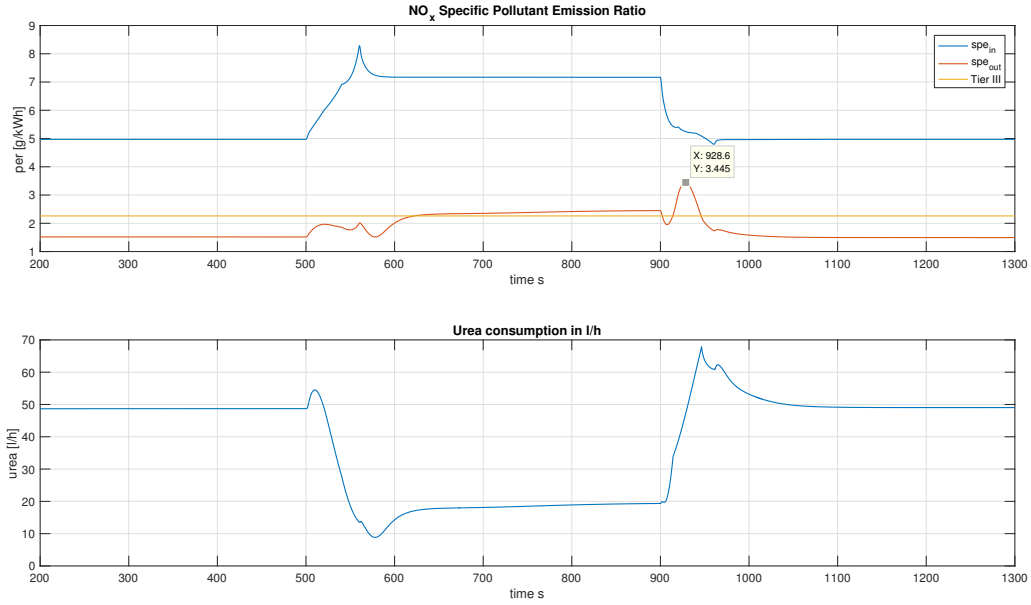

Figure 7.16: NOx per, spe and urea consumption for 100% → 25% → 100% (60secs)

The overall reduction and the urea consumption feature a much more stable behaviour and this is positively reflected on the NOx emission ratio, where the maximum peak is reduced by 30%.

8

CONCLUSIONS AND RECOMMENDATION

8.1. CONCLUSIONS

The main objective of this thesis was to gain insight into the behaviour of the marine SCR system under steady-state and transient conditions. To achieve this main goal, an in-depth literature study on the SCR process, chemical reactions, reaction kinetics and modeling approach has been performed. A 1D-single channel approach has been chosen to model the SCR system, consisting of two catalyst layers and an intra-catalyst volume. The resistance and volume element approach has been further used to allow for a possible integration with an existing diesel engine model. Before the integration, the SCR model has been tested, discussed and verified under various feed conditions in order to define which, and to what extent, process parameters affect the SCR behaviour. A simple control strategy, consisting of a feedforward branch, exploiting the information of the inlet NOx, and a feedback loop, providing a corrective action for steady-state errors, has been designed to simulate the injected urea. After that, the SCR model has been integrated with an existing diesel engine model capable of predicting, with enough accuracy, the SCR inlet parameters: mass flow, turbine outlet temperature and exhaust gas composition. The missing information regarding the NOx signal has been dealt with a look-up table approach, which correlates the NOx prediction with the engine load. Finally, three loading scenarios have been simulated to represent a more realistic view of the limiting conditions during rapid transients.
The conclusions are, therefore, treated in two separate subsections:

- SCR Model
- Diesel Integration and Control Strategy

8.1.1. SCR MODEL

The main objective set for the SCR model (section 3.2) was the accurate prediction of the NOx reduction and NH_3 slip under different operating conditions. In chapter 5, it has been demonstrated that for the adopted kinetic data:

- The optimal operating temperature is between 300 and 400°C. Above this window, the reduction efficiency decreases due to an overproduction of NO through oxidation of ammonia, which in turn is

minimized (no slip). On the other hand, below the optimal temperature range, both the NO and NH_3 increase because of the less effective action of the standard reaction at low temperatures

- A NO_2/NOx ratio close to 50% enhances the Fast reaction, helping the SCR to reach satisfying values of NOx reduction and ammonia slip, even for temperatures as low as 200°C

- There is a linear relation between ANR and NOx cut, when operating in the optimal temperature region. It is in that range, indeed, that the standard reaction plays its largest role, enabling the reduction of one mole of NO with one mole of NH_3

- For constant inlet reactants and mass flow, a step variation in temperature causes overshoots in the ammonia signal, when the temperature is increased, and in the NOx signal, when the temperature is decreased. These phenomena are connected with the great temperature dependence of both the desorption process and the standard reaction

8.1.2. DIESEL INTEGRATION & CONTROL STRATEGY

The main objective set for the engine integration (section 6.3) was, on one hand, the study of the engine response to the addition of the after-treatment system in terms of added flow resistance and, on the other hand, the investigation of the SCR behaviour under dynamic operations. It has been shown that:

- The added back pressure reaches a maximum of more than 40 millibar for 100% load. The main consequence is a decreased turbine pressure ratio, which negatively influences the engine thermal loading. The inlet receiver pressure drops and leads to a higher exhaust gas temperature, which directly affects the SCR as described in chapter 5. Lastly, a minor increment in fuel consumption is noticed

- The highly varying gas temperature is the main cause of instability during the transients. Especially In case of the 50% and 25% load scenarios, there is a great chance to exceed the Tier III limit, which is, however, a static limit based on the mean value over 4 load points

- For the tested system, the ammonia slip does not represent a limiting factor. This is due to the high operating temperatures predicted by the engine model, which enhance the oxidation of NH_3

- The SCR thermal inertia has an impact on the transient response as it acts like a lowpass filter with transport delay for the outlet temperature (Codan et al., 2010). This behaviour affects the turbine performance when a pre-turbo design is adopted (2-stroke engines)

8.2. RECOMMENDATION

During the thesis, a set of assumptions has been made in order to define appropriate project boundaries, which are needful, given the magnitude of the topic. Further investigations are therefore essential to validate the results and improve the model accuracy, especially when it comes to the integration with other systems. These considerations are summarized in the following points:

- Conduct experiments on marine SCR systems in order to develop more accurate kinetic data, which can then be used to optimize and validate the model results

- Include the sulphur influence on the reduction potential, catalyst deterioration and added back pressure by either adopting new kinetic data or using the results of the experiments

- Investigate the 2D model which takes the internal diffusion effects into account and simulates the concentration variations in the washcoat layer both in the axial and the radial directions. The SCR process might be diffusion limited (Heck et al., 2009) when constant operations below 300-250°C are needed
- Include the modeling of the urea injection and decomposition in the mixing duct. In this project, it has been assumed that complete conversion is achieved at any temperatures. This might not be the case when operating at low temperatures, where the decomposition rate drops
- Investigate more advanced control strategies. This can be done by optimizing the designed Feedforward+Feedback controller or by selecting strategies based on the control of the ammonia storage, such as the model-based predictive control (MPC) and adaptive control
- Examine the technical feasibility of the Diesel Oxidation Catalyst, SCR and Ammonia Slip Catalyst integration (DOC+SCR+ASC). This combination might be convenient when operating for long periods well below 300°C. This solution, is however applicable only if low sulphur fuels are adopted

BIBLIOGRAPHY

Åberg, A., Widd, A., Abildskov, J. and Huusom, J. K. (2017), 'Parameter estimation and analysis of an automotive heavy-duty scr catalyst model', *Chemical Engineering Science* **161**, 167–177.

Anderson, J. D. and Wendt, J. (1995), *Computational fluid dynamics*, Vol. 206, Springer.

Brandenberger, S., Kröcher, O., Tissler, A. and Althoff, R. (2008), 'The state of the art in selective catalytic reduction of nox by ammonia using metal-exchanged zeolite catalysts', *Catalysis Reviews* **50**(4), 492–531.

Ciardelli, C., Nova, I., Tronconi, E., Konrad, B., Chatterjee, D., Ecke, K. and Weibel, M. (2004), 'SCR-DeNO x for diesel engine exhaust aftertreatment : unsteady-state kinetic study and monolith reactor modelling', **59**, 5301–5309.

Codan, E., Bernasconi, S. and Born, H. (2010), Imo iii emission regulation: Impact on the turbocharging system, *in* 'CIMAC Congress'.

Cook, D. A. and Skinner, J. M. (2005), 'How to perform credible verification, validation, and accreditation for modeling and simulation', *The Journal of Defense Software Engineering* **18**(5), 20–24.

Davis, M. E. and Davis, R. J. (2012), *Fundamentals of chemical reaction engineering*, Courier Corporation.

Depcik, C. and Assanis, D. (2005), 'One-dimensional automotive catalyst modeling', *Progress in energy and combustion science* **31**(4), 308–369.

Dolanc, G., Strmčnik, S. and Petrovčič, J. (2001), 'Nox selective catalytic reduction control based on simple models', *Journal of Process Control* **11**(1), 35–51.

Döring, A., Bugsch, M., Hetzer, J., Bader, I., Struckmeier, D., Baydak, M., Losher, R. and Stiesch, G. (2016), The man scr system–more than just fulfilling imo tier iii, *in* 'CIMAC Congress Helsinki, Paper', Vol. 26.

Eastwood, P. (2000), *Critical topics in exhaust gas aftertreatment*.

Geertsma, R., Negenborn, R., Visser, K., Loonstijn, M. and Hopman, J. (2017), 'Pitch control for ships with diesel mechanical and hybrid propulsion: Modelling, validation and performance quantification', *Applied Energy* **206**, 1609–1631.

Glossary, M. &. S. . (2011), 'Modeling and Simulation (M & S) Glossary'.

Guan, B., Zhan, R., Lin, H. and Huang, Z. (2014), 'Review of state of the art technologies of selective catalytic reduction of NOx from diesel engine exhaust', *Applied Thermal Engineering* **66**(1-2), 395–414.

Güthenke, A., Chatterjee, D., Weibel, M., Krutzsch, B., Kočí, P., Marek, M., Nova, I. and Tronconi, E. (2007), 'Current status of modeling lean exhaust gas aftertreatment catalysts', *Advances in Chemical Engineering* **33**(07).

Guzzella, L. and Onder, C. (2009), *Introduction to modeling and control of internal combustion engine systems*, Springer Science & Business Media.

Heck, R. M., Farrauto, R. J. and Gulati, S. T. (2009), *Catalytic air pollution control: commercial technology*, John Wiley & Sons.

https://www.dieselnet.com/standards/inter/imo (2018).

https://www.epa.gov/ghgemissions/understanding-global-warming-potentials (2018).

Iwasaki, M. and Shinjoh, H. (2010), 'A comparative study of ?standard?,?fast? and ?no2? scr reactions over fe/zeolite catalyst', *Applied Catalysis A: General* **390**(1-2), 71–77.

Jacob, A., Kapteijn, F. and Mul, G. (1995), *Heterogeneous Catalysis for Chemical Engineers*, 6 edn, McGraw-Hill Education.

Janssen, F. J. J. G. (1987), The Selective Catalytic Reduction of Nitric Oxide with Ammonia: the Mechanism of the Reaction Over Various Vanadium and Titanium Containing Catalysts, PhD thesis, Universiteit Twente.

Koltsakis, G. C. and Stamatelos, A. M. (1997), 'Catalytic automotive exhaust aftertreatment', *Progress in Energy and Combustion Science* **23**(1), 1–39.

Lietti, L., Nova, I., Tronconi, E. and Forzatti, P. (1998), 'Transient kinetic study of the scr-denox reaction', *Catalysis Today* **45**(1-4), 85–92.

Lietti, L., Nova, I., Tronconi, E., Forzatti, P., Industriale, C. and Natta, C. G. (2000), 'Unsteady-State kinetics of DeNOx -SCR catalysis', **3**.

Magnusson, M., Fridell, E. and Härelind, H. (2016), 'Improved low-temperature activity for marine selective catalytic reduction systems', *Proceedings of the Institution of Mechanical Engineers, Part M: Journal of Engineering for the Maritime Environment* **230**(1), 126–135.

Magnusson, M., Fridell, E. and Ingelsten, H. H. (2012), 'The influence of sulfur dioxide and water on the performance of a marine scr catalyst', *Applied Catalysis B: Environmental* **111**, 20–26.

Nova, I. and Tronconi, E. (2014), *Urea-SCR technology for deNOx after treatment of diesel exhausts*, Springer.

Pace, A. (2013), "scr catalyst application under pressure on two-stroke marine engine", Master's thesis, Universita' di Padova.

Pontikakis, G., Konstantas, G. and Stamatelos, A. (2004), 'Three-way catalytic converter modeling as a modern engineering design tool', *Journal of engineering for gas turbines and power* **126**(4), 906–923.

Ruggeri, M. P., Nova, I. and Tronconi, E. (2012), 'Experimental and modeling study of the impact of interphase and intraphase diffusional limitations on the denox efficiency of a v-based extruded catalyst for nh3–scr of diesel exhausts', *Chemical engineering journal* **207**, 57–65.

Sapra, H., Godjevac, M., Visser, K., Stapersma, D. and Dijkstra, C. (2017), 'Experimental and simulation-based investigations of marine diesel engine performance against static back pressure', *Applied Energy* **204**, 78–92.

Schär, C. M. (2003), *Control of a selective catalytic reduction process*, ETH Zurich.

Schmidt, D. L. (1998), *The Engineering of Chemical Reactions*, Oxford University Press.

Schmitt, J. C. (2010), 'Selective catalytic reduction: testing, numeric modeling, and control strategies'.

Schulten, P. J. M. (2005), The interaction between diesel engines, ship and propellers during manoeuvring, PhD thesis, TU Delft, Delft University of Technology.

Shi, W. (2013), 'Dynamics of energy system behaviour and emissions of trailing suction hopper dredgers'.

Song, X. (2013), A SCR Model based on Reactor and Engine Experimental Studies for a Cu-zeolite Catalyst, PhD thesis, Michigan Technological University.

Stapersma, D. (2010*a*), *Diesel Engines Volume 1 Performance Analysis January 2010*, Vol. 1.

Stapersma, D. (2010*b*), *Diesel Engines Volume 3 Combustion April 2010*, Vol. 3.

Stapersma, D. (2010*c*), *Diesel Engines Volume 4 Emissions and Heat transfer April 2010*, Vol. 4.

Stapersma, D. (2010*d*), *Diesel Engines Volume 6 Thermodynamical Principles II April 2010*, Vol. 6.

Struckmeier, D. (2015), 'MDT Four-stroke SCR system kit to fulfill IMO Tier III (MAN Seminar)'.

Vannice, M. A. and Joyce, W. H. (2005), *Kinetics of catalytic reactions*, Vol. 134, Springer.

Wärtsilä (2011), 'Wärtsilä NOX Reducer: Environmental Efficiency'.

Wärtsilä (2013), 'Wärtsilä Environmental Product Guide'.

Wik, C. (2012), 'Wärtsilä R&D Presentation'.

Williams, J. L. (2001), 'Monolith structures, materials, properties and uses', *Catalysis Today* **69**(1-4), 3–9.

Woodyard, D. (2003), *Pounder's Marine Diesel Engines: and Gas Turbines*, Butterworth-Heinemann.

Yun, B. K. and Kim, M. Y. (2013), 'Modeling the selective catalytic reduction of nox by ammonia over a vanadia-based catalyst from heavy duty diesel exhaust gases', *Applied Thermal Engineering* **50**(1), 152–158.

A

REACTION KINETIC DATA

Table A.1: Adopted Kinetic Data (Åberg et al., 2017)

Reaction	Parameter	Value	Unit
Adsorption	k_0	467	[1/s]
	E_a	0	[kJ/mol]
Desorption	k_0	$7{,}9 \cdot 10^5$	[1/s]
	E_a	60,4	[kJ/mol]
	α	0,17	[-]
Oxidation	k_0	$3{,}27 \cdot 10^{16}$	[mol/m^3/s]
	E_a	221,1	[kJ/mol]
Standard SCR	k_0	$1{,}83 \cdot 10^9$	[1/s]
	E_a	75,3	[kJ/mol]
Fast SCR	k_0	$3{,}14 \cdot 10^{12}$	[m^3/mol/s]
	E_a	73,6	[kJ/mol]

For sake of consistency, the summary of the adopted kinetic expressions (Åberg et al., 2017) is given below.

Adsorption

$$\begin{aligned} r_{ads} &= k_{ads} C_{NH_3} (1 - \theta_{NH_3}) \\ k_{ads} &= k^0_{ads}\ exp\left(-\frac{E_{ads}}{RT_m}\right) \end{aligned} \tag{A.1}$$

Desorption

$$\begin{aligned} r_{des} &= k_{des} \theta_{NH3} \\ k_{des} &= k^0_{des}\ exp\left(-\frac{E^0_{des}}{RT_m}(1 - \alpha\theta_{NH_3})\right) \end{aligned} \tag{A.2}$$

Standard SCR

$$\begin{aligned} r_{std} &= k_{std} C_{NO} \theta_{NH_3} \\ k_{std} &= k^0_{std}\ exp\left(-\frac{E_{std}}{RT_m}\right) \end{aligned} \tag{A.3}$$

Fast SCR

$$r_{fast} = k_{fast} C_{NO} C_{NO_2} \theta_{NH_3}$$
$$k_{fast} = k^0_{std} \; exp\left(-\frac{E_{fast}}{RT_m}\right) \tag{A.4}$$

Oxidation

$$r_{ox} = k_{ox} \theta_{NH_3}$$
$$k_{ox} = k^0_{ox} \; exp\left(-\frac{E_{ox}}{RT_m}\right) \tag{A.5}$$

B

GAS PROPERTIES CALCULATION

The gas properties are continuously calculated once the temperature, pressure and composition vector are known. In fig.B.1, the "Properties" block is shown.

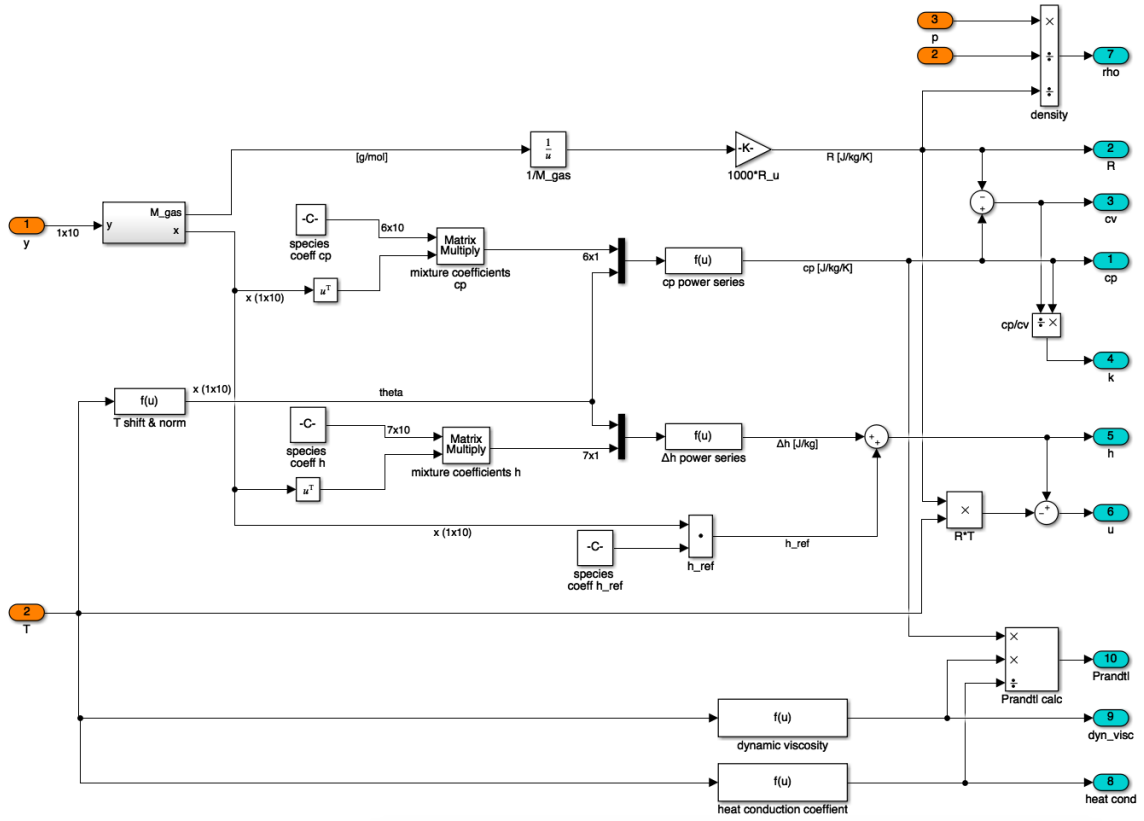

Figure B.1: Properties calculation block

The composition vector, described in section 4.2.1, is used to calculate the mixture molar weight and the

composition vector on a mass fraction basis:

$$M_{gas} = \sum_{j=1}^{nc} y_j \cdot M_j \tag{B.1}$$

$$x_j = \frac{y_j \cdot M_j}{\sum_{j=1}^{nc} y_j \cdot M_j} \tag{B.2}$$

where x_j stands for the mass fraction of the j^{th} component.
Generally speaking, mass and molar (˜) amounts are related by the molecular weight. The gas constant R on a mass basis is therefore calculated as:

$$R_{gas} = \frac{\tilde{R}}{M_{gas}} \tag{B.3}$$

The density follows from the ideal gas equation.

$$\rho_{gas} = \frac{p_{gas}}{R_{gas} \cdot T_{gas}} \tag{B.4}$$

The specific heat at constant pressure is not held constant but varies with the composition and the gas temperature. When a generic j component is considered, the following holds (Stapersma, 2010*d*):

$$c_{p_j} = R_j \sum_{k=1}^{m} \alpha_{k_j} \cdot \theta^{k-1} = \sum_{k=1}^{m} a_{k_j} \cdot \theta^{k-1} \tag{B.5}$$

where R is the gas constant, on a mass basis, of species j, α_k are the power series coefficients of j, m is the number of coefficients and θ stands for the normalised temperature:

$$\theta = \frac{T - T_{shift}}{T_{norm}} \tag{B.6}$$

The α_k coefficients of all the components, except NO_2 and NH_3, for which they are assumed to be 0, can be found in (Stapersma, 2010*d*). This assumption does not appreciably influence the properties calculation since both NO_2 and NH_3 accounts for less than the 0.1% of the exhaust flow composition. When the series extension for the specific heat in powers of absolute temperature is used, the T_{shift} is zero and thus:

$$\theta = \frac{T}{T_{norm}} \tag{B.7}$$

The adopted normalised temperature is 1000K.
To calculate the specific heat of the mixture, the additional information of the composition vector on a mass basis is used:

$$c_{p_{gas}} = \sum_{k=1}^{m} (\sum_{j=1}^{nc} x_j \cdot a_{k_j}) \theta^{k-1} \tag{B.8}$$

Once c_p is known, the heat coefficient at constant volume is easily given by:

$$c_{v_{gas}} = c_{p_{gas}} - R_{gas} \tag{B.9}$$

The enthalpy of an ideal component j is calculated by:

$$h_j = h_j^{ref} + \int_{T_{ref}}^{T} c_{p_j} \cdot dT \tag{B.10}$$

when the normalised temperature is considered, the enthalpy function becomes:

$$h_j = h_j^{ref} + T_{norm} \cdot \int_{\theta_{ref}}^{\theta} c_{p_j} \cdot d\theta \tag{B.11}$$

where θ_{ref} is the normalised reference temperature and h^{ref} is the enthalpy at reference conditions which, in simple words, correspond to the standard enthalpy of formation described in section 4.3.2. The adopted standard enthalpies of formation are given in table B.1.

Table B.1: Standard enthalpy of formation for different species

Species	$\mathbf{h}^{ref}$ **[kJ/mol]**
N_2	0
O_2	0
Ar	0
CO_2	-393,509
H_2O	-241,818
SO_2	-296,83
CO	-110,525
NO	+90,25
NO_2	+33,18
NH_3	-45,94

By combining equations (B.5) and (B.11), the difference between actual and reference enthalpies is calculated:

$$\Delta h_j = h_j - h_j^{ref} = \sum_{k=1}^{m} \frac{a_{k_j}}{k} \cdot T_{norm} \cdot \theta^k - \sum_{k=1}^{m} \frac{a_{k_j}}{k} \cdot T_{norm} \cdot \theta_{ref}^k \tag{B.12}$$

When the following new constants are introduced:

$$b_{1_j} = \sum_{k=1}^{m} \frac{a_{k_j}}{k} \cdot T_{norm} \cdot \theta_{ref}^k \tag{B.13a}$$

$$b_{k_j} = \sum_{k=1}^{m} \frac{a_{k_j}}{k} \cdot T_{norm} \qquad k = 2, ..., m+1 \tag{B.13b}$$

equation (B.12) can be rewritten as follows:

$$\Delta h_j = h_j - h_j^{ref} = \sum_{k=1}^{m+1} b_{k_j} \cdot \theta^{k-1} \tag{B.14}$$

As done for the heat coefficient at constant pressure, the composition vector is used to calculate the enthalpy of the gas mixture.

$$h_{gas}^{ref} = \sum_{j=1}^{nc} x_j \cdot h_j^{ref} \tag{B.15}$$

$$\Delta h_{gas} = h_{gas} - h_{gas}^{ref} = \sum_{k=1}^{m+1} \sum_{j=1}^{nc} x_j \cdot b_{k_j} \cdot \theta^{k-1} = \sum_{k=1}^{m+1} b_{k_{gas}} \cdot \theta^{k-1} \tag{B.16}$$

with

$$b_{k_{gas}} = \sum_{j=1}^{nc} x_j \cdot b_{k_j} \tag{B.17}$$

Finally, the actual gas enthalpy is simply calculated through:

$$h_{gas} = \Delta h_{gas} + h_{gas}^{ref} \tag{B.18}$$

For the internal energy, rather than using the series expansion, the following definition is used:

$$u_{gas} = h_{gas} - p \cdot v = h_{gas} - T \cdot R \tag{B.19}$$

The remaining fluid properties used in the temperature balances are:

- Dynamic viscosity (μ)
- Heat conduction coefficient (λ)
- Prandtl number

While for the first two properties a power law is adopted (the same of the Diesel model), the Prandtl number is simply calculated through:

$$Pr = \frac{c_{p_{gas}} \cdot \mu_{gas}}{\lambda_{gas}} \tag{B.20}$$

C

MASS AND ENERGY EQUATIONS

Through the assumptions of section 3.3, it is possible to model the reactor with a 1D single channel approach The entire catalyst can then be modeled by means of mass and energy equations for the bulk gas and the surface (washcoat+substrate) phase. The following model formulation is based on Depcik and Assanis (2005); Güthenke et al. (2007).
The equations that need to be included are:

- Bulk Gas Species (BGS)
- Bulk Gas Temperature (BGT)
- Surface Species (SS)
- Surface Temperature (ST)
- Intermediate Species (IS)

The housing temperature is not included due to the adiabaticity of the reactor.
Further applicable assumptions (Depcik and Assanis, 2005) are:

- Mach number less than 0.3 (incompressible flow)
- Constant cross section
- Constant flow velocity across the channel

C.1. BULK GAS SPECIES

For every species in the bulk gas (g) participating in the reaction mechanisms, a proper bulk gas equation must be written

$$\epsilon \cdot \frac{\partial C_{g,i}}{\partial t} + u_{gas} \cdot \epsilon \cdot \frac{\partial C_{g,i}}{\partial x} = -k_{m,i} \cdot G_a \cdot (C_{g,i} - C_{s,i}) \tag{C.1}$$

Starting from the left-hand side, the first term is the accumulation of concentration of species i in moles per volume times the void fraction ϵ (i.e. a measure of the void spaces in the catalyst that can be occupied by the bulk gas). The second term is the change in concentration in the axial direction due to mass flow times the

void fraction and flow velocity. The term on the right-hand side is the mass transfer from/to the surface of the catalyst (*s*) times the geometric surface area-to-volume ratio G_a that for a square catalyst is:

$$G_a = \frac{4\epsilon}{d_m}$$

where d_m is the hydraulic diameter of the monolith cell. Finally, $k_{m,i}$ is the mass transfer coefficient.

C.2. SURFACE SPECIES

This equation is used to model the layer of gas on the surface of the catalyst:

$$\epsilon_s \cdot (1-\epsilon) \cdot \frac{\partial C_{s,i}}{\partial t} = k_{m,i} \cdot G_a \cdot (C_{g,i} - C_{s,i}) + (1-\epsilon) \cdot \sum_{k=1}^{n_r} \sigma_k \cdot r_k \tag{C.2}$$

Here, the accumulation of surface species depends on the mass transfer term and on the summation of all the reactions k in which species i is involved. The accumulation takes place only in the fraction of the catalyst volume defined by the term $(1-\epsilon)$. The ϵ_s stands for the porosity of the catalytic bed. The r_k represents the rate of reaction k and σ_k the stoichiometric number. Nearly all the investigated literature omits the left-hand side of this equation based on the fact that the storage of gas in the catalyst is small in comparison to the other phenomena happening; typically the reaction rates are much larger in magnitude. Therefore, it is possible to rewrite the C.2 as follows:

$$-k_{m,i} \cdot G_a \cdot (C_{g,i} - C_{s,i}) = (1-\epsilon) \cdot \sum_{k=1}^{n_r} \sigma_k \cdot r_k \tag{C.3}$$

Given the above simplification, it is possible to substitute C.3 into C.1. Thus, both the bulk gas species (BGS) and the surface species (SS) equations can be joined together resulting in:

$$\epsilon \cdot \frac{\partial C_{g,i}}{\partial t} + u_{gas} \cdot \epsilon \cdot \frac{\partial C_{g,i}}{\partial x} = (1-\epsilon) \cdot \sum_{k=1}^{n_r} \sigma_k \cdot r_k \qquad i=NH_3,NO,NO_2 \tag{C.4}$$

In this way, a single molar balance is needed for each species i involved in the SCR process.

C.3. INTERMEDIATE SPECIES

The intermediate species is represented by the ammonia stored in the catalyst. It is supposed that only ammonia is being strongly adsorbed by the active elements (the mechanism is better described is section 2.4.3). Only the mass equation is presented here and is given by:

$$\frac{d\theta_{NH_3}}{dt} = \frac{1}{\Omega} \cdot \sum_k \sigma_k \cdot r_k \tag{C.5}$$

where Ω is the surface site density in $[mol/m^3]$ and θ_{NH_3} is the surface coverage fraction of ammonia.

C.4. BULK GAS TEMPERATURE

The temperature of bulk gas can be expressed with the following equation:

$$\epsilon \cdot \rho_g \cdot c_{v,g} \cdot \frac{\partial T_g}{\partial t} + u_{gas} \cdot \rho_g \cdot c_{p,g} \cdot \epsilon \cdot \frac{\partial T_g}{\partial x} = -h_{g \to m} \cdot G_a \cdot (T_g - T_m) \tag{C.6}$$

The first left-hand side term is the accumulation of heat in control volume where ρ_g is the exhaust gas density, c_g are the exhaust gas specific heat capacities (at constant pressure p and volume v) and T_g the gas temperature. The second term on the left-hand side denotes the heat convection by the exhaust gas mass flow through the catalyst. The term on the right-hand side is the inter-phase heat transfer from gas to monolith, where the $h_{g \to m}$ stands for the convective heat transfer coefficient between bulk gas and monolith in $[\frac{W}{m^2 K}]$.

C.5. SURFACE TEMPERATURE

When accumulation, axial heat conduction, gas/solid heat transfer and heat source from catalytic reactions are included, the surface temperature can be described by:

$$\rho_m \cdot c_{p,m} \cdot \frac{\partial T_m}{\partial t} = \lambda_m \cdot \frac{\partial^2 T_m}{\partial x^2} + \frac{h_{g\rightarrow m} \cdot G_a}{1-\epsilon} \cdot (T_g - T_m) + \frac{1}{1-\epsilon} \cdot \sum_{k=1}^{n_r} -\Delta H_{r,k} \cdot r_k \tag{C.7}$$

D

VOLUME AND RESISTANCE EQUATIONS

The description of the equations adopted in the volume and resistance blocks is in accordance with Schulten (2005).

D.1. VOLUME ELEMENT

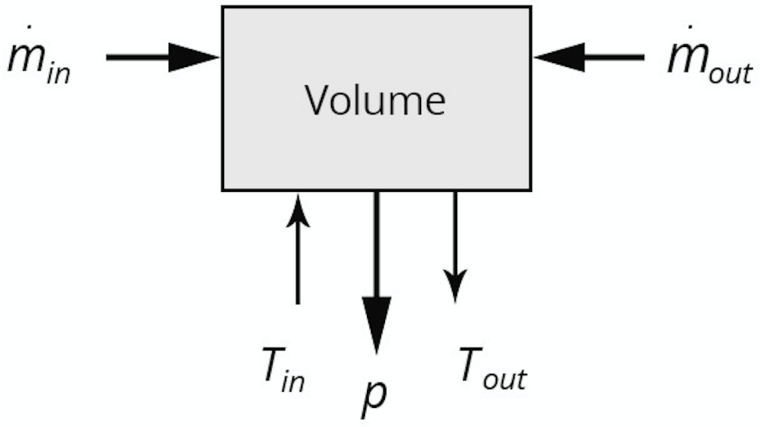

Figure D.1: Volume Block

The volume element calculates, by means of the flow in and out, the state of the volume.
The instantaneous mass is calculated via the integration of the net mass flow:

$$\frac{dm}{dt} = \dot{m}_{out} - \dot{m}_{in} = \dot{m}_{net} \tag{D.1}$$

When the kinetic and potential energies are neglected, the first law of thermodynamics states:

$$\frac{d(m \cdot u)}{dt} = \sum_e u_e \cdot \dot{m}_e + \dot{Q} - \frac{dW}{dt} \tag{D.2}$$

where u stands for the internal energy, e denotes the inflow and outflow, $\dot{Q}$ is the heat flow and W is the work. Only flow work applies:

$$\frac{dW}{dt} = \sum_e -p_e \cdot v_e \cdot \dot{m}_e \tag{D.3}$$

where v denotes the flow velocity (in the rest of the thesis the exhaust gas velocity is named u_{gas}). When enthalpy h is introduced, the following holds:

$$\sum_e u_e \cdot \dot{m}_e + \sum_e -p_e \cdot v_e \cdot \dot{m}_e = \sum_e (u_e + p_e \cdot v_e) \cdot \dot{m}_e = \sum_e h_e \cdot \dot{m}_e \tag{D.4}$$

Inserting in the energy balance and applying the chain rule to the mass and internal energy derivatives:

$$u \cdot \frac{dm}{dt} + m \cdot \frac{du}{dt} = \sum_e h_e \cdot \dot{m}_e + \dot{Q} \tag{D.5}$$

Inserting the mass balance (eq. D.1) and rearranging gives the following:

$$m \cdot \frac{du}{dt} = \sum_e (h_e - u) \cdot \dot{m}_e + \dot{Q} \tag{D.6}$$

In case of ideal gas, equation reduces to:

$$m \cdot c_v \frac{dT}{dt} = \sum_e (h_e - u) \cdot \dot{m}_e + \dot{Q} \tag{D.7}$$

The calculation for enthalpy, internal energy and heat coefficients is given in appendix B.
Once the temperature is known, the pressure in the volume element can be calculated:

$$p = \frac{m \cdot R \cdot T}{V} \tag{D.8}$$

D.2. RESISTANCE ELEMENT

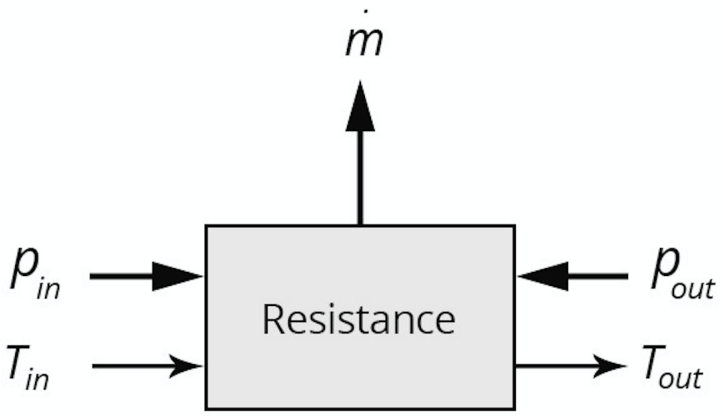

Figure D.2: Volume Block

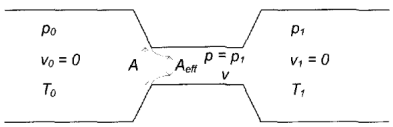

Figure D.3: Flow through a resistance (Schulten, 2005)

The momentum equation for steady-state, incompressible flow with an extra pressure loss included is given by:

$$\frac{p_0}{\rho g} + \frac{v_0^2}{2g} = \frac{p}{\rho g} + \frac{v^2}{2g} + \frac{p_{loss}}{\rho g} \tag{D.9}$$

where the pressure loss is written as:

$$p_{loss} = \zeta_{in} \cdot \frac{\rho v^2}{2} \tag{D.10}$$

If $v_1 = 0$, the combination of equations D.9 and D.10 gives:

$$v = \sqrt{\frac{2(p_0 - p_1)}{(1+\zeta_{in}) \cdot \rho}} \tag{D.11}$$

The mass flow through the resistance is:

$$\dot{m} = \rho \cdot A_{eff} \cdot v \tag{D.12}$$

If the density in the resistance is assumed to be the same as the inlet:

$$\rho \approx \rho_0 = \frac{p_0}{R_0 \cdot T_0} \tag{D.13}$$

the combination of equations D.11 and D.12 gives:

$$\dot{m} = \frac{A_{eff}}{\sqrt{1+\zeta_{in}}} \cdot \frac{p_0}{\sqrt{R_0 \cdot T_0}} \cdot \sqrt{2} \cdot \sqrt{(1 - \frac{p_1}{p_0})} \tag{D.14}$$

Instead of the first term on the left hand side, a resistance factor ϕ is introduced:

$$\phi = \frac{1}{\sqrt{1+\zeta_{in}}} \tag{D.15}$$

Furthermore, the effective area can be rewritten as:

$$A_{eff} = \mu \cdot A \tag{D.16}$$

where μ represents the contraction factor.
Given the above considerations, equation D.14 results in:

$$\dot{m} = (\mu \cdot \phi) \cdot A \cdot \frac{p_0}{\sqrt{R_0 \cdot T_0}} \cdot \sqrt{2} \cdot \sqrt{(1 - \frac{p_1}{p_0})} \tag{D.17}$$

E

NO_x Look-up Table

The values for the NOx look-up table (E.1) are taken from the measurements of a W34DF in diesel mode for generator load. The absence of measured emissions for the adopted engine, led to the adoption of an engine showing similar temperature trends (fig.E.1).

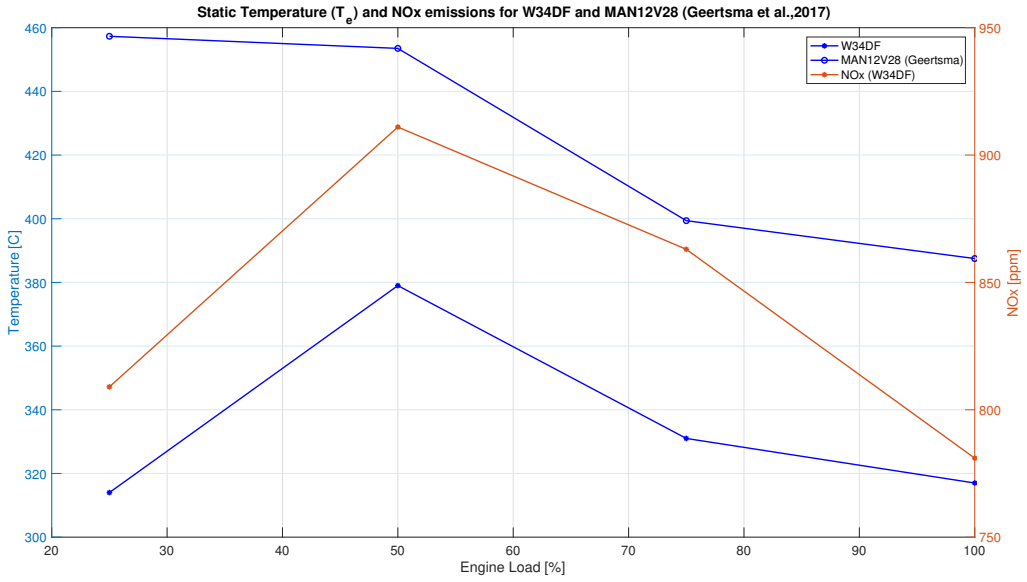

Figure E.1: Outlet turbine temperature and NOx emissions for W34DF and MAN12V28

Table E.1: NOx Look-up Table

NOx Lookup Table	
Load [%]	NOx [ppm]
100	781
75	863
50	911
25	809

NOMENCLATURE

VARIABLES

A	Area	[m^2]
C	Concentration	[mol/m^3]
c_p	Specific heat at constant pressure	[J/kg/K)]
c_v	Specific heat at constant volume	[J/kg/K)]
d_h	Hydraulic diameter	[m]
E_a	Activation energy	[J/kg]
G_a	Geometric surface area to volume ratio	[m^2/m^3]
H^0	Standard enthalpy of reaction	[kJ/mol]
h	Enthalpy	[J/kg]
$h_{g\rightarrow w}$	Heat transfer coefficient	[$W/m^2/K$]
k	Rate constant	Reaction dependent
k^0	Pre-exponential factor	Reaction dependent
L	Length	[m]
M	Molar weight	[g/mol]
m	Mass	[kg]
m	Number of cells	[-]
$\dot{m}$	Mass flow rate	[kg/s]
n	Moles number	[mole]
Nu	Nusselt number	[-]
p	Pressure	[Pa]
Pr	Prandtl number	[-]
$\dot{Q}$	Heat flow	[W]
R	Specific Gas constant	[J/kg/K]
$\tilde{R}$	Universal Gas constant	[J/mol/K]
r	Reaction rate	[$mol/m^3/s$]
Re	Reynolds number	[-]
sfc	Specific fuel consumption	[g/kW/h]
spe	Specific pollutant emission ratio	[g/kW/h]
T	Temperature	[K]
t	Time	[s]
u_{gas}	Gas velocity	[m/s]
V	Volume	[m^3]
x	Mass fraction	[-]
y	Mole fraction	[-]

GREEK SYMBOLS

ϵ	Void fraction	[-]
Δ	Difference	
λ	Thermal conductivity	[W/m/K]
λ	Air excess ratio	[-]
θ	Adsorption site	[-]
μ	Contraction factor	[-]
ξ	Extent of a reaction	[mol]
ρ	Density	[kg/m^3]
τ	Thickness	[m]
σ	Stoichiometric coefficient	[-]
ϕ	Resistance factor	[-]
Ω	Adsorption capacity	[mol/m^3]

SUBSCRIPTS

ads	Adsorption
des	Desorption
g	Gas
in	Inlet
i	Generic cell
j	Generic species
k	Generic reaction
m	Monolith
nc	Number or components
nr	Number or reactions
out	Outlet
ox	Oxidation
s	Surface
std	Standard
w	Wall